THE UNIVERSITY OF CHICAGO

THE ROLE OF H2-O AND ADDITIONAL NOVEL LOCI IN ANTIGEN PRESENTATION AND THE IMMUNE RESPONSE AGAINST BACTERIA AND VIRUSES IN MICE

A DISSERTATION SUBMITTED TO

THE FACULTY OF THE DIVISION OF THE BIOLOGICAL SCIENCES

AND THE PRITZKER SCHOOL OF MEDICINE

IN CANDIDACY FOR THE DEGREE OF

DOCTOR OF PHILOSOPHY

INTERDISCIPLINARY SCIENTIST TRAINING PROGRAM:

IMMUNOLOGY

BY

EMILY CULLUM

CHICAGO, ILLINOIS

JUNE 2022

TABLE OF CONTENTS

LIST OF FIGURES

LIST OF TABLES

SUMMARY

Whether or not a host organism mounts a protective immune response to invading pathogens is determined by a number of factors, including the genetic makeup of the host. Here, the role of a particular protein, H2-O, in the response against viruses and bacteria is explored in depth.

The loss-of-function of H2-O in the I/LnJ strain of mice is identified as dependent on three amino acid mutations in the Ig domain of the H2-Oβ protein; however, the precise mechanism why polymorphism in this domain of the protein alters its function is not yet clear. We hypothesize it may be due to Ig-domain mediated interaction between H2-Oβ and novel factors yet to be identified. Supporting this hypothesis, we have discovered that two additional loci (other than H2-O, H2-M, or MHC-II) control antigen presentation and work to uncover the identities of the genes encoded in these loci is currently underway. Our current data suggest that loci on chromosomes 1 and 15 harbor these two factors.

Classical MHC proteins influencing H2-O-dependent antibody responses was also investigated. While BALB/cJ mice harboring the MHC locus from the I/LnJ strain ($H2^J$-congenic mice) mount potent neutralizing antibody responses against both MMTV and MuLV, H2-O deficiency alone only confers protection from MMTV and not MuLV. The lack of response against MuLV appears to be due to the $H2^d$ haplotype of MHC present in the BALB/cJ strain, as $H2^b$-congenic BALB/cJ mice (BALB.B mice) are capable of producing neutralizing antibodies against the virus, although at lower titers than $H2^J$-congenic BALB/cJ mice.

While the response of H2-O-deficient mice on the C57BL/6J background mount neutralizing antibody responses against MMTV upon infection, the response of these animals to bacteria was completely unexplored. H2-O was found to influence multiple microbial communities, and our data suggest this may be independent of the quantity or specificity of IgA present in the gut. H2-O-deficient mice were also found to be more resistant to persistent

colonization by the bacterium *Staphylococcus aureus* as well as restrict early phase replication of the bacterium *Citrobacter rodentium.* Study of the mechanism of H2-O control of these pathogens is underway, but preliminary experiments suggest a dependence on B cells in the *S. aureus* infection model.

The resistance of H2-O-deficient animals to various pathogens in our studies made us question the physiological importance of this protein (as multiple models of infection suggested H2-O was maladaptive). The predominant hypothesis in the field of H2-O biology proposed H2-O played a role in the prevention of autoimmune disease, but conclusive studies to this end were lacking. To address this gap, we tested the susceptibility of H2-O-deficient mice in three models of autoimmunity, each utilizing a distinct genetic background. We did not find any evidence to suggest H2-O prevents autoimmunity. Instead, we found evidence to suggest H2-O is important in the restriction of a γherpesvirus, which exploits H2-O expressing cells during its replication. This suggests the physiological function of this gene may be related to high prevalence of such infections during the course of mammalian evolution.

Determining the true importance of a gene during infection requires the use of physiologically relevant infection systems. H2-O deficiency is not sufficient to confer neutralizing antibody responses to C57BL/6J mice when infected via breastmilk, the natural route for MMTV. Mice infected as neonates by their mother's viremic breastmilk exhibit life-long unresponsiveness to viral antigens. The role of H2-O in the induction or maintenance of this critical viral tolerance was explored. We found that H2-O-deficient neonatally infected mice were still partially tolerant to viral antigens, but to a lesser degree than H2-O-sufficient mice. However, H2-O-deficient mice did not exhibit any overall lack of oral tolerance to other dietary antigens, suggesting H2-O plays a role in the induction or maintenance of this virus-specific tolerance. It is tempting to speculate that MMTV may exploit H2-O in order to induce a state of immunological unresponsiveness against itself. In addition, we tested if H2-O-deficient

splenocytes transferred into neonatally infected hosts would produce antibodies, or if this response would be suppressed in a tolerant host. We found that H2-O-deficient (but not H2-O sufficient) splenocytes transferred into tolerant hosts were able to produce antibodies, suggesting tolerance may be induced in a B-cell intrinsic fashion.

INTRODUCTION

Effective immune responses to pathogens is a major determinant of an individual's evolutionary fitness. The responses to invading microorganisms undertaken by the host will be determined, in large part, by the host's genetic makeup. This work attempts to better understand the role of a particular mouse gene, *H2-Ob*, in immune responses against viruses, bacteria, and self.

Overview of mammalian immune responses

In mammals, immune responses are orchestrated by a wide variety of dedicated cell types which specialize in combating potential microbial invaders in specific ways. One of the most common ways to categorize these cell types is to divide them into cells that participate in "innate" or "adaptive" immunity. Innate immunity broadly refers to the ways in which an organism responds to microbial invaders in a rapid, but largely nonspecific way, targeting general molecular patterns which characterize "non-self", such as microbial carbohydrates or nucleic acids [1-4]. These microbial characteristics are often referred to as pathogen associated molecular patterns, or PAMPs [1-4]. In addition to those associated with pathogens, innate immune cells also harbor the capacity to recognize and respond to damage associated molecular patterns (also called DAMPs), such as exclusively intracellular molecules only released during non-programmed cell death [2]. While the cells of the innate immune system and the mechanisms by which they respond to pathogens and tissue damage are the subject of much study, they are not the primary focus of the work contained herein.

Activated innate immune cells are critical for activation of the more pathogen-specific adaptive immune system. Adaptive immunity broadly refers to the way in which an organism responds to non-self in a highly specific manner which is also capable of being recalled upon subsequent challenges with the same (or highly similar) pathogen. The necessary trade-off for the exceptional specificity of these responses is time—unlike the minutes or hours required for activation of innate immunity, full-blown responses via the adaptive immune response take days to weeks [4, 5]. The adaptive immune response to pathogens is primarily driven by T lymphocytes and B lymphocytes. Broadly, T and B cells use highly diverse receptors on their cell surface (called T cell receptors, or TCRs, and B cell receptor, or BCRs, respectively) to recognize the presence of intracellular or extracellular foreign macromolecules (usually protein). These foreign macromolecules are otherwise known as antigens (where macromolecules that are not foreign, or “self” are referred to as self antigens). These highly diverse receptors are generated through a process of recombination in which allows a pair of genetic loci to give rise to millions of different receptors with varying specificities [4]. Cells harboring receptors which are non-functional or self-reactive (i.e. recognize self antigens) are eliminated during processes termed positive and negative selection, respectively[4]. The mechanisms of TCR/BCR recombination and selection are also fields of intense study, and are not the primary focus of the work contained herein.

T cells and B cells recognize foreign antigen in the context of major histocompatibility complex (MHC) molecules [4]. MHC molecules are proteins located on the surface of cells and contain a binding groove which will bind small antigen-derived peptides. The mammalian genome encodes two types of MHC proteins: MHC-I and MHC-II. MHC-I proteins are found in all cells and bind and present peptides derived from intracellular proteins, such as self peptides or peptides derived from microbes replicating intracellularly [4]. MHC-II proteins are found only in a specialized subset of cells called antigen presenting cells (APCs) which include dendritic cells, macrophages, and B cells. MHC-II proteins present peptides derived from extracellular

proteins which have been phagocytosed and degraded in the lysosome prior to MHC-II loading and presentation [4]. Peptides presented by MHC-I are recognized by the TCRs of a specific subset of T cells expressing the co-receptor CD8 (CD8+ T cells) and peptides presented by MHC-II are recognized by TCRs of a specific subset of T cells expressing the co-receptor CD4 (CD4+ T cells).

The result of TCR recognition of peptide:MHC is activation of the T cell if a costimulatory signal, in the form of an additional receptor:ligand interaction between the MHC presenting cell (i.e. activated innate immune cell) and the T cells occurs. Activated T cells can either contribute to clearance of an infection directly or indirectly. Typically, T cells participating directly in the elimination of a pathogen will be cytotoxic CD8+ T cells. T cells participating indirectly in the elimination of a pathogen can do so by a number of mechanisms relying on secreted proteins or by aiding in the production of antibodies by B cells. T cells which help activate B cells to produce antibodies are CD4+ T cells, otherwise known as T helper cells (Th cells).

While antibodies are produced exclusively by B cells, Th cells are critical for initiating this response in many cases. The process by which B cells become activated in a T cell dependent manner is called the germinal center response, as it occurs in specific microstructures within lymphoid organs called germinal centers [4]. In the germinal center, antigens are presented via MHC-II by follicular dendritic cells (named for the anatomic structure of the spleen, called the follicle, in which the germinal centers can be found) to B cells for recognition via the BCR. If the BCR:antigen interaction is sufficiently strong, the B cell will be able to capture the antigen and internalize it via BCR-mediated endocytosis and process this antigen for presentation on its own MHC-II. Antigen presented on the B cell via MHC-II can be recognized by a specific subset of CD4+ T cells residing in near the germinal center, the T follicular helper cell, or Tfh cell, via the TCR and provides a help signal to the presenting B cell via a CD40/CD40L interaction. The B cell may cycle through this process several times, each time mutating its BCR via a process termed somatic hypermutation (SHM), which is mediated by AID. This eventually results in a B

cell clone with very high BCR affinity for the antigen of interest, thus resulting in production of high affinity antibodies. It is also typically during this germinal center response that the B cell is able to modify its heavy chain locus to produce antibodies of the IgG1, IgG2a (or IgG2c), IgG2b, IgG3, IgA, or IgE isotype. This process, called class switch recombination (CSR) is, like SHM, mediated by AID. Which isotype a B cell will switch to during CSR is dependent on a number of factors, one of which is the types of cytokines present during the GC reaction. Typically, the type of invading microbe elicits certain cytokines be secreted by other immune cells drives and results in a characteristic isotype switch which in turn aids in clearance of the specific type of invading microbe. The intricacies of the germinal center response and class switch recombination are subjects of intense study. However, they are not the primary focus of this work.

Antigen presentation

As antigen presentation of MHC-II is absolutely required for the initiation of CD4+ T cell responses and B cell responses, it follows that the details of this presentation, such as what peptides are presented and to what level they are presented, are of great importance. The process of MHC-II antigen presentation begins with acquisition of the antigen by the APC either by general endocytosis/pinocytosis or by receptor-mediated endocytosis. APCs that are also highly phagocytic, such as dendritic cells and macrophoages, are efficient as acquiring antigen via endocytosis and pinocytosis. In contrast, B cells do not endocytose material efficient except via the BCR. Therefore, dendritic cells and macrophages are far more likely to present a wide variety of antigens on their cell surfaces and B cells are more likely to present antigens derived from the target of their BCR. In either case, endocytosed material, which is found in cellular structures called phagosomes, is degraded by cellular proteases once the phagosomal-lysosomal fusion occurs. These cellular proteases generate the array of peptides that will be presented on MHC-II. This lysosomal compartment is also the site of MHC-II:peptide loading.

Prior to its arrival in the antigen-containing lysosomal compartment, MHC-II (like all proteins of the secretory pathway) is produced in the endoplasmic reticulum. Here, it is produced in complex with another protein, class-II associated invariant chain (or CD74). This complex traffics to the lysosome, where lysosomal proteases degrade most of the invariant chain, leaving only the class-II associated invariant chain peptide (CLIP) in the MHC-II peptide binding groove. Once in the lysosome, the MHC-II:CLIP will either be loaded with peptide or CLIP will remain in the binding groove, and the complex will traffic to the cell surface where it can be recognized by TCRs and BCRs.

H2-M (HLA-DM) and H2-O (HLA-DO)

Importantly, the process of peptide loading onto MHC-II is regulated by two known key proteins: H2-M (HLA-DM in humans) and H2-O (HLA-DO in humans). In both humans and mice, both genes are located within the MHC locus (found on chromosome 6 in humans and chromosome 17 in mice). As with many of the MHC molecules encoded in these loci, H2-M (and its homologs) and H2-O (and its homologs) are thought to be the result of gene duplication events. Interestingly, while MHC classical MHC molecules are found among many vertebrate species, homologs of H2-M are not seen in ecotherms but are first seen in endotherms and homologs of H2-O do not arise until the divergence of placental from non-placental mammals [6]. Both H2-M and H2-O are αβ heterodimers. H2-Mα is encoded by *H2-Ma* and H2-Mβ is encoded by *H2-DMb1*. The production of functional H2-M is restricted to MHCII antigen presenting cells as well as medullary thymic epithelial cells. Similarly, H2-Oα is encoded by *H2-Oa* and H2-Oβ is encoded by *H2-Ob* and exhibits the same expression pattern as H2-M [7, 8]. Within the cell, both H2-M and H2-O reside in the late endosomal compartments, where they can easily interact with materials recently phagocytosed by the antigen presenting cell [8-10]. Both proteins are obligate heterodimers, meaning both subunits are required for functional protein. Since these genes are thought to have arisen via duplication events, H2-M and H2-O

are sometimes contrasted to the “classical” MHC molecules and called “non-classical” MHC molecules.

The function of H2-M is to bind MHC-II:CLIP and catalyze the removal of CLIP from the peptide binding groove and load antigenic peptide [11, 12]. H2-M is also said to have MHC-II peptidome “editing” function, as loaded low affinity peptides will quickly be removed and replaced with higher affinity peptides. This function of H2-M has been demonstrated both in vitro and in vivo (with the use of H2-M-deficient mice) [10]. In vivo, the MHC-II complexes on the cell surface of H2-M-deficient mice are almost exclusive bound to CLIP, rather than antigenic peptides[10]. Importantly, the function of H2-M is regulated by its inhibitor, H2-O [13, 14]. The outcome of H2-O activity is a reduction in H2-M activity, and therefore fewer MHC-II:CLIP complexes at the cell surface without overall changes in MHC-II levels [15]. Like H2-M, the function of H2-O was also probed in vivo using H2-O deficient mice. As H2-O is essentially an inhibitor of antigen presentation, it was first hypothesized that H2-O may function to prevent autoimmunity [13]. Several groups have tested this hypothesis, with inconsistent results [16-19]. While some of these groups report spontaneous autoimmunity found in their H2-O-deficient mice, such as presence of autoantibodies [20], these phenotypes do not appear to affect the overall health of the animal and furthermore, are not reproduced by other laboratories, including ours. Other reports of increased susceptibility to induced autoimmunity are not well controlled and exhibit poor phenotype penetrance [19]. While multiple studies from various research groups have reached similar conclusions regarding H2-O as an inhibitor of H2-M, an alternate hypothesis has been proposed that H2-O and H2-M act in concert to catalyze peptide loading on MHCII [21]. This study was conducted in a cell-free *in vitro* system using purified proteins, and so its relevance to *in vivo* systems is unclear.

Other groups have attempted to address the importance of H2-O to the process of antigen presentation in various ways. As the MHC-II antigen presentation machinery functions within the thymic epithelium to aid in the selection of T cells during development, one group

asked if H2-O effects the T cell repertoire by analyzing TCR Vβ chain usage in H2-O-sufficient and H2-O-deficient mice, finding no striking differences [22]. Two other groups used a mass spectrometry based approach to identify the peptides presented by DO-sufficient and DO-deficient human cell lines [23] and in H2-O-sufficient and H2-O-deficient mouse splenocytes [19, 23]. Both groups' data support the conclusion that H2-O (or HLA-DO)-deficient antigen presenting cells present a smaller diversity of peptides with an overall higher affinity for MHC-II than the peptides presented by H2-O (or HLA-DO)-sufficient antigen presenting cells. The primary limitation of these studies is the use of animals at "steady state"—arguably, the most important result of antigen presentation is the mounting of an effective immune response against a pathogen.

Canonically, H2-O is thought to work by acting as a competitive inhibitor of H2-M:MHC-II binding [24]. These studies were conducted in vitro, using HLA-DM and HLA-DO constructs expressed in *Drosophila melanogaster* S2 cells, and therefore their relevance to the mouse homologs in vivo is currently not well understood. However, these studies combined with close structural similarity between the human and mouse homologs make it reasonable to hypothesize that H2-O may inhibit H2-M via a mechanism based on competitive inhibition. However, data from our laboratory, which are discussed below, indicate the mechanisms of H2-O regulation of H2-M activity is more complex than simple competitive inhibition.

Response of H2-O-deficient mouse strains to MMTV

The goal of the studies described here was to investigate the role of a particular gene, *H2-Ob*, to immune responses against microbes in mice.

These studies are largely based on experiments conducted by the lab which found I/LnJ mice are highly resistant to mammary tumors caused by the betaretrovirus Mouse Mammary Tumor Virus (MMTV) [25, 26]. As with all viruses in the retroviridae family, MMTV replication depends on reverse transcription of its ssRNA genome to dsDNA, which is integrated into the

host cell genome in order for viral genes to be expressed. MMTV enters the cell via receptor-mediated endocytosis after binding of the envelope glycoprotein to the host transferrin receptor 1 (CD71) [27, 28]. The virus is spread to neonates via viremic breastmilk. The virus gains entry to the Peyer's patches found in the small intestine via M cells, and subsequently spreads first to dendritic cells (DCs) and then to B and T cells found in the Peyer's patches. Viral T cell superantigens elicit a proliferation of superantigen-cognate T cells which further supports replication of the virus. This superantigen-mediated T cell stimulation is critical for viral infection, as mice that do not have superantigen-cognate T cells will not be productively infected by the virus [29]. B cells are also critical for the life cycle of the virus, as mice deficient in B cells do not shed virus in the breastmilk [30]. As a result of the proliferation of infected lymphocytes, the virus is able to spread to the mammary glands [31]. Infected females will subsequently shed infectious virus into their breastmilk, infecting offspring. In susceptible strains of mice, viral infection is transmitted indefinitely. As retroviruses integrate into the host genome, integration can cause disruption of or upregulation of cellular genes. If these genes are capable of altering cell physiology in a way that predisposes the cell to unregulated cell replication, these genes are referred to as proto-oncogenes. It is due to the insertion of MMTV near cellular proto-oncogenes in the mammary gland that gives rise to mammary tumors [27]. The resistance of I/LnJ mice to these tumors was further investigated and was found to be due to a failure of the virus to be transmitted from the Peyer's patches to the mammary glands [25]. It follows that pups sucking the milk infected I/LnJ females (whether they are of the I/LnJ strain or another more MMTV susceptible strain) do not become infected.

Later, I/LnJ resistance to MMTV was identified to depend on the presence of neutralizing antibodies against the virus produced by I/LnJ mice but absent from susceptible strains such as C57BL6/J, BALBc/J, and C3H/HeN [15, 32, 33]. This resistance mechanism, which was shown to be inherited in a recessive fashion [25], was later shown to be controlled by a loss of function allele of the gene *H2-Ob* found in the I/LnJ strain [15]. The allele of *H2-Ob* in the I/LnJ strain

differs from MMTV-susceptible strains by 4 amino acids [15]. Three of these four mutations are found in the protein's immunoglobulin (Ig) domain, which is structurally part of the protein's lysosomal luminal domain. The fourth mutation is found in the protein's cytoplasmic tail domain (Ct), which resides outside of the lysosome in the cytoplasm of the cell. This region of the protein, compared to other regions of H2-Oβ, is relatively more polymorphic. For example, C57BL/6 mice have a unique Ct compared to BALB/cJ and C3H/HeN mice, which does not confer any resistance to MMTV. The contribution of these mutations are explored in detail in Chapter 1. The discovery of a unique null allele of *H2-Ob* prompted study of the mechanism of its loss of function. The most obvious explanation would be, of course, that the mutations found in the I/LnJ allele lead to loss of protein production. However, H2-Oβ protein in I/LnJ mice is made and can bind H2-M, yet the H2-O complex lacks the ability to inhibit H2-M [15]. *H2-Ob*$^{-/-}$ mice on the C57BL/6J (B6J) background also produce MMTV-neutralizing antibodies, supporting the conclusion that the I/LnJ *H2-Ob* allele is a loss-of-function allele [15]. Currently, accepted dogma in the field of H2-O biology proposes H2-O binding to H2-M is both necessary and sufficient for H2-O to exert its inhibitory function [24]. However, study of the I/LnJ allele of *H2-Ob* has made clear that this model of H2-O function is incorrect, as the I/LnJ allele can bind to, but not inhibit, H2-M [15]. Further complicating the understanding of the function of H2-O is the fact that many have suggested the function of H2-O is to prevent development of autoimmunity [18, 34] yet autoimmune disease has not been reported in either the I/LnJ strain or H2-O-deficient mice from the B6 or BALB/cJ strains, indicating that prevention of autoimmunity cannot be the function of H2-O (this idea is explored in detail in Chapter 4). Therefore, the function of this gene represents a crucial gap in our understanding of immunology, especially as this gene appears to be conserved among most mammals [35].

Outline

This work is divided into five chapters, each of which attempt to address an unanswered question in the field of H2-O biology:

First, what is the mechanism by which H2-O inhibits H2-M? Contrary to what has been assumed by the field for many years, binding of H2-M by H2-O is not sufficient to mediate inhibition. Work to understand which mutations are most critical for loss-of-function revealed the importance of the Ig domain, as well as novel unknown players in the MHC-II antigen presentation pathway.

Second, what is the role of classical MHC to H2-O-dependent antiretroviral antibody responses? To address this question, we used BALB/cJ and BALB/c $H2^b$ congenic (BALB.B) mice which are susceptible to both MMTV and murine leukemia virus (MuLV).

Third, what influence does H2-O-deficiency have on immune responses against bacteria, both commensal and pathogenic? While prior work in the lab definitively demonstrated a role for H2-O-deficiency in the immune response against retroviruses, it was unknown H2-O could regulate immune responses against other microbes, such as bacteria. We tested the influence of H2-O on several different models of bacterial colonization, such as consortia of commensal bacteria, non-pathogenic non-commensal bacteria, and pathogenic bacteria.

Fourth, what is the adaptive advantage of H2-O? Canonically, it is thought to prevent autoimmunity. However, preliminary data in the lab argued against this conclusion. Therefore, our laboratory in collaboration with others, tested the role of H2-O-deficiency in several models of autoimmunity, both systemic and organ specific, and failed to find any evidence that H2-O suppresses onset or progression of autoimmune disease.

And lastly, what is the role of H2-O in antiretroviral antibody responses in mice infected with MMTV as neonates via the natural oral route? For many experiments to be feasible, we must resort to a non-physiological method of MMTV infection in our experiments: intraperitoneal injection of purified virus. Therefore, we explored the role of H2-O in antibody responses against MMTV in mice infected via milk as neonates and found that H2-O plays a role in a unique tolerance to viral antigens induced by the virus upon infection and that this tolerance is likely maintained by B cells in adult mice.

RESULTS

Chapter 1: Investigation of the mechanism by which H2-O inhibits H2-M

Preface

Studies of I/LnJ H2-O/H2-M interactions demonstrated that H2-O binding to H2-M was not sufficient to inhibit H2-M, as the I/LnJ protein was capable of such interactions yet was shown to be loss-of-function [15]. Therefore, a more detailed study of how H2-O inhibits H2-M was undertaken. These studies were recently published [36], and the text below under the heading "Published Data" is taken directly from that publication and can be found online on the *Journal of Immunology* website at the following URL: https://www.jimmunol.org/content/207/1/5.abstract. The vast majority of the experiments contained in that publication were performed either by the author, or by the author with help from Tatyana Golovkina. Bone marrow chimera experiments were designed and performed by Lisa Denzin, and biochemical analysis of Ob KI alleles was performed by both me and Lisa Denzin. Flow cytometry experiments analyzing levels of H2-O and H2-M in various cell types were performed by Austin Graves.

Summary

In our published studies, we use a CRISPR-Cas9 based approach to introduce single mutations or combinations of mutations found in the loss-of-function I/LnJ allele of *H2-Ob* onto the C57BL/6J background. The four candidate mutations were S128N, V148I, L167H, and E239K/S240L (B6J mice have a unique allele compared to other MMTV-susceptible strains containing S240, where other virus susceptible strains, such as BALB/cJ and C3H/HeN contain L240). Single amino acid changes and the double S128N/V148I change were not sufficient to lead to loss of function of H2-O. However, a loss-of-function allele containing three mutations, S128N/V148I/L167H, was found in the CAST/EiJ strain of mice.

We also discovered other loci, other than those containing H2-O and H2-M, which are capable of regulating antigen presentation on MHC-II. We provisionally call these two loci *c2pmA* and *c2mpB.* While the identities of genes in these loci are presently unknown, our data indicate the presence of two recessive loci in the C57BL/6N strain which lead to altered antigen presentation similar what is seen in B6J.*Ob*$^{-/-}$ mice.

A small portion of the unpublished studies in this chapter solidify the importance of the three Ig domain mutations as we were able to produce a mouse containing all three mutations on a single allele on the B6J background. This mouse line exhibits decreased H2-O function consistent with our hypothesis that these three mutations, when present together, lead to H2-O loss off function in I/LnJ mice.

The majority of the unpublished studies in this chapter focus on identification of loci encoding the *c2pmA* and *c2mpB*. This is primarily being accomplished by a genome-wide scan for polymorphisms found between B6J and B6N mice of N2 mice phenotyped to be CLIP^{High} or CLIP^{Low}. This approach has identified two loci of interest, and several candidate genes within these loci, which are discussed in detail herein.

Published Data

MHC Class II presentation is affected by polymorphism in the H2-Ob gene and additional loci

Emily Cullum[1], Austin M. Graves[2], Vera L. Tarakanova[3], Lisa K. Denzin[2,4] and Tatyana Golovkina[1,5,6 *]

[1]Committee on Immunology, University of Chicago, Chicago, IL, 60637

[2]Graduate School of Biomedical Sciences, Rutgers, The State University of NJ, New Brunswick, NJ, 08901

[3]Microbiology and Immunology, Cancer Center, Medical College of Wisconsin, Milwaukee, WI 53226

[4]Child Health Institute of NJ, Department of Pediatrics, Rutgers Robert Wood Johnson Medical School, The State University of NJ, New Brunswick, NJ, 08901

[5]Committee on Microbiology, University of Chicago, Chicago, IL, 60637

[6]Department of Microbiology, University of Chicago, Chicago, IL, 60637

*Address correspondence to Dr. T. Golovkina, Tel. (773) 8347988; E-mail address: tgolovki@bsd.uchicago.edu

Funding sources: This work was supported by PHS grant AI117535 to T. G. and L.K.D., by P30 CA014599 to the University of Chicago, by the National Center for Advancing Translational Sciences of the National Institutes of Health through Grant Number UL1 TR000430 to the University of Chicago.

Running Title: *H2-Ob* and non-*H2-Ob* polymorphisms modify MHC II presentation

Abstract

Pathogen-derived peptides are loaded on Major Histocompatibility Class II (MHCII) and presented to $CD4^+$ T cells for their activation. Peptide loading of MHCII occurs in specialized endosomal compartments and is controlled by the non-classical MHCII molecules H2-M and H2-O, which are both constitutive αβ heterodimers. H2-M catalyzes MHCII peptide loading, whereas H2-O modulates H2-M activity by acting as an MHCII mimic. Recently, we discovered that the *H2-Ob* allele inherited by retrovirus-resistant I/LnJ mice results in nonfunctional H2-O. I/LnJ H2-O binds to but does not inhibit H2-M. Compared to H2-Oβ from virus-susceptible mice, H2-Oβ from I/LnJ mice has 4 unique amino acid (AA) substitutions: three in the immunoglobulin (Ig) domain and one in the cytoplasmic tail. Here we show that the three AAs in the Ig domain of I/LnJ Oβ are critical for the H2-O inhibitory activity of H2-M. Unexpectedly, we found that MHCII presentation was significantly different in antigen presenting cells from two closely related mouse strains, B6J and B6N, which carry identical alleles of MHCII, H2-O, and H2-M. Using a positional cloning approach, we have identified two loci, polymorphic between B6J and B6N, that mediate the difference in MHCII presentation. Collectively these studies reveal extra complexity in MHCII/H2-M/H-2O interactions that likely involve yet to be identified modulators of the pathway.

Key Points

Three key H2-Oβ Ig-domain residues control H2-O function

MHCII presentation and anti-viral Ab responses are diverse in B6J and B6N mice

Two non-MHC loci mediate the difference in MHCII presentation in B6J and B6N mice

Introduction

The individual outcomes that follow exposure to viral pathogens vary significantly among individuals in both humans and animals. In part, such variations are determined by genetic diversity of the immune response. Similar to mice from other strains, I/LnJ mice become infected with retroviruses from distinct genera, such as Mouse Mammary Tumor Virus (MMTV) and Murine Leukemia Virus (MuLV), but unlike mice from other strains I/LnJ mice produce virus-neutralizing antibodies (Abs) and shed uninfectious virions [32, 33]. We found that this unique mechanism of retroviral resistance was controlled by a single recessive locus, virus infectivity controller 1 (*vic1*), mapped to the MHC locus on Chromosome 17 [37], which functioned in bone marrow (BM)-derived cells to drive the Ab response [38].

The gene encoding Vic1 was subsequently identified as *Ob* based on polymorphism found in this gene in virus-susceptible and virus-resistant mice [15]. *Ob* encodes the β chain of the highly conserved MHCII-like αβ obligate heterodimer H2-O [10], which is a negative regulator of MHCII-peptide presentation [39]. Peptide loading of MHCII molecules is catalyzed in specialized endosomes by H2-M, another MHCII-like αβ heterodimer. H2-M binds to MHCII and replaces MHCII-associated invariant chain peptides (CLIP) with high affinity, pathogen-derived peptides generated by lysosomal proteases, such as cathepsin L and S. H2-O binds to H2-M and acts as an MHCII mimic, blocking the ability of H2-M to bind to MHCII and catalyze MHCII peptide loading. This concept is based on the crystal structure of the DM/DO (human homologues of H2-M and H2-O) complex [40] and a plethora of other supporting biochemical data from numerous groups [13, 14, 17, 23, 41-43].

Based on the recessive nature of the Ab responses in I/LnJ mice, the I/LnJ *Ob* allele was presumed to be a loss-of-function allele. In support of this, mice from other genetic backgrounds with targeted *Ob* deletion were capable of producing retrovirus-neutralizing Abs similar to I/LnJ mice and antigen presenting cells (APCs) expressing I/LnJ Oβ exhibited increased antigen presentation [15]. In the absence of H2-O, H2-M is uninhibited and results in small changes in the MHCII-bound peptidome favoring presentation of high affinity peptides [23,

44]. Thus, these small changes appear to be sufficient to direct potent virus-neutralizing Ab responses [15] most likely due to enhanced presentation of high affinity viral peptides. Although the I/LnJ *Ob* was shown to be null, biochemical analyses revealed that I/LnJ mice had Oβ protein levels that were similar to Oβ levels in susceptible mice and produced H2-O that associated with H2-M [15]. Thus, the I/LnJ *Ob* allele resulted in H2-O that was capable of binding to H2-M but yet did not modulate H2-M-mediated peptide loading.

We have also identified human *DOA* and *DOB* alleles with altered DO function, a few of which phenocopied I/LnJ H2-O as they inefficiently inhibited DM, despite binding to DM [15, 45]. Therefore, these unexpected results challenged the current paradigm that H2-O functions alone to inhibit H2-M activity and suggested existence of unknown factors contributing to H2-O function. Using a genetic approach, we have identified three AA mutations within the Ig of *Ob* which control H2-O function. We have also discovered two new non-MHC-linked loci which modify MHCII antigen presentation.

Results

Generation and characterization of B6J.Oβ knockin mice.

Specific amino acid (AA) polymorphisms found in I/LnJ Oβ do not perturb H2-O protein levels or alter the ability of I/LnJ H2-O to associate with H2-M [15]. However, despite these seemingly normal biochemical features, I/LnJ H2-O fails to inhibit H2-M function [15]. Compared to Oβ from virus-susceptible mice, Oβ from virus-resistant I/LnJ mice has 4 unique missense mutations: three in the Ig domain (S128N, V148I and L167H) and one in the cytoplasmic tail (Ct) (E239K) [[15] and Figure 1A]. We reasoned that determining the polymorphic AA(s) that hinder H2-O function should lead to the elucidation of the mechanism behind the protein's loss-of-function. Thus, using a CRISPR/Cas9 approach we generated Mouse Mammary Tumor Virus (MMTV) susceptible C57BL/6J (B6J) mice encoding nucleotide substitutions in the *Ob* gene that resulted in the Oβ proteins with single (S128N, V148I and L167H) or double (S128N/V148I and E239K/S240L; B6J mice have unique substitution S240L not found in mice from other

backgrounds, Figure 1A) AA changes. Two to three independent founders per each line were bred to B6J mice for two generations. Heterozygous mice from each line were intercrossed to establish homozygous KI lines.

We first confirmed that KI mutations did not result in large alterations in H2-O and H2-M protein levels. Western blotting of B cell lysates from all the KI mice showed only small variations in H2-O and H2-M protein levels compared to the levels in B6J B cells. However, these variations did not change ratios of H2-M:H2-O (Figure 1B; bottom panels and Supplemental Figure 1A). Our previous studies showed that the mutations found in I/LnJ *Ob* did not alter H2-M/H2-O interactions [15]. However, it was important to confirm that B6J.*Ob*KI mice produced Oβ that did not impact H2-M/H2-O interactions in isolation from the other I/LnJ genes. Therefore, H2-M and any co-associated H2-O was captured from B6J and B6J.*Ob*KI B cell lysates by immunoprecipitation with a heterodimer-specific anti-H2-M monoclonal Ab followed by western blotting with Abs specific for the Cts of Oβ and Mβ(Figure 1B; left, top panel). In the case of the E239K/S240L double mutant, a polyclonal serum specific for the Oβ luminal domain was used since the KI mutations in the Ct impaired the binding of the Ab specific for the Oβ cytoplasmic tail (Figure 1B; right, top panel). We also performed the converse experiment in which H2-O was immunoprecipitated followed by western blotting for Oβ and Mβ (Figure 1B; middle panels). These experiments revealed similar levels of H2-M co-associated with H2-O as well as similar ratios of H2-M:H2-O in B cells from all B6J.*Ob*KI mice compared to B6J mice (Figure 1B and Supplemental Figure 1B). Thus, these single or double KI AA mutations within Oβ did not alter H2-O or H2-M protein levels or perturb H2-O/H-2M interactions.

Cells that lack H2-O or express I/LnJ H2-O have lower than normal levels of MHCII-CLIP complexes as H2-M function is enhanced in the absence of inhibition by H2-O [15, 18]. Thus, cell surface MHCII-CLIP levels can be used as a read-out to measure the impact of the Oβ AA substitutions on H2-O protein function. Therefore, we used the 15G4 mAb that specifically recognizes I-A^b-CLIP complexes [[17] and Supplemental Figure 2] to measure MHCII-CLIP

levels on splenic B cells from B6J.*Ob* KI mice and B6J control mice (see Supplemental Figure 3 for details). B cells from none of the KI lines exhibited the decrease in MHCII-CLIP levels characteristic of $Ob^{-/-}$ cells (Figure 1C) and cells expressing I/LnJ Oβ [15].

As expected, when challenged with MMTV, none of the B6J.*Ob* KI mice produced virus-neutralizing Ab titers that were comparable to the titers in infected $Ob^{-/-}$ mice (Figure 1D). The V 148I *Ob* allele appears to be a gain of function allele (Figure 1C). However, this was not the mutation driving the virus-neutralizing Ab responses (Figure 1D). Collectively these data show these individual or double mutations in Oβ were insufficient to confer loss of function H2-O.

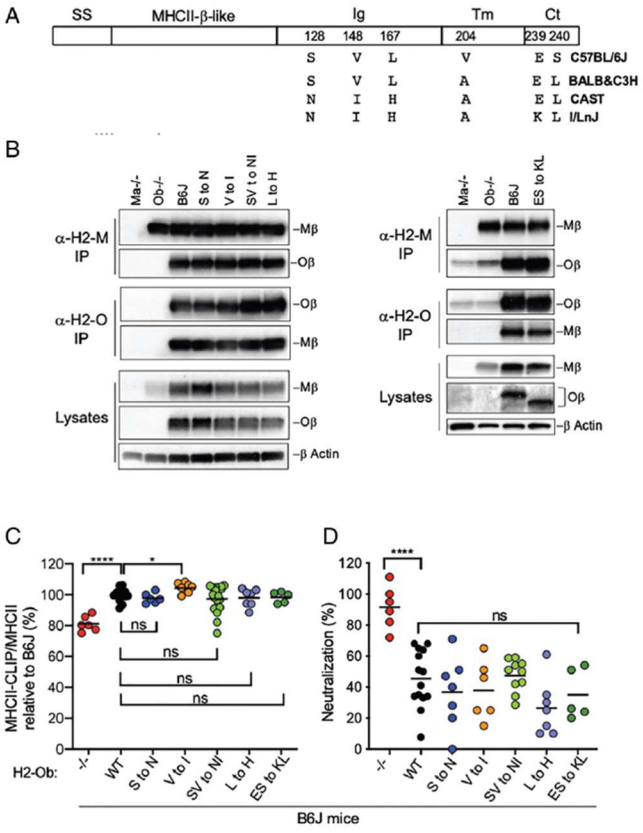

FIGURE 1.1. Ob proteins with single or double mutations in the Ig domain or Ct do not affect H2-O function. (A) The domain structure of Ob. Also shown: Amino acid substitutions (and their positions) found in Ob from various mice compared with Ob of B6 mice. (B) Ob and Mb protein levels and H2-M/H2-O interactions in Ob.KI mice. H2-M or H-2O captured by immunoprecipitation from lysates of purified B6J, B6J.Ob S to N, B6J.Ob V to I, B6J.Ob SV to NI, B6J.Ob L to H, and B6J.Ob ES to KL splenic B cells were analyzed by Western blotting with Abs specific for the Ct of Mb and Ob (left panel) or the Ct of Mb and Ob luminal domain (right panel) and also for b-actin (loading control). Purified B6J.Ma/ and B6J.Ob/ B cells were used as controls. Data are representative of four (left panel) and four (right panel) independent experiments. See Supplemental Fig. 2 for quantification of results across all experiments. (C) Comparison of MHCIICLIP levels on B cells of Ob.KI mice. Quantification of the gMFI of I-AbCLIP on B cells, defined as CD191 from homozygous Ob KI mice relative to that obtained for control WT (WT/WT and WT/KI) B6J B cells. To correct for small differences in total MHCII levels among different samples, the ratio of MHCIICLIP/(total) MHCII was calculated by dividing the gMFI obtained for MHCIICLIP by that obtained for MHCII for each sample. Graphs show quantification of the gMFI of MHCIICLIP/MHCII for mice from the indicated strains relative to that obtained for B6J mice. Dots represent individual mice. The data are combined from multiple independent experiments. Horizontal lines indicate the mean of values obtained for each group of mice. (D) Mice with indicated genotypes were infected with MMTV at 8 wk of age (via i.p. injection), and their sera were screened for capacity to neutralize virus at 3 mo postinfection. Neutralization (percentage) was calculated as described in Ref. 5. Dots represent individual mice. Horizontal lines indicate the mean of values obtained for different mice from the same group. Significance was calculated using an unpaired t test. ****$p < 0.0001$, *$p < 0.05$. Ig, Ig domain; MHCII b-like, MHCII b-like domain; SS, signal sequence; Tm, transmembrane domain.

Identification of three AAs in the Oβ Ig domain as mediating H2-O loss-of-function.

Using a publicly available data base with sequenced genomes of various inbred mouse lines (Sanger Institute Mouse Genomes Project), we found that the *Ob* allele of the wild-derived CAST/EiJ (CAST) mice had the three Ig domain mutations found in I/LnJ mice: S128N, V148I and L167H (Figure 1A). To test whether CAST mice produced virus-neutralizing Abs similar to I/LnJ mice, we injected them with MMTV and screened their sera for the ability to neutralize the virus. Similar to I/LnJ mice, CAST mice produced anti-MMTV Abs (Figure 2A, top) that efficiently neutralized virus (Figure 2A, bottom). These data suggest that the combination of the three mutations found in the CAST *Ob* allele could be sufficient to mediate H2-O loss-of-function. To directly test this possibility, we compared the ability of CAST H2-O to inhibit H2-M function in B cells from (B6J.$Ob^{-/-}$ x CAST)F1 (F1.$Ob^{CAST/-}$) and (B6J x CAST)F1 (F1.$Ob^{CAST/B6}$) (Figure 2B, top) by measuring MHCII-CLIP levels. Importantly, all other genes in F1.$Ob^{CAST/-}$ and F1.$Ob^{CAST/B6}$ mice are heterozygous (one B6 allele and one CAST allele) and thus, could not be considered as contributing to the phenotype. B cells from F1.$Ob^{CAST/-}$ exhibited significantly lower levels of MHCII-CLIP compared to F1.$Ob^{CAST/B6}$ B cells (Figure 2B, bottom). These data indicate that the CAST *Ob* allele is a loss-of-function allele. I/LnJ mice have similar levels of H2-O and H2-M protein and H2-M/H2-O interactions appeared to be similar to those in B6J mice, despite I/LnJ *Ob* being a loss-of-function allele [15]. Therefore, we next asked if CAST H2-O and H2-M protein levels were normal and H2-O/H2-M interactions were similar to those observed in virus-susceptible BALB/cJ mice (Figure 2C). BALB/cJ mice were used for these studies since the Cts of BALB/cJ and CAST mice are identical, allowing for the use of a polyclonal serum specific for the Oβ Ct tail. CAST mice had, on average, 17% less H2-O than BALB/cJ mice. As a result, total ratio of H2-M:H2-O has somewhat increased with less co-associated H2-O when H2-M was captured from B cell lysates (Figure 2C and 2D). It is unlikely, however, that such a small decrease in the H2-O level has influenced MHCII-CLIP levels because H2-$O^{+/+}$ and H2-$O^{+/-}$ mice (which have 2-fold difference in H2-O) maintain similar

levels of MHCII-CLIP [46]. Nevertheless, to demonstrate that CAST mice possess a null allele of *Ob* more conclusively and to make a connection of this allele with the production of virus-neutralizing Abs*,* we undertook a genetic approach. We have demonstrated that two genes in the I/LnJ mice are necessary and sufficient to allow for antibody responses to MMTV following neonatal infection [46]. The first gene, *vic1,* which encodes the loss-of-function *Ob* allele, is sufficient to confer Ab responses to mice infected as adults. An additional locus, which acts as a modifier of *vic1*, termed *vic2*, confers the ability to produce Abs following natural infection of neonates with MMTV via breastmilk. *Vic2* is dominant and modifies the function of recessive *vic1,* meaning that the presence of two alleles of *vic1* and one allele of *vic2* of the I/LnJ origin are necessary and sufficient for Ab responses against MMTV in mice infected as neonates [46]. Therefore, to test whether CAST mice have a loss of function *Ob* similar to I/LnJ mice, we generated (I x CAST)F1 mice along with control (I x B6)F1 and ($B6^{vic1i/i}$ x CAST)F1 mice and fostered them by viremic mothers as neonates. Both B6 and CAST mice have susceptible allele of *vic2* [[46] and data not shown]. Thus, only (I x CAST)F1 mice were expected to produce virus-neutralizing Abs if I/LnJ and CAST mice have identical loss-of-function alleles of *Ob*. As expected, only (IxCAST)F1 mice produced virus-neutralizing Abs (Figure 2E, top and bottom), whereas control F1 hybrids failed to do so. Collectively, these studies strongly suggested that the three polymorphic AAs in the Ig-like domain of CAST and I/LnJ Ob proteins were responsible for the loss of H2-O function.

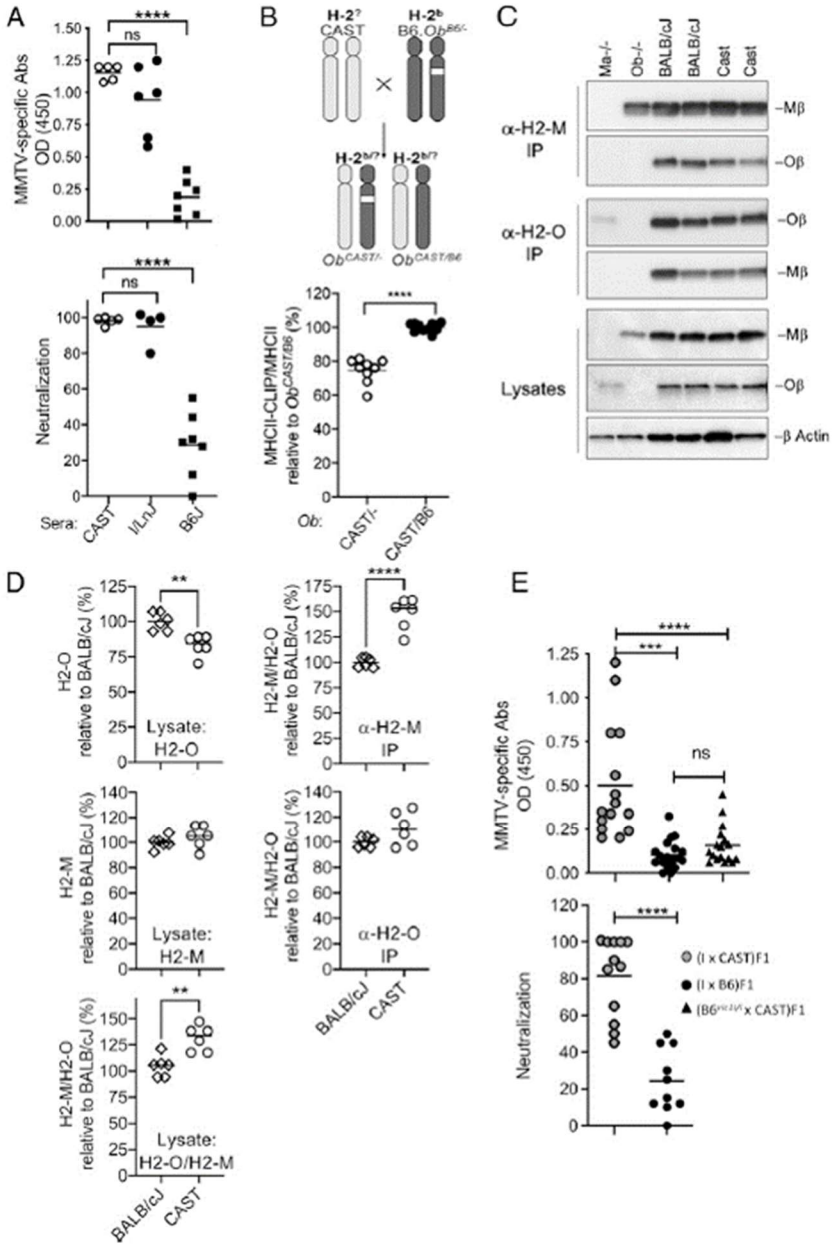

FIGURE 1.2. Identification of the combination of mutations within the Ig domain of Ob that result in the loss-of-function H2-O. (A) Similar to I/LnJ mice, MMTV-infected CAST mice produce virus-neutralizing Abs. CAST mice were infected with MMTV at 8 wk of age (via i.p. injection), and their sera were screened for antivirus IgGs (top panel) and for virus neutralization 3 mo postinfection (bottom panel). OD450 is the absorbance at 450 nm. Each symbol represents an individual mouse. Horizontal lines indicate the mean of values obtained for mice from the same group. (B) Like I/LnJ mice, CAST mice inherit loss-of-function H2-O. (B, top panel) Genetic cross to produce H-2?/b ObCAST/ and H-2?/bObCAST/B6 F1 mice; the CAST MHC haplotype is unknown. (B, bottom panel) Quantification of the gMFI of MHCIICLIP on B cells, identified as CD191 from F1.ObCAST/ mice relative to that obtained for F1.ObCAST/B6 B cells. To correct for small differences in total MHCII levels among different samples, the ratio of MHCIICLIP/(total) MHCII was calculated by dividing the gMFI *(legend continued on next page)*

FIGURE 1.2, continued obtained for MHCIICLIP by that obtained for MHCII for each sample. Graphs show quantification of the gMFI of MHCIICLIP/MHCII for mice from both groups relative to that obtained for F1.ObCAST/B6 mice. Each symbol represents an individual mouse. Data are combined from two independent experiments. Horizontal lines indicate the mean of values obtained for each group of mice. (C) H2-O and H2-M protein levels and H2-M/H2-O interactions in CAST mice. H2-M or H2-O captured by immunoprecipitation from lysates of purified BALB/cJ and CAST splenic B cells were analyzed by Western blotting with Abs specific for the Ct of Mb and Ob. Purified B6J.*Ma*$^{-/-}$ and B6J.*Ob*$^{-/-}$ B cells were used as controls. Total lysates were also probed by Western blotting with Abs specific for Mb, the Ct of Ob, and b-actin (loading control). BALB/cJ and CAST Ob proteins have identical Cts, allowing for the use of Ob Ab reagents specific for the Ct to perform these analyses. Data are representative of three independent experiments comprising two BALB/cJ and two CAST mice each. (D) Quantification of total H2-O (top left) and H2-M (middle left) protein levels, the ratio of H2-M/H2-O (bottom left) in B cell lysates and H2-M/H2-O ratios measured after immunoprecipitation with H2-M (top right), or H2-O (bottom right) across the three independent experiments. Data are normalized to the levels obtained for BALB/cJ mice (see Materials and Methods for details). Each symbol represents an individual mouse, and horizontal bars represent the mean of values obtained for different mice of the same group. (E) Newborn mice from the indicated crosses were fostered by MMTV(LA)infected mothers. Four months postinfection, mice were confirmed to be infected by measuring deletion of SAg-cognate T cells and were screened for anti-virus Abs by ELISA (top panel) and neutralization of MMTV (bottom panel). OD450 is absorbance at 450 nm. Neutralization (percentage) was calculated as described in Ref. 5. Results are expressed as mean of OD (top panel) or as mean of percentage of neutralization (bottom panel) produced by sera from uninfected mice of the same cross. Significance was calculated using unpaired t tests. ****$p < 0.0001$, ***$p < 0.001$, **$p < 0.01$.

Novel modifiers of the MHCII pathway.

Our published data [15] and the data presented here suggest that H2-O requires an unknown factor(s) to inhibit H2-M since I/LnJ and CAST H2-O efficiently bind H2-M but yet fail to inhibit H2-M function. If so, then animals with the WT allele of H2-O but without the functional allele of this provisional factor(s) should exhibit the phenotype of H2-O-deficient mice. The inbred mouse strain B6J was established at The Jackson Laboratory in 1948. In 1951, at the F32 generation of inbreeding, it was passed on to the National Institutes of Health, leading to development of the C57BL/6N (B6N) mouse strain. The C57BL/6NTac (B6NTac) sub-strain was established at F151, following the transfer of the B6N line to Taconic Farms in 1991. Unexpectedly, we found that when compared to B6J, both B6N and B6NTac mice have significantly lower MHCII-CLIP levels on the surface of their B cells and DCs, similar to the levels in B6J.*Ob*$^{-/-}$ cells (Figures 3A and 3B, respectively).

Low MHCII-CLIP (MHCII-CLIP^{Low}) levels in B6J.*Ob*$^{-/-}$ mice correlate with production of virus-neutralizing Abs [[15] and Figures 1C and D]. To determine whether the MHCII-CLIP^{Low} levels in B6N mice also correlated with an efficient anti-viral Ab response, we infected B6N and B6J mice with MMTV and three months later screened their sera for virus-neutralizing Abs. B6N (but not B6J) mice produced high titers of anti-MMTV Abs (Figure 3C) that efficiently neutralized the virus (Figure 3D).

To determine whether the mechanism underlying the MHCII-CLIP^{High} phenotype in B6J mice was dominant, we crossed B6J by B6N mice to produce F1 mice. B cells from these F1 mice had MHCII-CLIP levels similar to that of B6J mice (Figure 3A), indicating that the MHC-CLIP^{High} level is a dominant trait. To determine the number of genes controlling the MHCII-CLIP^{High} phenotype in B6J mice, we backcrossed F1 mice to B6N mice to generate N2 mice and measured MHCII-CLIP levels on their splenic B cells. Whereas 89/121 (74%) of N2 mice had levels of MHCII-CLIP comparable to the levels in B6N mice, 32/121 (26%) had levels similar that of B6J mice (Figure 3A). This distribution of phenotypes indicates that two dominant genes

control the MHCII-CLIP^{High} phenotype in B6J mice as only ~25% of N2 mice are expected to have MHCII-CLIP^{High} level and the rest (~75%) are expected to be MHCII-CLIP^{Low} (Figure 3E). In contrast, B6N mice inherit 2 recessive alleles of these genes which we provisionally called class II presentation modifier A and B (*c2pmA and c2pmB*). Our data suggest that H2-O exerts its negative function on H2-M only in mice inheriting dominant alleles of both *c2pmA* and *c2pmB*.

The genomes of B6J and B6N mice have been sequenced [47]. Between the two genomes, 51 coding variants that include coding SNPs, insertions and deletions were identified [48] but no polymorphisms were found within the coding regions of H2-M, MHCII, H2-O, invariant chain, or cathepsins S and L [47] indicating that *c2pmA and c2pmB* are not these genes. Moreover, overall levels of H2-O, H2-M, and MHCII in B cells and DCs from B6J, B6N, and B6NTac mice were similar as were H2-O/H2-M interactions (Figure 4A, Figure 4B and Supplemental Figure 4). Thus, B6N and B6J mice inherit identical alleles of known genes that mediate the main functions within the MHCII presentation pathway and yet B6N mice exhibit the MHCII-CLIP^{Low} phenotype characteristic of H2-O-deficient B6J mice.

To test whether *c2pmA* and *c2pmB* are expressed in cells of bone marrow (BM) origin we used a BM chimera (BMC) approach. Lineage marker negative (lin^{-}) B6J BM cells were transferred intravenously (i.v.) into lethally irradiated B6N mice (B6J→B6N). The converse chimeras were also established (B6N→B6J) as well as the requisite control chimeras (B6J→B6J and B6N→B6N). The chimeric mice were sacrificed nine weeks post-transplant and MHCII-CLIP levels on splenic B cells were measured by flow cytometry. The results showed that MHCII-CLIP^{High} levels on B6J B cells remained high on the cells that developed in B6N mice and MHCII-CLIP^{Low} remained low on B6N B cells that developed in B6J mice (Figure 4C). Thus, *c2pmA* and *c2pmB* are expressed in cells of the BM origin.

To determine whether *c2pmA* and *c2pmB* function in B cells, an additional set of BMCs were established in which lethally irradiated B6N mice were reconstituted either with a 50:50 mix of lin^- BM cells derived from B6J.μMT (B-less mice) and B6N (the source of B cells) mice or with control B6N BM. At 12 weeks post-transplant, the levels of MHCII-CLIP and MHCII on peripheral blood B cells were measured by flow cytometry (Figure 4D and Supplemental Figure 4). B6N-derived B cells in both groups of BMCs maintained the donor-derived MHCII $CLIP^{Low}$ phenotype. Two possibilities could explain these results. First, *c2pmA* and *c2pmB* could be B-cell intrinsic intracellular factors. Alternatively, *c2pmA* and *c2pmB* could be autocrine factors secreted by B cells and acting upon B cells. However, in either case *c2pmA* and *c2pmB* function in B cells.

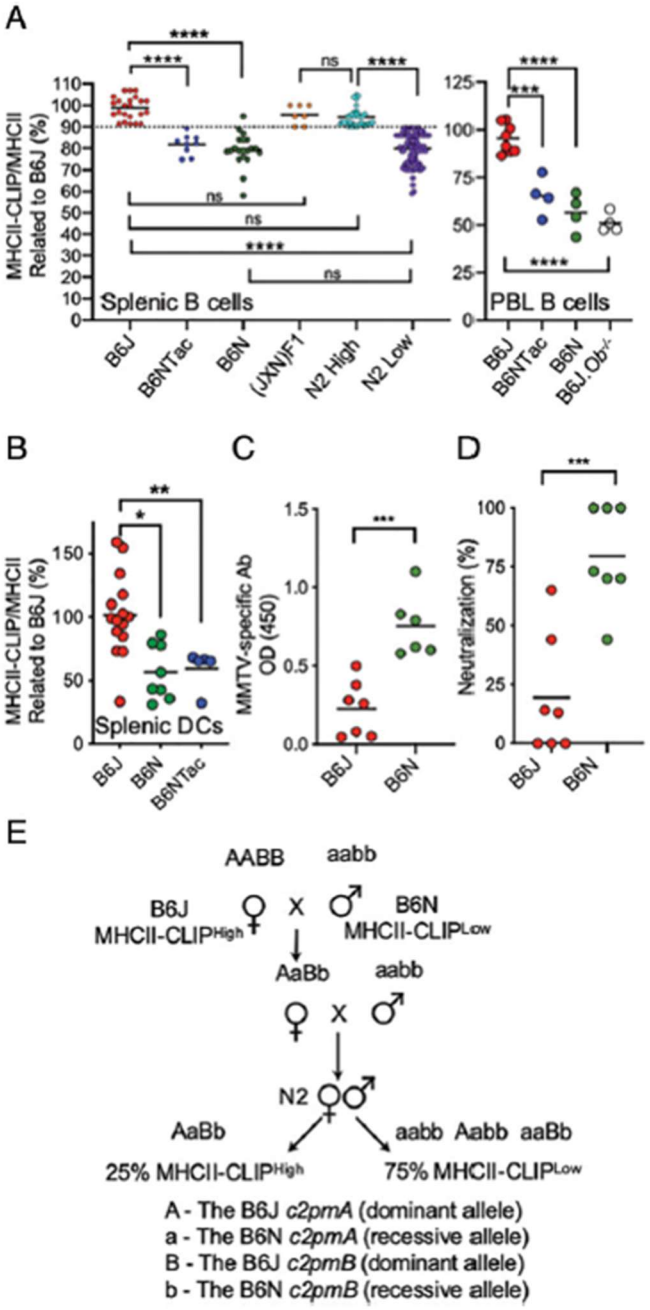

FIGURE 1.3. Low MHCIICLIP levels on B cells and DCs of B6N mice correlates with their ability to produce virus-neutralizing Abs. (A) Comparison of MHCIICLIP levels on splenic B cells of B6N, B6J, F1, and N2 mice (left) and on B cells among PBLs (right). F1 are mice obtained from crossing B6J to B6N mice. N2 are mice obtained from backcrossing F1 mice to B6N mice. N2 mice were analyzed in groups (1020 mice per group) at 8 wk of age along with age-matched B6J mice (35 mice per group), and their splenic B cells, identified as CD191, were stained with 15G4 (MHCIICLIP) or M5/114 (total MHCII). To correct for small differences in total MHCII levels among different samples, the ratio of MHCII-CLIP/(total) MHCII was calculated by dividing the gMFI obtained for MHCIICLIP by that obtained for MHCII for each sample. The averaged MHCIICLIP/MHCII gMFI obtained for B6J mice was *(legend continues on next page)*

FIGURE 1.3, continued defined as 100%. Data for all mice are expressed as percentage of B6J gMFI. The values for B6J mice ranged from 91.4 to 107% (mean ± SD = 98.8 ± 5.3). The values for B6N ranged from 58 to 95% (mean ± SD = 79.3 ± 7.8). The values for (B6J B6N)F1 mice ranged from 90 to 110% (mean ± SD = 95.6 ± 4.5). With an arbitrary cut off at 90% (dotted line), all N2 MHCII- $CLIP^{High}$ were at $90%, and all N2 MHCII- $CLIP^{Low}$ are at #89.5% relative to B6J mice. The range of N2 MHCII- $CLIP^{High}$ was 90105% (mean ± SD = 94.6 ± 4.4), whereas the range of N2 MHCII- $CLIP^{Low}$ was 5989.5% (mean ± SD = 79.9 ± 7.2). Dots represent individual mice. Horizontal lines indicate the mean of values obtained for different mice from the same group. (B) Quantification of the gMFI of Ab-CLIP on the cell surface of splenic DCs from mice of indicated strains and crosses. To correct for small differences in total MHCII levels among different samples, the ratio of MHCII- CLIP/(total) MHCII was calculated by dividing the gMFI obtained for MHCIICLIP by that obtained for MHCII for each sample. Graphs show quantification of the gMFI of MHCIICLIP/MHCII for mice from indicated strains/crosses relative to that obtained for B6J mice. B cells were defined as CD191 and DCs as CD3 CD19 CD11c1. Dots represent individual mice. Horizontal lines indicate the mean of values obtained for each group of mice. (C) Unlike B6J mice, MMTV-infected B6N mice produce potent virus-neutralizing Abs. B6N and B6J mice were infected with MMTV at 8 wk of age and screened for anti-virus IgGs 3 mo later. OD450 is the absorbance at 450 nm. Dots represent individual mice. Horizontal lines indicate the mean of values obtained for different mice from the same group (D) Sera from mice (shown in C) were tested for virus neutralization. Dots represent individual mice. Horizontal lines indicate the mean of values obtained for different mice form the same group. (E) Genetic cross used to produce N2 mice for c2pmA and c2pmB mapping. *p < 0.05, **p < 0.01, ***p < 0.001, ****p < 0.0001. ns, not significant.

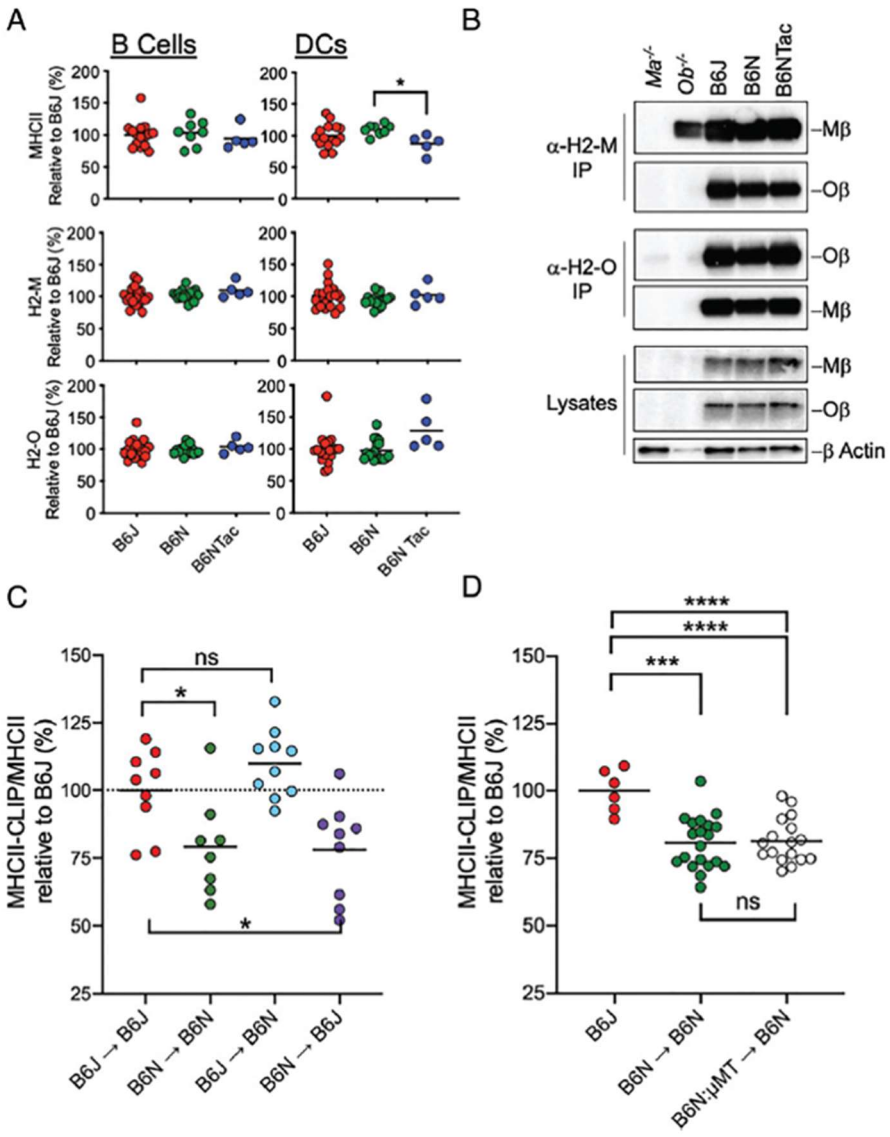

FIGURE 1.4. c2pmA and c2pmB are expressed in the BM compartment and function in B cells. (A) MHCII, H2-M, and H2-O levels are similar in B6J, B6N, and B6Tac B cells and DCs. Splenic B cells were surface stained with fluorochrome-labeled mAbs to identify B cells (CD3 CD11c CD191) or DCs (CD3 CD19 CD11c1) and for MHCII followed by fixation and permeabilization and intracellular staining with fluorochrome-labeled mAbs specific for H2-O (mAb Mags.Ob3) and H2-M (mAb 2C3A) (Supplemental Fig. 3). Graphs show quantification of the gMFI of MHCII, H2-O, or H2-M in indicated strains of mice relative to that obtained for B6J. Horizontal lines indicate the mean of values obtained for different mice from the same group. Dots represent individual mice. Data were combined from two (MHCII) or three (H2-O and H2-M) similar experiments. (B) c2pmA and c2pmB do not alter levels of H2-M, H2-O, or MHCII. H2-M or H2-O captured by immunoprecipitation from lysates of purified B6J, B6N, and B6NTac, B6J.Ob/, or B6JMa/ splenic B cells were analyzed by blotting with Abs specific for the Cts of Mb or Ob or b-actin. Blotting of lysates used for the immunoprecipitations are included as controls. Data are representative of two similar experiments. See Supplemental Fig. 3C for quantification of cumulative data. (C) c2pmA and c2pmB are expressed in cells of the BM origin. Six-week-old B6J or B6N recipient mice were lethally irradiated and *(legend continues on next page)*

FIGURE 1.4, continued reconstituted with lin donor B6J or B6N BM. Nine weeks posttransplantation, the levels of MHCII and MHCIICLIP were measured on the surface of CD191 splenic B cells from the chimeric mice. To correct for small differences in total MHCII levels among different samples, the ratio of MHCIICLIP/(total) MHCII was calculated by dividing the gMFI obtained for MHCIICLIP by that obtained for MHCII for each sample. Graphs show quantification of the gMFI of MHCIICLIP/MHCII for mice from different groups relative to that obtained for B6J mice. Dots represent individual mice. Horizontal lines indicate the mean of values obtained for different mice from the same group. Data were pooled from two independent experiments. (D) c2pmA and c2pmB function in B cells. Six-week-old B6N recipient mice were lethally irradiated and reconstituted with lin donor B6N (control) BM or a 50:50 mix of lin BM from B6J.mMT (B-less mice) and B6N BM. Twelve weeks posttransplantation, the levels of MHCII and MHCIICLIP were measured on the surface of CD191 peripheral blood B cells or splenic B cells (Supplemental Fig. 4) from the chimeric mice. To normalize each sample's MHCIICLIP level to this sample's level of MHCII, the gMFI obtained for 15G4 (MHCIICLIP) was divided by the gMFI obtained for M5/114 (MHCII). Graphs show quantification of the gMFI of MHCIICLIP/MHCII for mice from different groups relative to that obtained for B6J mice. Data were pooled from two independent transplantation experiments. Dots represent individual mice. Horizontal lines indicate the mean of values obtained for different mice of the same group. Significance was calculated using an unpaired t test. *$p < 0.05$, ***$p < 0.001$, ****$p < 0.0001$

Discussion

Since its discovery over two decades ago, considerable work has been done to describe the function and structure of H2-O/DO. Multiple groups have reported H2-O as an inhibitor H2-M and therefore a negative regulator of peptide loading on MHCII-CLIP using *in vitro* cell line and biochemistry-based approaches [8, 11, 13]. It has also been demonstrated *in vivo* in mice that successful inhibition of H2-M by H2-O results in a higher proportion of CLIP-bound MHCII complexes on APCs [15]. The inhibitory nature and similarity of H2-O to MHCII in structure suggests H2-O acts as a competitive inhibitor of MHCII:H2-M binding [40]. However, previous work from our laboratories demonstrated that H2-O found in mice of the I/LnJ strain was non-functional yet maintained interaction with H2-M [15]. This indicates that, contrary to the current paradigm, H2-O/H2-M binding alone is not sufficient to block H2-M function *in vivo*.

H2-O is a constitutive heterodimer, composed of Oα and Oβ chain. Compared to the *Ob* allele of retrovirus-susceptible mice, the *Ob* allele of retrovirus-resistant I/LnJ mice encodes for three distinct AA mutations in Ig domain and a single AA mutation in the Ct domain (Figure 1A). We present data demonstrating that *Ob* alleles that encode for single or double AA mutations found in the Ig domain or Ct domain of I/LnJ Oβ do not alter the function of H2-O (Figure 1B and 1C). In contrast, the CAST *Ob* allele that encodes for three Ig AA mutations found in I/LnJ Oβ results in H2-O with loss-of-function (Figure 2A and 2B). Although CAST mice have slightly lower H2-O levels, CAST H2-O retains the ability to interact with H2-M. The fact that this loss-of-function H2-O is still capable of binding to H2-M (Figure 2C) is not surprising as the DM/DO crystal structures shows that DM/DO interactions are mainly driven by contacts between DOα and DM and that the 3 Ig domain mutations likely point away from the DM/DO interface [40]. Based on these data we propose that H2-O requires yet to be identified factors to inhibit H2-M and that these factors may interact with the Ig domain of Oβ.

Serendipitously, we also discovered that two closely related strains of B6 mice, B6J and B6N, exhibit different MHCII-CLIP levels in B and DC cells: high in B6J and low in B6N mice (Figures

3A and 3B). The low MHCII-CLIP levels, indicative of uninhibited H2-M in B6N cells, correlated with the production of a potent neutralizing Ab response against a retrovirus (Figure 3C and 3D) as seen in B6J.*Ob*$^{-/-}$ mice [Figure 1D and [15]]. Genetic crosses between the B6J and B6N mice identified two dominant loci (which we provisionally call *c2pmA* and *c2pmB*) that are inherited by B6J mice and control the MHCII-CLIP^{High} phenotype (Figure 3A and 3E*).* BMC experiments showed that *c2pmA* and *c2pmB* are expressed in the BM cells and function in B cells (Figures 4C and 4D). Whether these genes function in other cells expressing H2-O remains to be investigated.

c2pmA and *c2pmB* do not encode for H2-M, MHCII, H2-O, invariant chain, or cathepsins L and S as there are no polymorphisms identified between the B6N and B6J alleles of these genes. In addition, as the levels of MHCII, H2-M and H2-O proteins are similar in B6J and B6N B cells as are H2-M/H2-O interactions (Figures 4A, 4B and Supplemental Figure 4), it is unlikely that *c2pmA* and *c2pmB* affect the expression of these MHCII pathway proteins. *c2pm*A and *c2pmB* might potentially encode for genes participating in processes such as trafficking, uptake, and antigen processing or represent negative regulators, enhancers, microRNAs and other control elements. But until these genes are identified it is too premature to discuss their functions.

To our knowledge, this is the first report showing that there are additional factors other than H2-M and H2-O that control peptide loading of MHCII molecules. These data highlight that modulation of antigen presentation by H2-M and H2-O is more complex than previously appreciated. Our data indicate that binding of H2-M by H2-O is not sufficient for H2-M inhibition as previously suggested [15] and that regions of H2-O distinct from the site of H2-M/H2-O interaction are likely critical for H2-O function. The mechanism underlying H2-O function is still unclear, but H2-O may exert its function by binding to and altering the conformation of H2-M in a manner dependent on the AA composition of the Ig domain of Oβ. The unknown factors encoded by the *c2pmA* and *c2pmB* loci can alter MHCII presentation directly by altering the

activity of H2-M, indirectly by modifying the activity of H2-O via targeting the Ig domain, or by altering another yet to be defined pathway. The precise nature of these interactions will be revealed via the positional cloning of genes encoded by *c2pmA* and *c2pmB*.

Unpublished Data

Follow up studies are currently in progress, and those that are not yet published are described here.

To determine if the NIH combination of mutations found in CAST mice were sufficient to regulate MHCII antigen presentation, B6J mice harboring the all three mutations, S128N, V148I, and L168H, were generated. The function of H2-O in these mice was determined by measuring MHCII:CLIP levels and the production of MMTV-neutralizing antibodies upon infection as adults. Mice homozygous for the NIH mutant allele of *H2-Ob* were found to exhibit decreased H2-O function, as measured by increased antibody titers upon MMTV infection (**Figure 1.5A**) and decreased MHCII-CLIP levels on splenic B cells (**Figure 1.5B**). These results indicate that this combination of mutations contribute to loss-of-function of H2-O in I/LnJ mice. The generation of these mice is a critical tool in the effort to understand how I/LnJ *H2-Ob* is a loss-of-function mutant. As H2-O binding to H2-M is not sufficient for inhibition of H2-M, this would suggest that other factors are required for H2-O to exert its full effect. In future studies to fully understand this pathway, Ob.NIH mice will be invaluable for testing how these mutations affect interactions with other factors while holding all other genes constant. While these studies are undertaken, another approach to identify genes that could affect MHCII presentation other than H2-O and H2-M was used. This approach is described in detail in [36], but significant work has been done to attempt to identify *c2mpA* and *c2pmB,* which is described here.

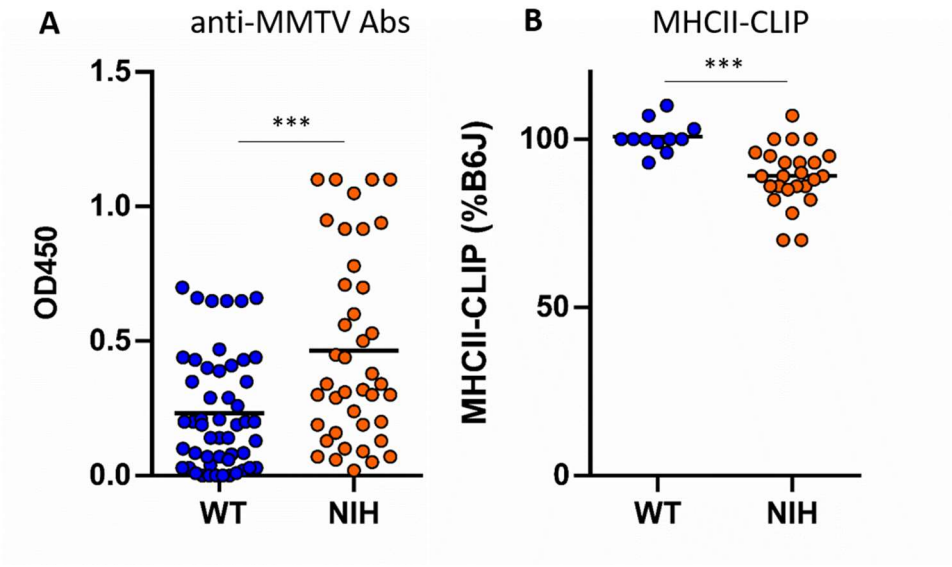

FIGURE 1.5. *H2-Ob*.NIH mice exhibit H2-O with decreased function. B6J mice harboring the NIH mutations in the Ig domain were generated using CRISR-Cas9. The functional capacity of this mutant allele of *H2-Ob* was measured using (A) ability to produce antibodies upon MMTV infection and (B) levels of MHCII-CLIP on splenic B cells. Significance determined using unpaired t-tests. ***=p<0.001

In order to determine the locations of *c2pmA* and *c2mpB*, a genome-wide scan of the N2 mice described produced in [36] was performed (**Figure 1.6**). This scan provides genotype data for experimental mice at approximately ten thousand positions throughout the genome [49]. However, as B6J and B6N mice are closely related strains, about 2% of these positions are polymorphic between the two strains and therefore are useful in differentiating the genomic composition of N2 mice. Select N2 mice were used for this screen—those which were unambiguously $CLIP^{High}$ or $CLIP^{Low}$. Quantitatively, these were animals with either a MHCII-CLIP levels of higher than 92% of the B6J control group mean (for $CLIP^{High}$) or lower than 88% of the B6J control group mean (for $CLIP^{Low}$). Based on the crosses performed to obtain N2 animals, all loci will either be homozygous B6N/B6N or heterozygous B6N/B6J.

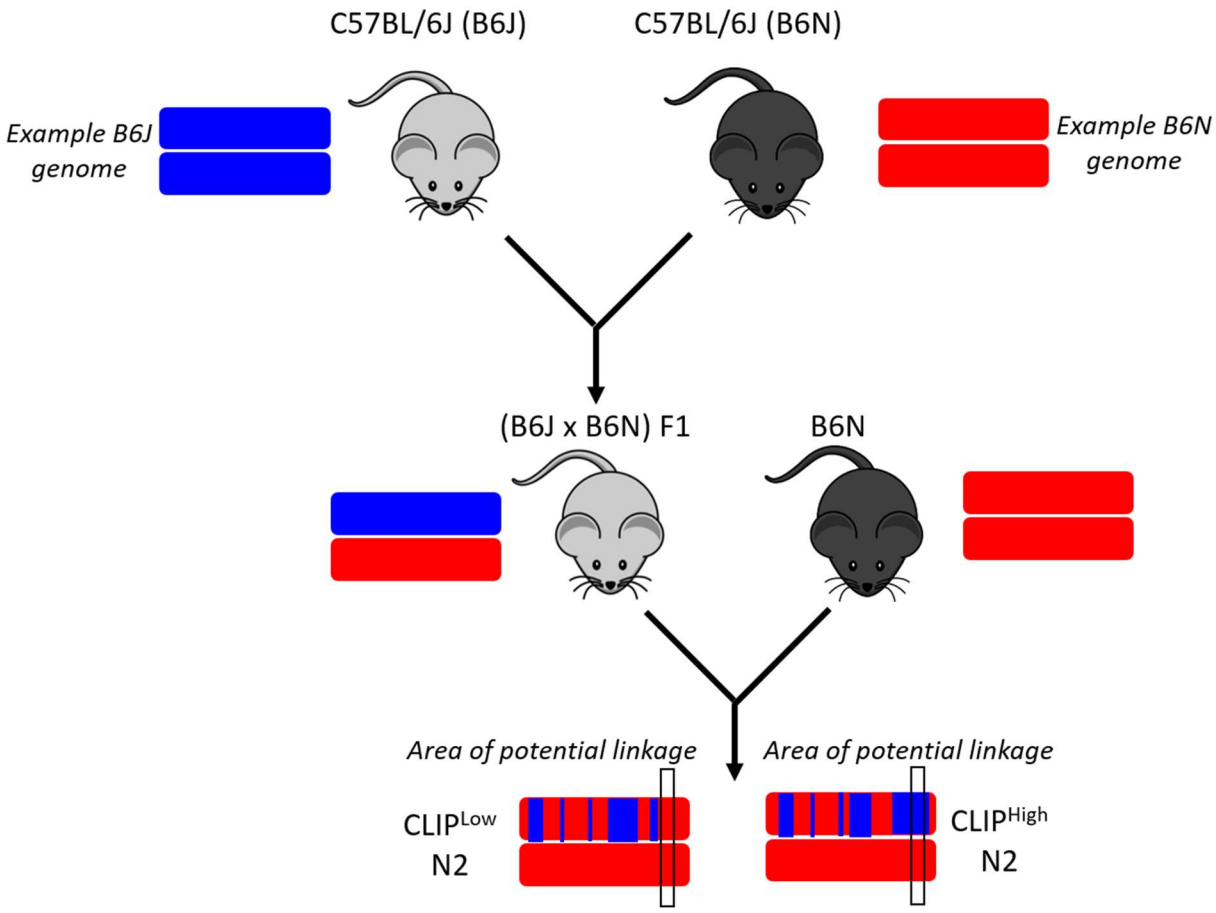

FIGURE 1.6. Generation of N2 mice for genome wide scan. N2 mice were generated by crossing (B6J x B6N)F1 mice to B6N mice. N2 mice have a distribution of phenotypes, due to independent assortment and recombination of parental chromosomes during meiosis (shown as mixed blue and red genetic material). Areas which are of homozygous B6N origin in most $CLIP^{Low}$ mice and are heterozygous in most $CLIP^{High}$ mice are areas of potential linkage. An example of such a region is shown outlined in the black box, which is homozygous B6N/B6N (red/red) in $CLIP^{Low}$ N2 mice and heterozygous B6N/B6J (red/blue) in $CLIP^{High}$ mice. Approximately 50 mice of each phenotype were used for genomic analysis.

Loci which are predominantly heterozygous in mice exhibiting the CLIP^{High} phenotype while also being predominantly homozygous in mice exhibiting the CLIP^{Low} phenotype are candidate loci for encoding *c2pmA* and *c2pmB*. A combination of SNPs included in the Transnetyx miniMUGA panel and those designed by us to increase coverage were used to scan the genome at approximately 10 Mb intervals. The proportion of animals in each phenotype group heterozygous at each SNP was calculated (**Figure 1.7**). Based on the distribution of phenotypes of the F1 and N2 crosses in [36], we predict two loci will show linkage to the High/Low CLIP phenotype. However, our data indicate clear linkage only on chromosome 1, between 39 and 64 megabases (Mb). Several additional chromosomes show weak linkage, such as 11, 14, 15, and 17. The technique of screening genomes for areas of potential linkage is limited by several factors, including the penetrance of the phenotype under study, the density of markers used to genotype experimental mice, and the number of experimental mice used. Any combination of these factors could explain a lack of strong linkage to *c2pmB* in our experiments. To better narrow down candidate chromosomes for *c2pmB*, analysis of select N2 genomes was done only on those which showed heterozygosity at the potential *c2pmA* locus (Chr1 between 39 and 64 Mb). This approach was taken because we predict that the vast majority of CLIP^{High} mice will also be heterozygous at *c2pmB* if they are heterozygous at *c2pmA* and the vast majority of CLIP^{Low} mice will he homozygous at *c2pmB* if they are heterozygous at *c2pmA.* A caveat of this approach is of course the assumption that *c2pmA* is encoded on Chr1 in the critical region identified by the linkage analysis. When this approach was taken, chromosome 15 was identified as a candidate chromosome harboring *c2pmB,* with a location likely between 24 and 70 Mb (**Figure 1.8**). Unfortunately, high-throughput identification of candidate genes in this region containing coding region polymorphisms is limited by poor quality of the available C57BL/6N sequenced genome in this region. Potential coding region polymorphisms will need to be sequenced individually to confirm whether they indeed are polymorphic, and this is currently underway. In addition, no genes on chromosome 15 which are

differentially expressed in B6N and B6J mice fall within the potential Chr15 critical region, limiting identification of *c2pmB* candidates via this method. Due to the relatively weak linkage observed in the present group of N2 animals, additional animals are being bred to validate this candidate chromosome further prior to in depth investigation.

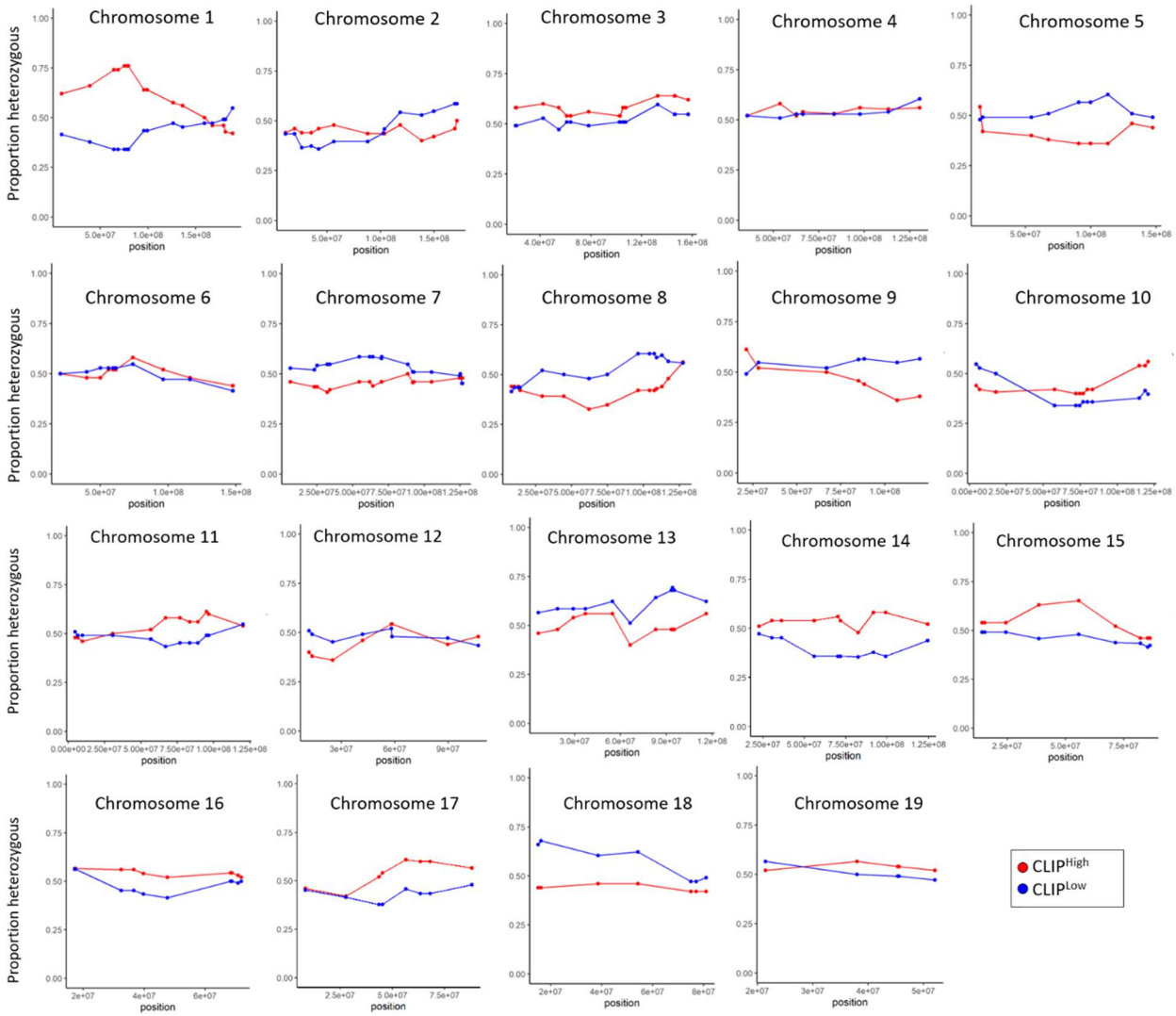

FIGURE 1.7. Chromosome 1 shows clear genetic linkage to CLIP phenotype in N2 mice. DNA from N2 animals phenotyped as CLIP^{High} or CLIP^{Low} was subjected to a genome-wide scan to determine the genotype (heterozygous B6J/B6N or homozygous B6N/B6N) at several hundred regions throughout the genome. Chromosomes with areas of genetic linkage were identified by plotting the proportion of CLIP^{High} (red) and CLIP^{Low} (blue) N2 mice heterozygous at each marker. Based on the predicted inheritance of the *c2pmA* and *c2pmB* loci (Figure 1.3E), 100% of CLIP^{High} mice are predicted to be heterozygous at either locus (genotype *AaBb*) and 33% of CLIP^{Low} mice are predicted to be heterozygous at either locus (genotypes *aaBb, aabb,* or *Aabb*). Loci which have no linkage to the CLIP phenotype *(legend continued on next page)*

FIGURE 1.7, continued are expected to be 50% heterozygous, as randomly selecting a mouse with genotype *Aa* or *aa* is equally likely. Chromosomes were considered as an area of possible linkage if there were locations in which CLIP^{High} mice were >65% heterozygous and CLIP^{Low} mice were <40% heterozygous. Data are combined from two independent experiments. CLIP^{High} n=50 and CLIP^{Low} n=53.

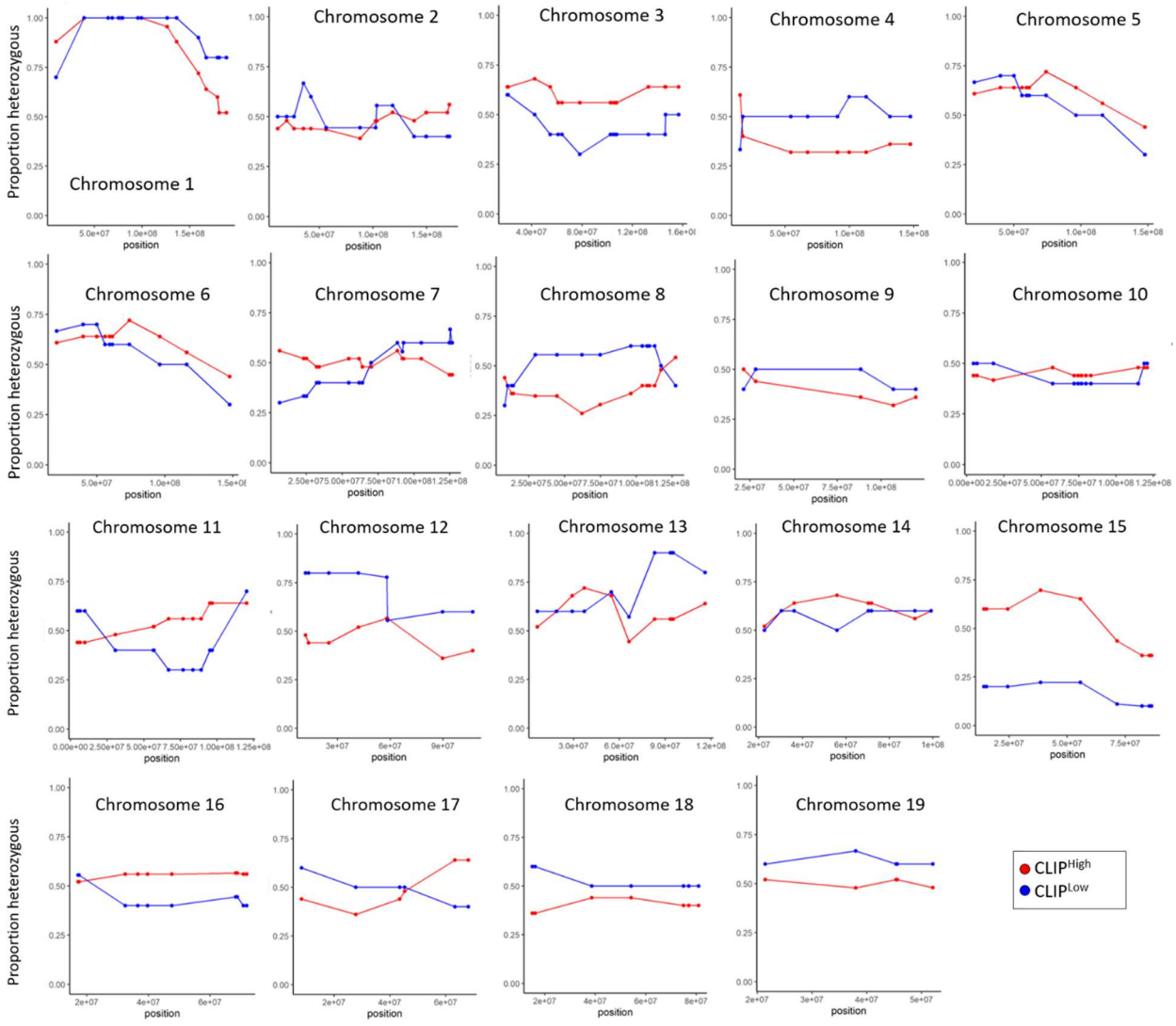

FIGURE 1.8. Linkage analysis under specific conditions assuming c2pmA is located on chromosome 1 identifies chromosome 15 as a candidate encoding c2pmB. Linkage analysis was repeated using a select group of animals which were heterozygous at the critical region identified on chromosome 1 (evident by 100% heterozygosity in both CLIP^{High} and CLIP^{Low} mice on chromosome 1 in this figure). We predict that all CLIP^{High} mice will be heterozygous at *c2mpB* if they are heterozygous at *c2pmA* and no CLIP^{Low} mice will be heterozygous at *c2mpB* if they are heterozygous at *c2pmA.* The chromosome most closely matching this prediction is chromosome 15, which also showed weak linkage under normal analysis conditions (Fig 1.8).

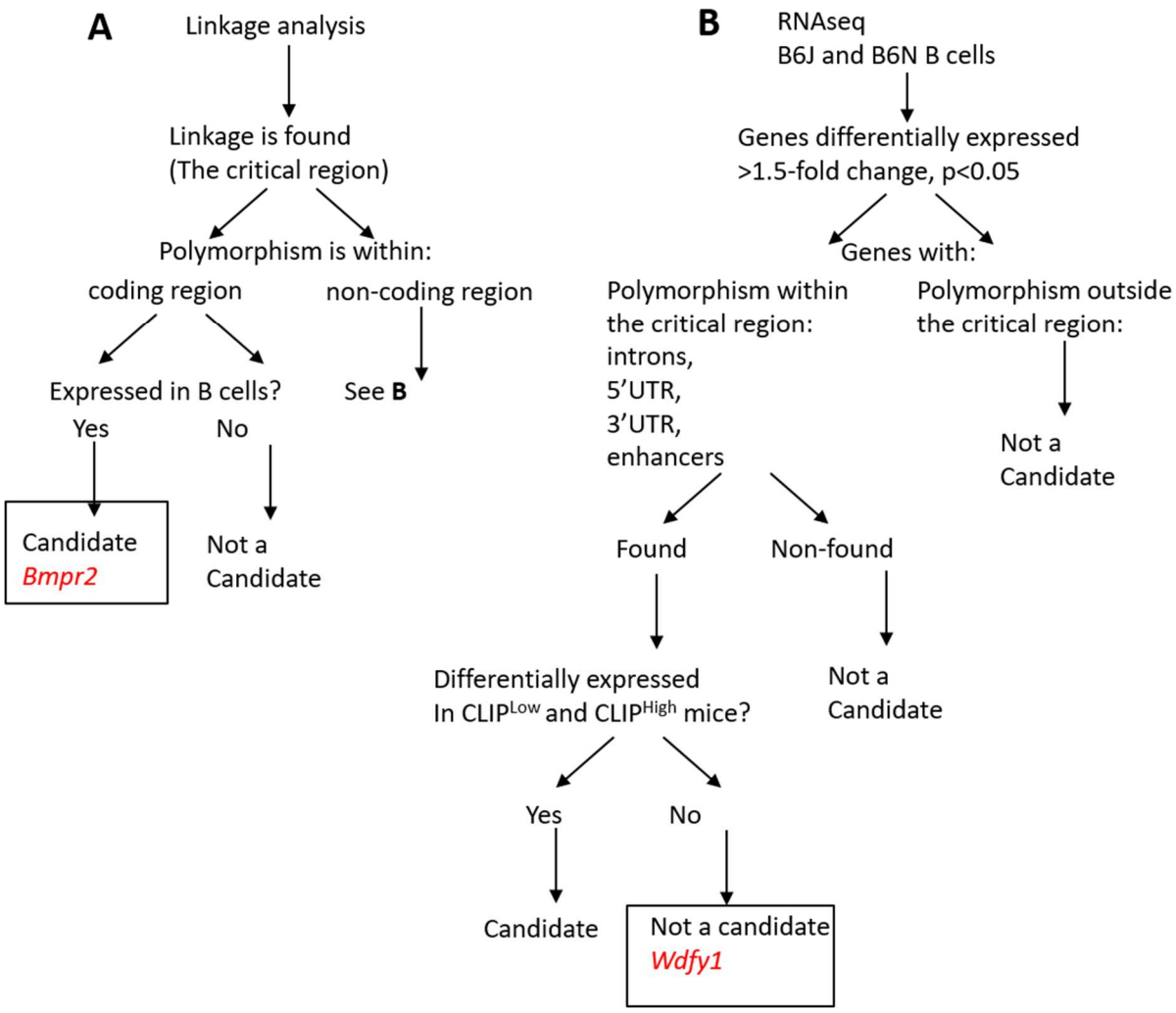

FIGURE 1.9. Schematic of approach to identify candidate genes on chromosome 1. Description of criteria applied to identify candidate genes on chromosome 1. A. Only one gene, *Bmpr2*, is reported to have a missense mutation in B6N mice. B. RNAseq was performed to identify differentially regulated genes in B cells of B6J and B6N mice. Only one differentially regulated gene, *Wdyf1,* was reported to have a polymorphism and was located near the critical region. *Wdfy1* expression was not found to correlate with CLIP levels upon further analysis.

A two-pronged approach was used to identify potential genes in these regions driving differences in MHCII-CLIP levels (**Figure 1.9**). Genetic differences between the two strains could affect a protein directly (i.e. polymorphism affecting the protein sequence) or affect a protein indirectly (i.e. alter transcript expression and thereby alter protein levels). To address the first possibility, the Sanger Mouse Genome Project database was used to search for polymorphisms in protein coding regions of the loci identified by the genome wide scan. On Chr1, this approach yielded only a single candidate, *Bmpr2*. As mentioned above, the publicly available genomic sequence of the C57BL/6N mouse is of poor quality in regions of Chr15, and reported polymorphisms compared to the C57BL/6J genome are of low confidence. Therefore, we are currently in the process of validating reported low confidence coding region polymorphisms in order to generate a list of candidate *c2pmB* genes on this chromosome.

To address the second possibility, RNA sequencing of transcripts isolated from bulk splenic B cells from B6J and B6N mice was performed, followed by differential expression analysis (published experiments [36] indicated that at least one of *c2pmA* and *c2pmB* are expressed in B cells). Differentially expressed transcripts identified by RNA-seq were investigated to determine their chromosomal location and if any polymorphisms in or nearby the gene existed. Genes were considered to be differentially expressed if the fold-change in expression between B6N and B6J was at least 1.5-fold with a multiple comparison-adjusted p value of less than 0.05. The complete RNAseq results table is provided as **Table S1** and the list of differentially expressed transcripts is provided as **Table S2** (supplemental materials) available online. Those with such polymorphisms that were located in the identified critical regions from the genome wide scan were considered candidates. Using this approach, only a single gene was identified as a possible candidate, *Wdfy1.* In order to determine if this gene may be connected with the $CLIP^{High}$ vs $CLIP^{Low}$ phenotype, RNA was isolated from the spleens of a select group of N2 mice phenotyped as $CLIP^{High}$ or $CLIP^{Low}$. qPCR measurement of *Wdfy1*

expression levels was performed to determine if any correlation existed (**Figure 1.10**). While we were able to detect a difference in expression level in B6N and B6J B cells (left) and bulk spleens (middle) as we would expect, we did not detect any difference in expression levels of the phenotyped N2 mice (right). Theoretically, if *Wdfy1* controlled CLIP levels, there would be a difference in expression levels in N2 mice dependent on their CLIP phenotype. Therefore, we were able to rule out *Wdfy1* as a candidate for *c2pmA/B.* This combination of approaches yielded a single candidate gene on chromosome 1, *Bmpr2*.

BMPR2 is a member of the bone morphogenic protein (BMP) receptor family of serine/threonine receptor kinases, of which BMPR2 is classified a type II receptor. Two type II receptor molecules, in conjunction with a two BMP type I receptor molecules, form a functional tetrameric signaling complex. The ligands for this receptor are TFGβ superfamily ligands. Functional signaling through this pathway is essential, as loss of BMPR2 in mice is embryonically lethal at day 9.5 [50]. B6N mice encode an R321Q mutation in *Bmpr2*, which is found in the intracellular kinase domain of the protein [51]. The presence of the missense mutation was identified by the Sanger Mouse Genomes Project database, and was validated via Sanger sequencing of exon 7 from B6J and B6N mice.

While unlikely due to the embryonic lethal phenotype of BMPR2 KO mice, the possibility that R321Q drastically altered protein levels in B6N mice was tested using Western blotting. Using this method, similar levels of BMPR2 in both B6J and B6N mouse B cells was detected (**Figure 1.11**). BMPR2 protein detected in purified B cells was not due to contamination by T cells as similar levels of protein was also detected in genetically T cell deficient B6J mice. These results are in agreement with the fact that no differences in RNA expression levels of *Bmpr2* was observed in either RNAseq or qPCR between B6J and B6N mice (**Figure 1.12**).

To demonstrate more definitively any role for the R321Q mutation in MHCII Ag presentation, B6J mice harboring the B6N allele of *Bmpr2* were generated. To accomplish this, a CRISPR-Cas9 approach was used. Guide RNA recognizing the region of *Bmpr2* containing

the R321Q missense mutation was injected into B6J embryos alongside Cas9 nuclease and a homology-directed repair template.

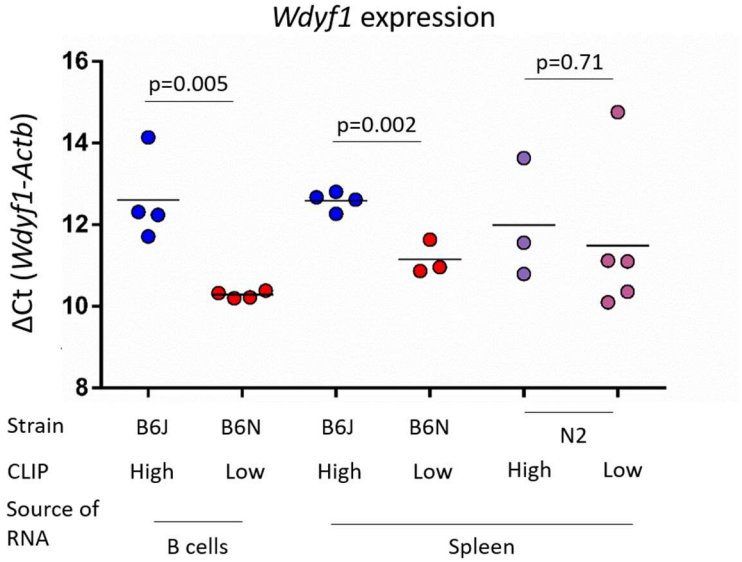

FIGURE 1.10. Wdyf1 is not differentially expressed in CLIP^{High} and CLIP^{Low} spleens. RNA was isolated from purified B cells of B6N and B6J mice (left), total spleen of B6N and B6J mice (middle), or total spleen of N2 mice phenotyped as CLIP^{High} or CLIP^{Low}. As expected based on detection of *Wdfy1* as a differentially regulated transcript in RNAseq, *Wdyf1* transcript levels were significantly lower in both B cells and bulk spleen of B6N mice controlled to B6J mice. However, transcript levels in the spleens of N2 mice phenotyped as CLIP^{High} or CLIP^{Low} and were found to be similar between the two groups. p values calculated using unpaired t-tests.

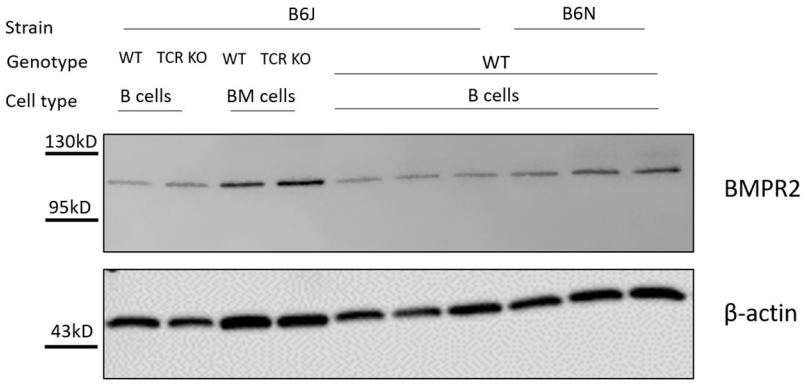

FIGURE 1.11. BMPR2 protein is detectable is B6J and B6N B cells. BMPR2 protein levels were measured via western blotting using monoclonal antibodies recognizing BMPR2 or β-actin (loading control) in B cells purified from spleens of B6J, B6N, or B6J.TCRb$^{-/-}$d$^{-/-}$ mice or bulk bone marrow cells isolated from B6J or B6J.TCRb$^{-/-}$d$^{-/-}$ mice.

Shortly prior to weaning, mice were analyzed for presence of the knock-in allele and for frame-shifting indels (the result of genome repair where the provided template was not used for repair). An outline of this design is shown in **Figure 1.13A**. The presence of frame-shifting indels was determined using gel electrophoresis and Sanger sequencing while the presence of the knock-in allele was determined using restriction digestion recognizing KI mutations and confirmed with Sanger sequencing (Schematic in **Figure 1.13B**, results in **Figure 1.13C-D**). Using these approaches, 2 mice with possible knock-out alleles were generated and 4 mice with knock-in alleles were generated. Currently, all four founder animals have been bred to wild type B6J mice and have confirmed transmission of the knock-in allele to their progeny.

Future experiments will include generation of homozygous knock-in animals (and heterozygous and homozygous wild-type controls) via intercrossing and subsequently measuring MHCII-CLIP levels on splenic B cells and antibody responses upon infection of mice with MMTV. These experiments will test whether the B6N allele of *Bmpr2* is sufficient to alter antigen presentation on MHCII. We would predict based on the observed inheritance pattern of *c2pmA* and *c2mpB* that homozygous *Bmpr2*.KI/KI mice will exhibit the $CLIP^{Low}$ phenotype. Additionally, much work remains to be done to identify candidate genes for *c2mpB.* To that end, we are currently generating a high-coverage whole genome sequence of the B6N strain to better understand the extent of polymorphism in the candidate region on chromosome 15.

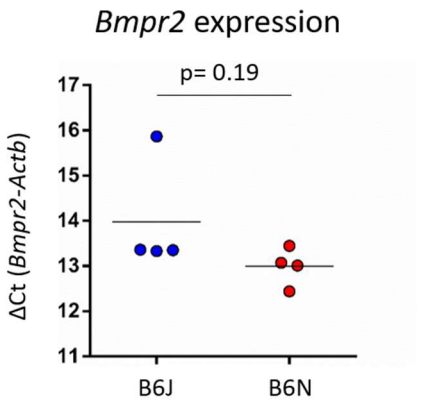

FIGURE 1.12. Bmpr2 is not differentially expressed in B6J and B6N B cells. *Bmpr2* transcript levels were measured via qPCR in RNA isolated from purified splenic B cells and were found to be similar between B6N and B6J mice. p value calculated using an unpaired t-test.

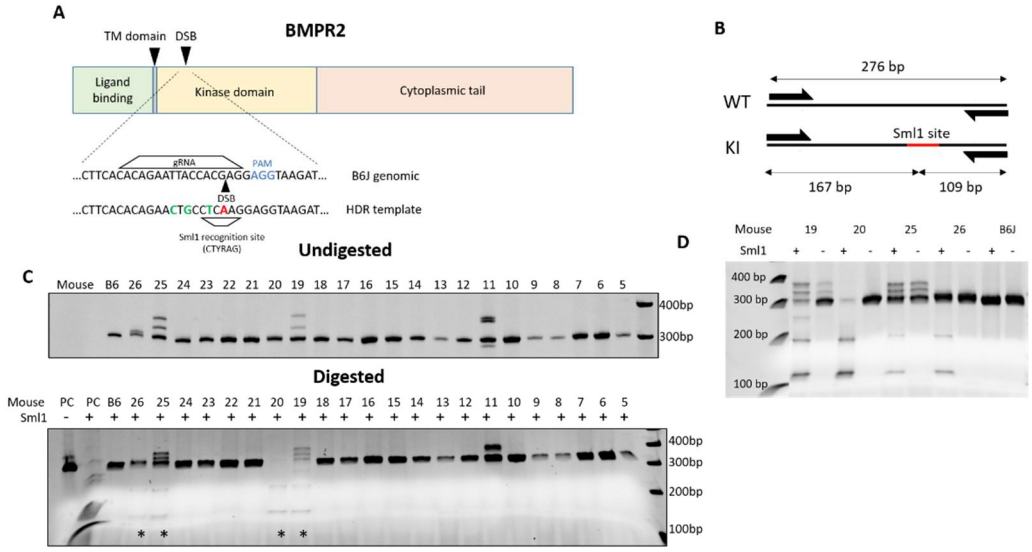

FIGURE 1.13. Genome editing approach to determine the role of BMPR2 in MHC-II:CLIP levels A. Schematic of the structure of BMPR2 depicting the ligand binding domain, transmembrane (TM) domain, kinase domain, and cytoplasmic tail regions as well as the site of Cas9-induced double stranded break (DSB). The partial sequence of the B6J *Bmpr2* genomic sequence as well as the homology directed repair (HDR) template oligonucleotide are indicated, with silent mutations highlighted in green and the single missense mutation highlighted in red. The amino acids affected by the silent mutations and missense mutation are also highlighted in green and red, respectively. The locations of the guide RNA (gRNA), protospacer adjacent motif (PAM) and Sml1 recognition site (CTYRAG) are also indicated. **B**. Schematic of genotyping approach used for founder mice resulting from embryo injection of Cas9, guide RNA, and HDR template oligonucleotide. **C.** Results of PCR amplification (top) and restriction enzyme digestion (bottom) outlined in B. **D.** Confirmation of presence of KI allele in founder animals 19, 20, 25, and 26.

Chapter 2: Investigation of the role of classical MHC in H2-O-mediated resistance to retroviruses.

Preface

The work in this chapter is unpublished. All of the work in this chapter was performed by the author or Tatyana Golovkina.

Summary

Previously, the laboratory found BALB/cJ mice congenic for the *vic1* locus (containing all MHC genes) from the I/LnJ strain were resistant to both MMTV and murine leukemia virus (MuLV), an unrelated retrovirus. In these studies, we use BALB/cJ.*H2-Ob*$^{-/-}$ mice, BALB.B mice, and BALB/cJ.vic1 mice to ask whether H2-O-deficiency alone is sufficient to confer resistance to these retroviruses to BALB/cJ mice. We find loss of H2-O is sufficient to provide resistance to MMTV, but not MuLV. We also find that this is likely due to the failure of the H2^{d} haplotype to present MuLV-derived antigens, as BALB/cJ mice immunized with virus and adjuvant fail to produce antibodies against the virus.

Results

Previous work in the lab found transfer of the *vic1* locus from the retrovirus resistant I/LnJ strain to the retrovirus susceptible BALB/cJ strain conferred resistance of BALB/cJ mice to both MMTV and MuLV. We wanted to understand if H2-O-deficiency alone was sufficient to confer this resistance, as many other genes, such as classical MHC molecules, are also found in the *vic1* locus. To test this, *H2-Ob*$^{-/-}$ mice were generated on the BALB/cJ background and confirmed to have total loss of H2-O protein via western blotting (**Figure 2.1A**). These mice were subsequently infected as adults with MMTV via ip injection and tested for the presence of neutralizing antibodies in the serum via ELISA (**Figure 2.2A**) and neutralization assay 3 months post infection (**Figure 2.2B**). We observed that BALBc/J.Ob$^{-/-}$ produced neutralizing antibodies

upon infection with MMTV, suggesting H2-O deficiency is sufficient to confer this response in this genetic background.

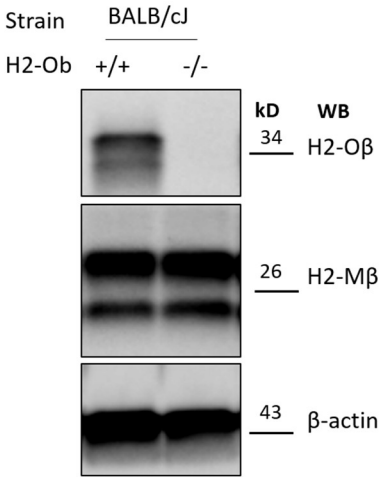

FIGURE 2.1 BALB/cJ H2-Ob$^{-/-}$ mice do not produce H2-O protein. Lysates from splenocytes isolated from BALB/cJ *H2-Ob*$^{+/+}$ and *H2-Ob*$^{-/-}$ mice were used for detection of H2-Oβ, H2-Mβ, and β-actin (loading control) proteins via Western blotting. *H2-Ob*$^{-/-}$ splenocytes do not have detectable H2-Oβ protein but have normal levels of H2-Mβ protein.

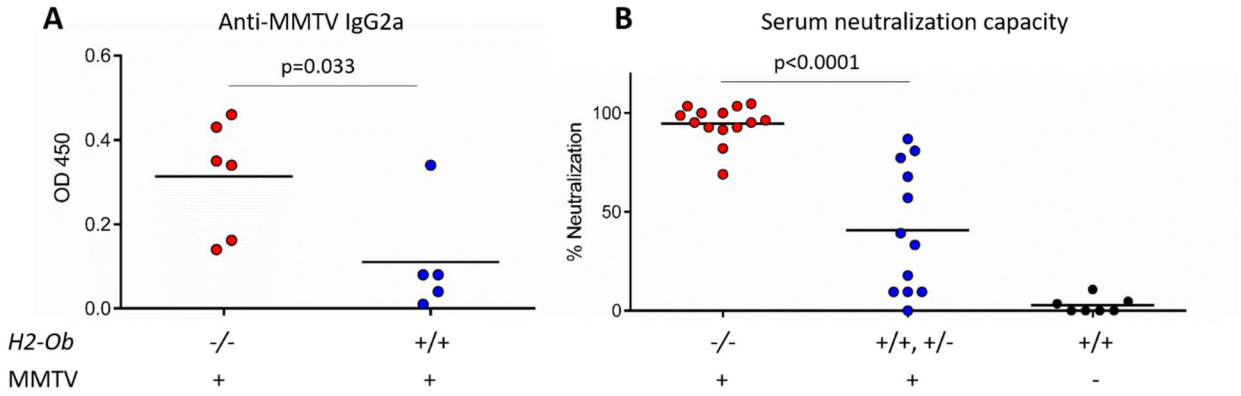

FIGURE 2.2. BALB/cJ *H2-Ob*$^{-/-}$ mice mount neutralizing antibody responses against MMTV upon infection A. Serum antibody levels of anti-MMTV antibodies measured via ELISA in *H2-Ob*$^{-/-}$ and *H2-Ob*$^{+/+}$ controls 15 weeks following MMTV infection via i.p injection of virus purified from milk. H2-O-deficient mice on the BALB/cJ background produce significantly higher titers of MMTV-specific antibodies of the IgG2a isotype upon infection. **B**. Neutralization capacity of serum obtained from infected H2-O-deficient (*H2-Ob*$^{-/-}$) and H2-O-sufficient (*H2-Ob*$^{+/-}$ and *H2-Ob*$^{+/+}$) controls as well as wild-type uninfected controls. Serum from MMTV-infected H2-O-deficient mice is more potently neutralizing compared to serum of infected H2-O-sufficient mice, which is somewhat capable of neutralizing. Serum of uninfected mice on the BALB/cJ background is not virus neutralizing. p values were calculated using unpaired t-tests.

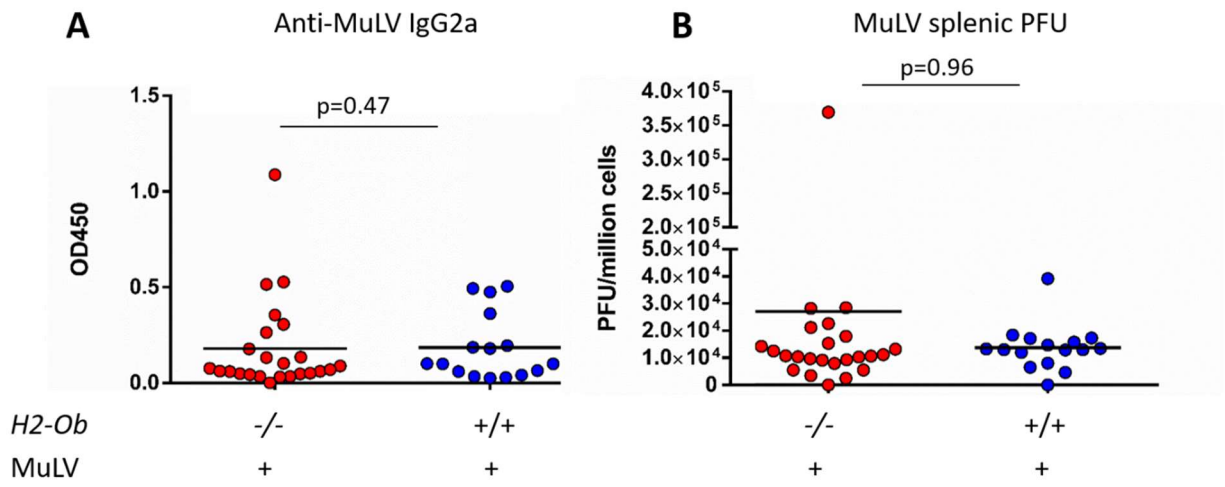

FIGURE 2.3. BALB/cJ *H2-Ob*$^{-/-}$ mice do not mount neutralizing antibody responses against MuLV upon infection. A. Serum antibody levels of anti-MuLV antibodies in *H2-Ob*$^{-/-}$ and *H2-Ob*$^{+/+}$ controls 12-16 weeks following MuLV infection via i.p. injection of 1000 PFU at 6-8 weeks of age. **B.** Splenic viral loads from the same *H2-Ob*$^{-/-}$ and *H2-Ob*$^{+/+}$ mice shown in A. p values were calculated using unpaired t-tests.

Next, we infected *H2-Ob*$^{+/+}$ and *H2-Ob*$^{-/-}$ BALBc/J mice with MuLV and tested for the presence of antiviral antibodies in the serum via ELISA (**Figure 2.3A**) and infectious virus in the spleen via XC plaque assay (**Figure 2.3B**). We observed that, unlike with MMTV infection, H2-O deficiency was not sufficient to confer the ability to produce virus-neutralizing antibodies upon infection with MuLV.

It is well known that susceptibility to MuLV in BALB/cJ mice is due, in large part, to the H2^{d} haplotype of MHC [52]. As BALB/cJ.vic1 mice encode the H2^{j} haplotype of MHC, it was possible that the resistance observed was due to MHC alone and not necessarily the absence of H2-O. Therefore, we tested the hypothesis that BALB/cJ mice simply are not capable of producing titers of antibodies against the virus sufficient for clearance due to their MHC by immunizing BALB/cJ (H2^{d}), BALB.B (H2^{b}) and BALB/cJ, vic1 (H2^{j}) with virus purified from the milk of viremic females in Complete Freund's Adjuvant (CFA). We observed, as expected, BALB/cJ.vic1 mice produced high titers of antiviral antibodies upon immunization (**Figure 2.4**). Furthermore, BALB.B mice also produced antibodies, although to a lesser degree. BALB/cJ mice did not produce as high of titers of antibodies upon immunization, which suggests that the lack of response to viral infection even in the absence of H2-O may be due to poor presentation of certain viral antigens on MHCII.

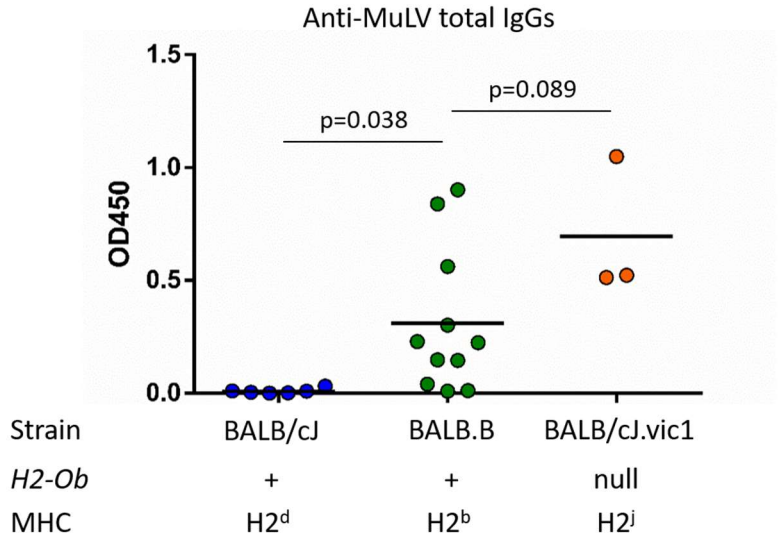

FIGURE 2.4. BALB/cJ *H2-Ob*$^{-/-}$ mice do not produce antibodies against MuLV upon immunization. Serum antibody levels of anti-MuLV antibodies wild-type BALB/cJ, BALB.B, and BALB/cJ.vic1 mice immunized with Triton X-100 inactivated MuLV virions isolated from milk with CFA. All three groups of mice were immunized first with milk-derived virions inactivated with 1% Triton X-100 emulsified in CFA (day 0) and boosted with an additional dose of milk-derived virons inactivated with 1% Triton X-100 emulsified in incomplete Freund's adjuvant (IFA) (day 14) prior to serum collection (day 24). BALB/cJ mice fail to produce antibodies even in the absence of viral infection against viral antigens, while BALB.B mice do not, suggesting confirming MHC haplotype is critical for response against MuLV using our laboratory's RL-MuLV isolate. p values were calculated using unpaired t-tests.

These results suggest that BALB/cJ mice may not be the ideal model for testing the contribution of H2-O to clearance of MuLV infection. Therefore, to determine if BALB.B mice may be used instead, we infected BALB/cJ, BALB.B, and BALB/cJ.vic1 mice with MuLV to determine how readily BALB.B mice control MuLV infection compared to highly susceptible and highly resistant control animals. We found BALB.B mice to be moderately resistant to infection, with most mice clearing the virus as measured via XC plaque assay (**Figure 2.5A**) and producing moderate titers of antibodies upon infection (**Figure 2.5B**). While this would suggest that most mice were completely resistant to the virus (as seen, for example, in BALB/cJ.vic1 mice), overall BALB.B mice had a trend toward higher spleen weights (**Figure 2.5C**) and significantly lower IgG2a antibody titers than BALB/cJ.vic1 mice. This suggests the virus in the spleen may have been below the limit of detection of the assay as performed. Perhaps using more splenocytes in the XC plaque assay would reveal low levels of virus in the spleen.

On the basis of the findings that BALB.B mice appear to exhibit intermediate resistance to MuLV infection, *H2-Ob*$^{-/-}$ BALB.B mice are currently being generated using a method similar to that in [15]. The utility of these mice will lie in their compatibility with already developed reagents (such as tetramers to detect virus-specific T cells) which depend on the $H2^b$ MHC haplotype. Furthermore, unlike MMTV, MuLV readily forms plaques which simplifies quantification of viral loads which will facilitate further study on the role of H2-O in these infections.

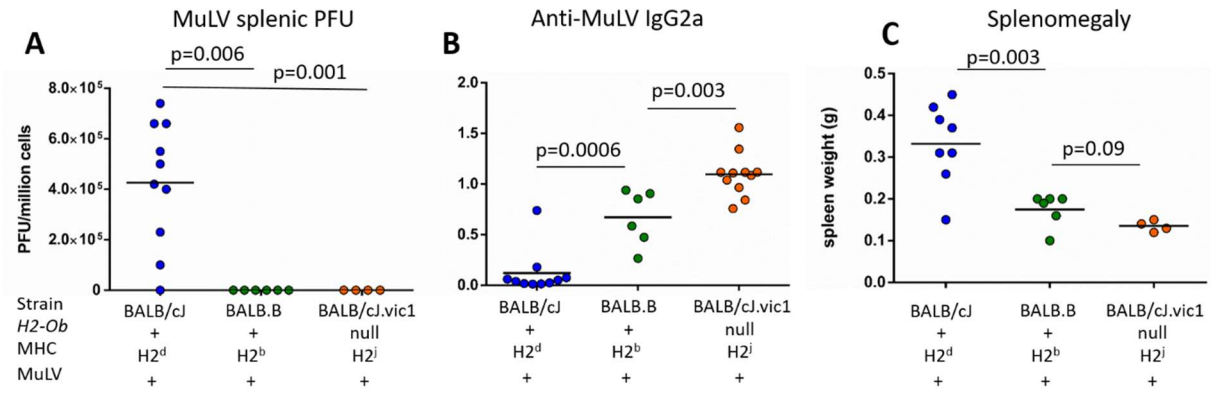

FIGURE 2.5. BALB.B mice mount neutralizing antibodies to MuLV upon infection. A. XC plaque assay measuring infectious virus loads in the spleens of BALB/cJ, BALB.B, and BALB/cJ.vic1 mice 12 weeks post-infection with 1000 PFU MuLV via i.p. infection at 8 weeks of age. Both BALB.B and BALB/cJ.vic1 mice have undetectable viral loads in the spleen. **B.** Anti-MuLV antibody titers in the serum 12 weeks post infection. BALB.B mice mount an intermediate response compared to BALB/cJ and BALB/cJ.vic1 mice. **C.** BALB.B mice have a trend toward higher spleen weights 12 weeks post infection than BALB/cJ.vic1 mice.

Chapter 3: Investigation of the role of H2-O in immune responses targeting commensal and pathogenic bacteria

Preface

The data contained in this chapter are all currently unpublished. Many collaborators were involved in the collection of data here. Dr. Federico Rey at the University of Wisconsin-Madison kindly provided the 22-member consortium (22-mix) used in the experiments shown in figure 3.10. The experimental model of *Staphylococcus aureus* colonization used in this chapter was developed by the labs of Olaf Schneewind and Dominique Missiakas, and preliminary experiments using this model in *H2-Ob*$^{-/-}$ mice were performed by Dr. Yan Sun in the Schneewind/Missiakas lab. The data in figure 3.14 were collected by Dr. Sun. Additional help generating bacterial strains and training on the colonization model was provided by Dr. Miaomiao Shi in the Schneewind/Missiakas lab. The model of *Citrobacter rodentium* infection is widely used, but protocols and bacterial strains were provided to us by Dr. Joseph Pickard in the lab of Dr. Gabriel Nuñez at the University of Michigan.

Summary

Previously, the laboratory established a role for H2-O in antiretroviral antibody responses. However, it remained unknown if H2-O played a role in immune responses against other microbes, such as bacteria. In these studies, the effect of H2-O-deficiency on commensal and pathogenic bacteria colonizing mucosal surfaces is explored. We found H2-O shapes the composition of the gut microbiota via a mechanism independent of IgA specificity or quantity. Furthermore, H2-O-deficient mice are relatively resistant to colonization by both S*taphylococcus aureus* and *Citrobacter rodentium.* While the mechanisms of resistance to these two model pathogens are still under study, preliminary data suggest resistance to *S. aureus* is dependent

(either directly or indirectly) on specificity of the B cell receptor in H2-O-deficient mice and resistance to *C. rodentium* is independent of adaptive immunity.

Results

Previous work in the lab has clearly demonstrated a role for H2-O in the response against retroviruses [15]. The goal of these studies was to determine if there was also a role for H2-O in immune responses against other microbes, namely commensal and pathogenic bacteria. To test the hypothesis that H2-O can regulate the commensal bacterial community, a gnotobiotic approach was taken. First, B6J.*H2-Ob*$^{-/-}$ mice were rederived as germ-free (GF) at Taconic farms. The *H2-Ob*$^{-/-}$ line is currently maintained GF conditions at the University of Chicago. To address the role of H2-O in regulating the microbiota, GF *H2-Ob*$^{+/+}$ and *H2-Ob*$^{-/-}$ adults were colonized with whole SPF cecum ("input"). The effect of H2-O-deficiency was determined in colonized adults (G0 generation) and/or their offspring (G1 generation) (**Figure 3.1**) by 16S rRNA amplicon sequencing of DNA isolated from cecal contents of experimental mice. Amplicon sequencing data was analyzed using the DADA2 pipeline [53]. This experiment was independently conducted three times, using whole cecum input derived from a similar source (C57/BL6NTac mice purchased from Taconic Farms) empirically found by previous experiments done in the lab to be well suited to this purpose. In each of the three experiments, different input samples were used as well as different generations of mice were analyzed to determine the effect of H2-O on the commensal community. In the first experiment ("experiment 1", red), only G1 mice were analyzed. In the second experiment, ("experiment 2", blue), only G0 mice were analyzed. And in the third experiment ("experiment 3", green), mice of both generations were analyzed (i.e. G0 mice as well as their G1 progeny, which all came from the same input sample).

In two independent experiments with different SPF inputs, *H2-Ob*$^{+/+}$ and *H2-Ob*$^{-/-}$ G1 mice were found to have distinct commensal bacterial communities (**Figure 3.2**). The

differences seen in *H2-Ob*$^{+/+}$ and *H2-Ob*$^{-/-}$ did not appear to be based on the richness of the communities, as both genotypes harbored similar numbers of taxa (**Figure 3.3A**). However, the *H2-Ob*$^{-/-}$ communities did appear to be more diverse, which is likely due to increased representation of rarer taxa at the expense of more abundant taxa (i.e. the community is more even) (**Figure 3.3B**). Supporting this fact, Linear discriminant analysis Effect Size (LEfSe) analysis [54] of the communities recovered from each experiment to identify differentially abundant taxa indicated a small number of taxa found at higher abundance in *H2-Ob*$^{+/+}$ mice and a large number of taxa at higher abundance in *H2-Ob*$^{-/-}$ mice, suggesting expansion of many rare taxa due to a restriction on few abundant taxa (**Figure 3.4**). All taxonomic and abundance information for all ASVs recovered in 16S sequencing are detailed in **Table S3** (supplemental).

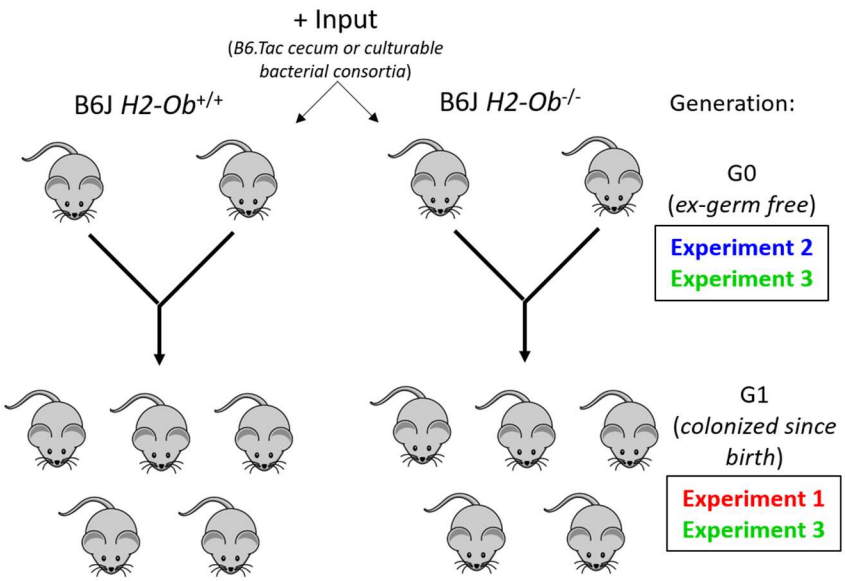

FIGURE 3.1. Breeding schematic of gnotobiotic mice. Germ free B6J *H2-Ob*$^{+/+}$ and *H2-Ob*$^{-/-}$ breeder mice were colonized with bulk cecal contents derived from an SPF B6.Tac mouse purchased from Taconic Farms. These ex-germ free mice (G0 generation) were either used for analysis or bred to produce G1 mice for cecal composition analysis. In some experiments, G0 mice were instead colonized with defined bacterial consortia rather than bulk cecal contents.

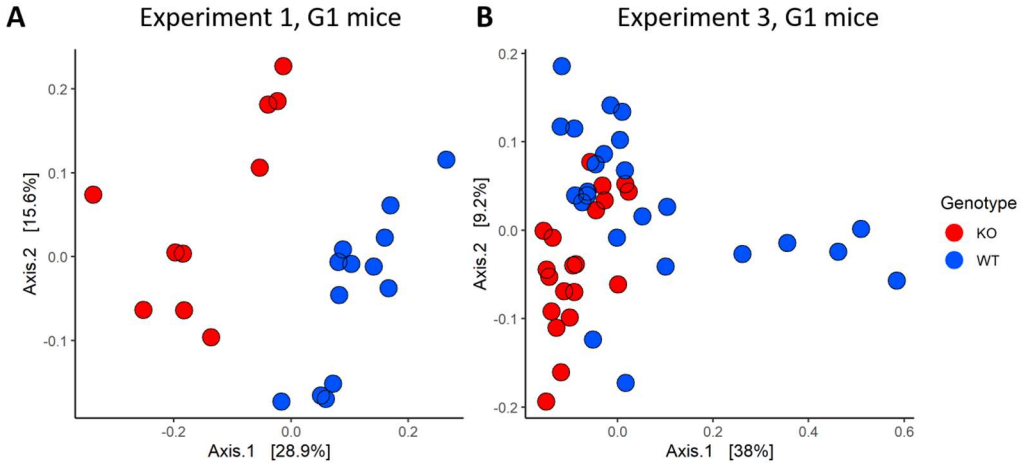

FIGURE 3.2. Comparison of cecal composition in G1 animals. G1 B6J *H2-Ob*$^{+/+}$ and *H2-Ob*$^{-/-}$ mice were aged to 8 weeks and the bacterial composition of their ceca analyzed using 16S rRNA amplicon sequencing. The similarity of the cecum compositions to one another are visualized using principal component analysis (PCoA) built using the Bray-Curtis dissimilarity index. Panels A and B represent two independent experiments.

We next wondered if differences in commensal composition due to H2-O-deficiency could be seen in colonized mice (G0 mice) in addition to their offspring (G1 mice, discussed above). To address this question, two independent experiments were conducted in which colonized adults were sacrificed 2-4 weeks after colonization for cecum collection and 16S rRNA amplicon sequencing. Principal component analysis of the communities in these two groups suggested only modest differences in commensal composition that were dependent on the input microbiota (**Figure 3.5**). This is supported by LEfSe analysis of these communities, as far fewer taxa were found to be differentially abundant compared to the communities recovered from G1 mice (**Figure 3.6**). Because one G0 experiment and one G1 experiment were done with the same input (G0 mice were bred to produce G1 and both groups analyzed), our results suggest that differences in commensal composition that are dependent on H2-O are more pronounced in the G1 generation (compare G0 mice from experiment 3, **Figure 3.5B**, with G1 mice from experiment 3, **Figure 3.3B**). However, as our results also indicate that the degree of H2-O-dependent regulation heavily depends on the composition of the input microbiota ([55] and discussion below), this observation may be true for some input microbiota and not for others. The influence of the generation of mice on the degree of H2-O-dependent regulation of the microbiota could be due to a variety of reasons, technical or biological. For example, taxa that are more likely to be regulated by H2-O could more easily colonize neonatal hosts rather than adult hosts, or more pronounced effects of H2-O on the microbiota could be seen after longer periods of colonization (G0 animals are only colonized for 2-4 weeks before analysis, whereas G1 mice are analyzed at 8 weeks of age). The precise mechanism underpinning the more robust regulation of the commensal composition in G1 mice will require additional experiments to understand.

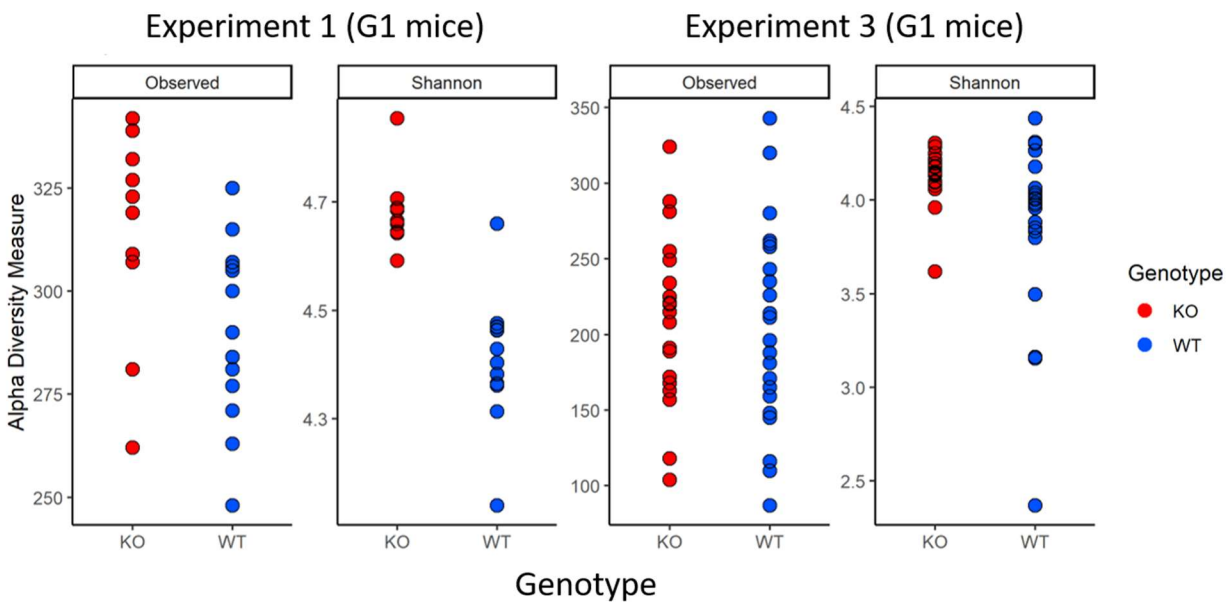

FIGURE 3.3. Alpha diversity of communities in G1 experiments. Comparison of alpha diversity in cecal communities in G1 experiments using taxon count ("Observed") and Shannon diversity index ("Shannon"). *H2-Ob*$^{+/+}$ and *H2-Ob*$^{-/-}$ communities do not have strikingly different numbers of taxa in either experiment, but show a trend toward higher diversity overall. This suggests that communities in *H2-Ob*$^{-/-}$ G1 mice are not richer, but are more even.

It is well understood that differences in the input microbiota will largely determine differences in recovered taxa [55]. To understand if differences in input microbiota could drive the dampened community differences observed in experiment 3, a simple comparison of all three input samples was made. Of the 100 most abundant taxa in each experiment, most taxa are unique, with only a small fraction shared between all three experiments (**Figure 3.7**). Furthermore, when analysis of the most differentially abundant taxa between *H2-Ob*$^{+/+}$ and *H2-Ob*$^{-/-}$ mice in each experiment is compared to the abundance in each input, it becomes clear that several taxa which are highly regulated by H2-O in experiment 1 are virtually absent from inputs in subsequent experiments, especially experiment 3 (**Figure 3.8**). Overall, these data suggest that while distinct input microbiota are regulated in an H2-O dependent manner, H2-O dependent regulation is a complex process depending on the makeup of the community in question.

With the understanding that certain communities are regulated by H2-O at the G0 generation, we next wondered if we could identify a simplified culturable consortium of bacteria which could be used as a more tractable experimental system in which to test how H2-O regulates the commensal composition. To do this, we colonized *H2-Ob*$^{+/+}$ and *H2-Ob*$^{-/-}$ adults with two culturable consortia: Altered Scheadler's Flora (ASF) [56] and a 22-member consortium (a gift from Dr. Federico Rey at the University of Wisconsin-Madison). In two independent experiments, no striking differences between *H2-Ob*$^{+/+}$ and KO mice were seen using ASF (**Figure 3.9**). However, using the larger consortium we observed differences between the two groups (**Figure 3.10A**). Several taxa were found to be differentially regulated in this community (**Figure 3.10B**). Interestingly, a similar trend was observed in this experiment as compared to the previously discussed experiments utilizing complex microbiota as inputs: a small number of highly abundant taxa were found to be restricted in the *H2-Ob*$^{-/-}$ mice alongside an expansion of several rarer taxa.

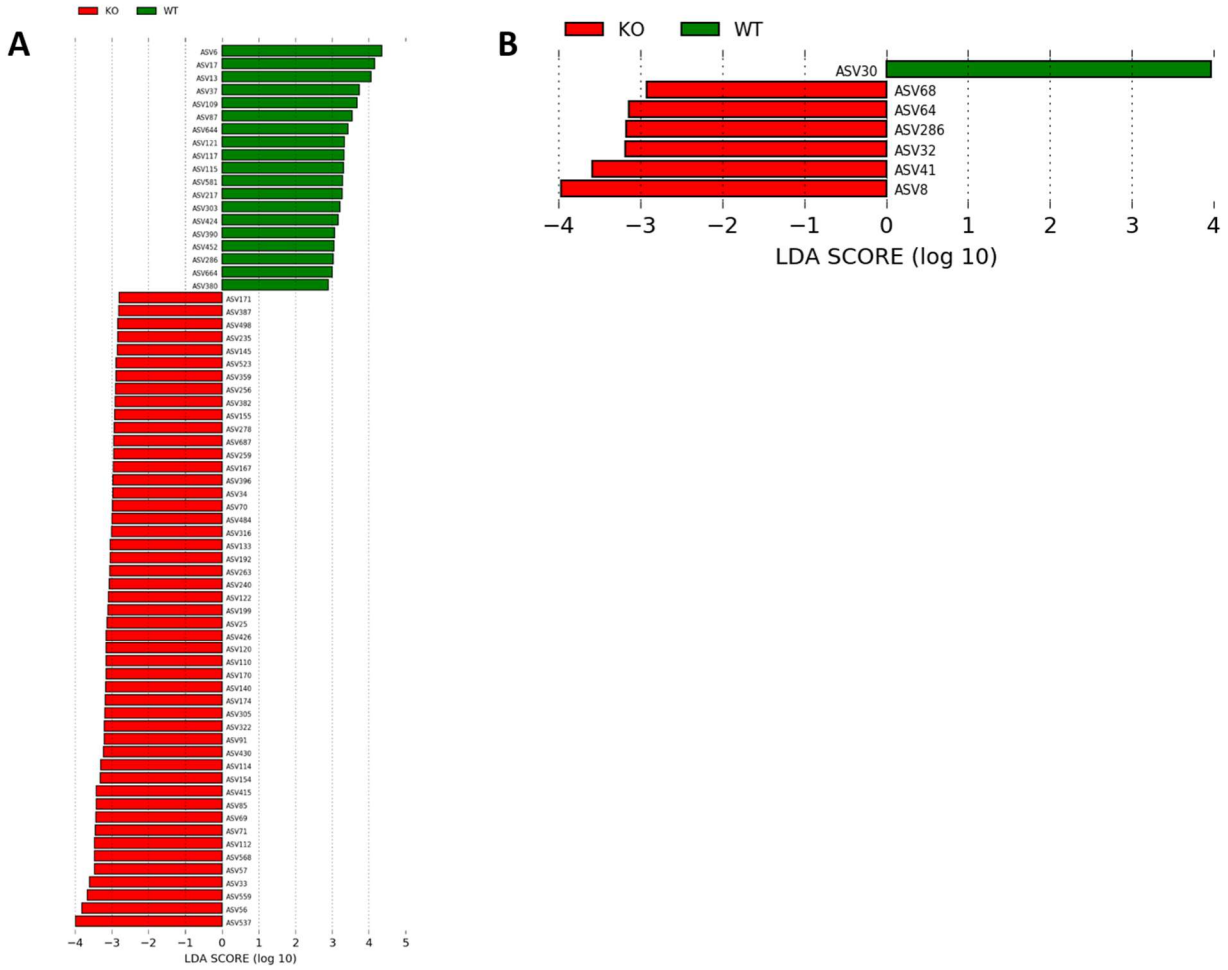

FIGURE 3.4. Identification of differentially abundant ASVs in G1 animals. Differentially abundant amplicon sequence variants (ASVs) assigned by the DADA2 16s analysis pipeline were identified using the LEfSe analysis tool. ASVs denoted with green bars are significantly more abundant in *H2-Ob*$^{+/+}$ mice, and those denoted by red bars are significantly more abundant in KO mice. (A) ASVs differentially abundant in experiment in Figure 3.3A. (B) ASVs differentially abundant in experiment in Figure 3.3B.

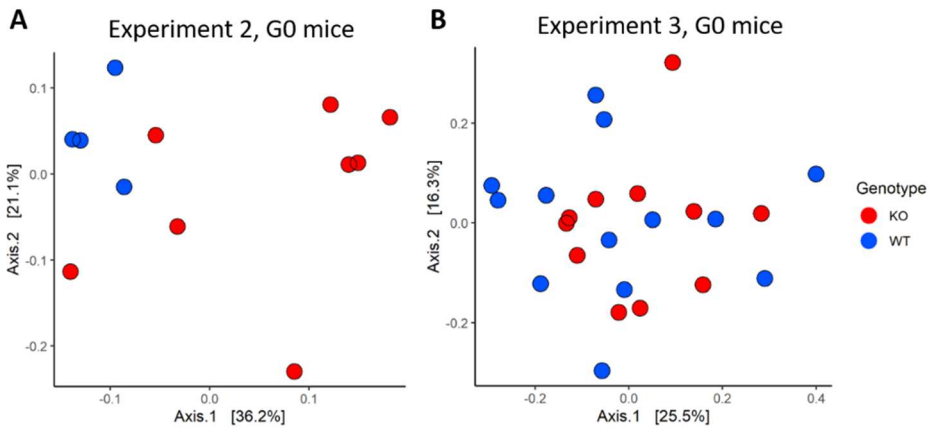

FIGURE 3.5. H2-O dependent regulation of commensal bacteria is attenuated at the G0 generation and depends on the input microbiota used. G0 B6J *H2-Ob*$^{+/+}$ and *H2-Ob*$^{-/-}$ mice were aged to colonized as adults of at least 8 weeks of age and the bacterial composition of their ceca analyzed using 16S rRNA amplicon sequencing 2-4 weeks after colonization. The similarity of the cecum compositions to one another are visualized using principal component analysis (PCoA) built using the Bray-Curtis dissimilarity index. Panels A and B represent two independent experiments.

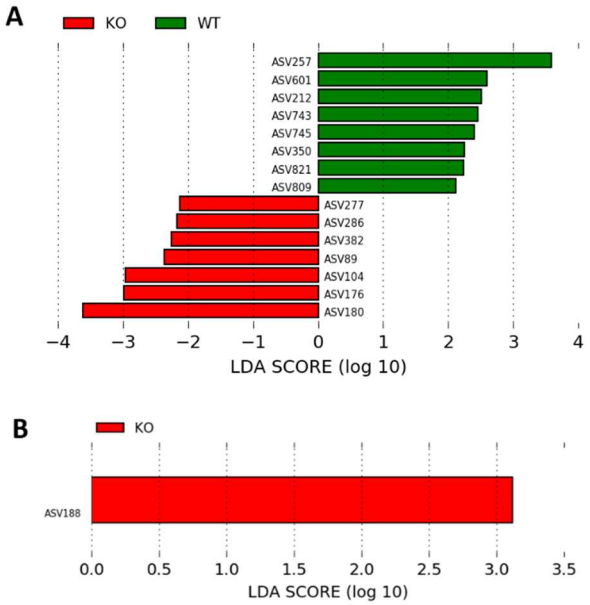

FIGURE 3.6. Identification of differentially abundant ASVs in G0 animals. Differentially abundant amplicon sequence variants (ASVs) assigned by the DADA2 16s analysis pipeline were identified using the LEfSe analysis tool. ASVs denoted with green bars are significantly more abundant in *H2-Ob*$^{+/+}$ mice, and those denoted by red bars are significantly more abundant in KO mice. (A) ASVs differentially abundant in experiment in Figure 3.5A. (B) ASVs differentially abundant in experiment in Figure 3.5B.

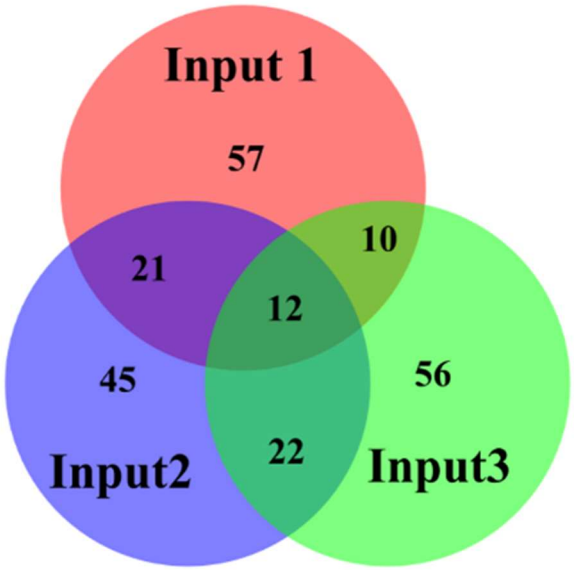

FIGURE 3.7. Many abundant taxa present in input microbiota samples are unique. Venn diagram compareing the top 100 most abundant ASVs from each input microbiota used for colonization. Many to most of the input taxa were unique to each input, with only a small fraction being shared between all three input samples.

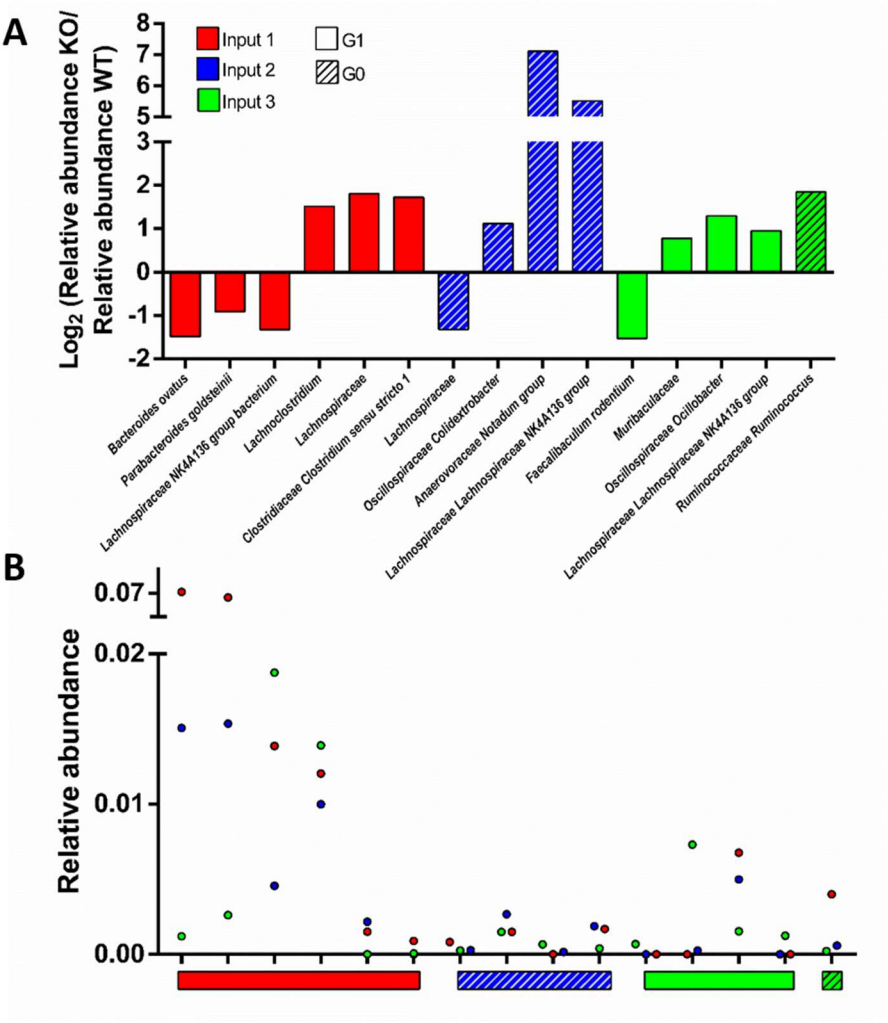

FIGURE 3.8. Input microbiota samples vary in the abundance of the taxa most regulated by H2-O. (A) Log2-transformed fold change (KO relative to *H2-Ob*$^{+/+}$) of the relative abundance of select differentially abundant taxa from each of the three independent experiments. The most differentially abundant (up to three) taxa with either positive or negative fold change were selected to display here. The taxonomic classification of selected taxa are on the x-axis. (B) The relative abundance in each experiment's corresponding input sample of all of the selected differentially abundant taxa from directly above. The abundance in each input is denoted in either red (abundance in input 1), blue (abundance in input 2), or green (abundance in input 3).

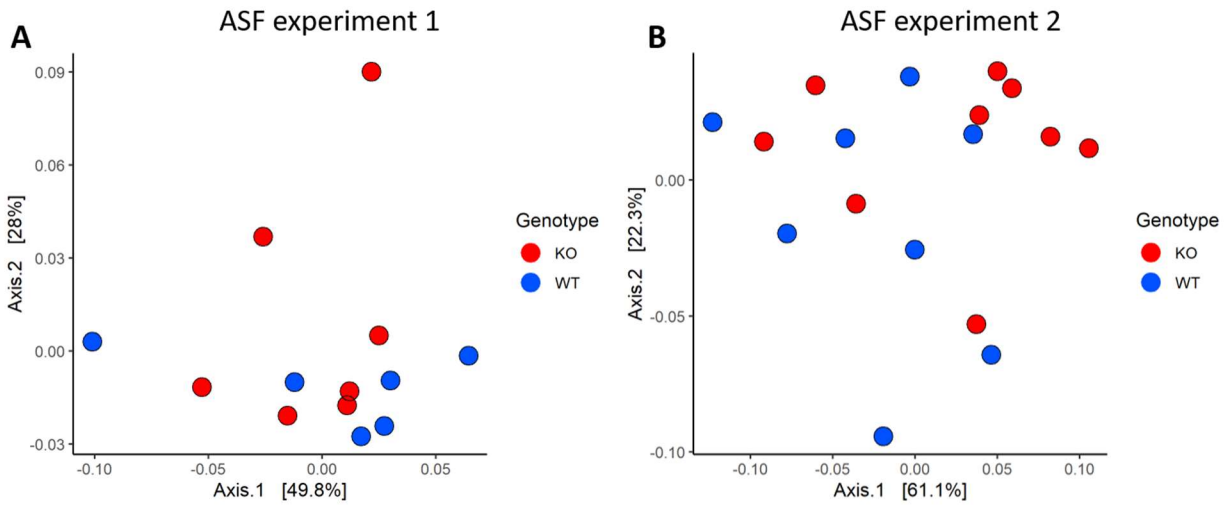

FIGURE 3.9. Comparison of cecal composition in ASF colonized G0 animals. G0 B6J *H2-Ob*$^{+/+}$ and *H2-Ob*$^{-/-}$ mice were colonized with the ASF consortium and the contents of their ceca analyzed using 16S rRNA amplicon sequencing 2 weeks post-colonization. The similarity of the cecum compositions to one another are visualized using principal component analysis (PCoA) built using the Bray-Curtis dissimilarity index. Panels A and B represent two independent experiments.

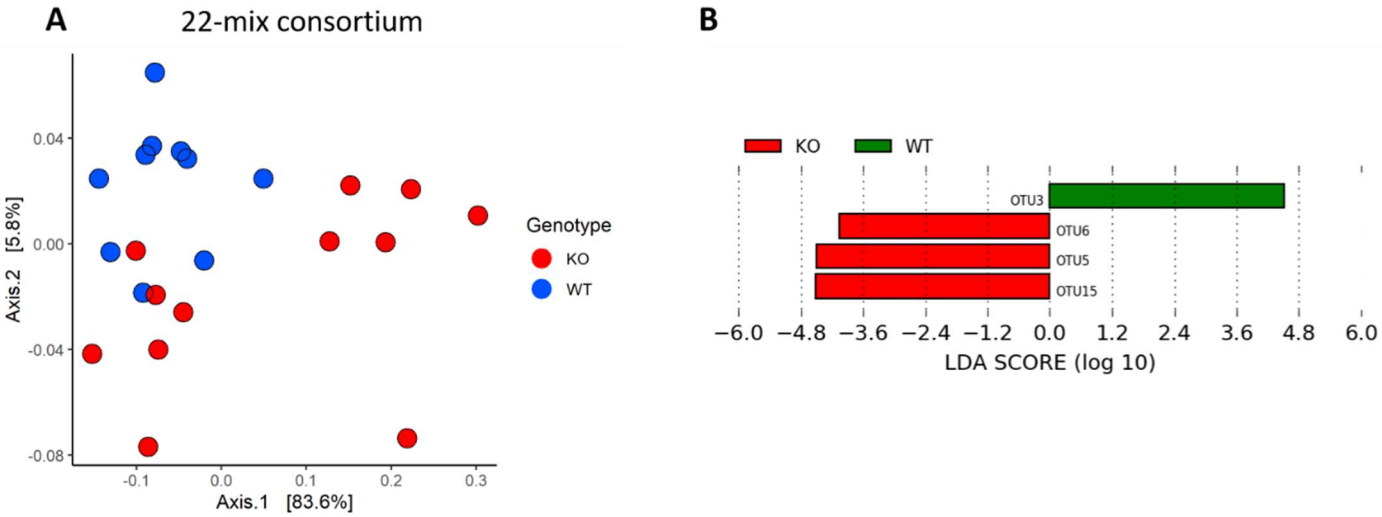

FIGURE 3.10. Comparison of cecal composition in 22-mix colonized G0 animals. (A) G0 B6J *H2-Ob*$^{+/+}$ and *H2-Ob*$^{-/-}$ mice were colonized with the 22-mix consortium and the contents of their ceca analyzed using 16S rRNA amplicon sequencing 2 weeks post-colonization. The similarity of the cecum compositions to one another are visualized using principal component analysis (PCoA) built using the Bray-Curtis dissimilarity index. (B) Differentially abundant amplicon sequence variants (ASVs) assigned by the DADA2 16s analysis pipeline were identified using the LEfSe analysis tool. ASVs denoted with green bars are significantly more abundant in *H2-Ob*$^{+/+}$ mice, and those denoted by red bars are significantly more abundant in KO mice.

We next wanted to better understand the mechanisms that may be driving differences in commensal composition in *H2-Ob*$^{+/+}$ and *H2-Ob*$^{-/-}$ mice. The hypothesis that specificity of IgA, the predominant immunoglobulin present in the intestines, was tested using a previously published IgA-seq approach [55] in which IgA-bound and IgA-unbound bacteria are MACS-purified and subjected to 16S rRNA amplicon sequencing. Bacteria from cecal contents from G1 mice from experiment 1 were purified by the presence of bound IgA and used for 16S amplicon sequencing. Taxonomic classifcations and abundance data of all ASVs identified in this experiment are provided in **Table S4** (supplemental, note: ASV designations do not match those of **Table S3**). Comparison of the IgA+ and IgA- populations from all mice revealed very few differences between *H2-Ob*$^{+/+}$ and *H2-Ob*$^{-/-}$ mice among IgA+ bacteria (**Figure 3.11C-D**) with clear differences driven by genotype among the IgA- bacteria (**Figure 3.11A-B**). These data suggest IgA specificity is not responsible for driving community differences in *H2-Ob*$^{+/+}$ and *H2-Ob*$^{-/-}$ mice. In support of this conclusion, overall intestinal and serum levels of IgA were also not found to be significantly different between *H2-Ob*$^{+/+}$ and *H2-Ob*$^{-/-}$ mice (**Figure 3.12**). These results were somewhat surprising, as IgA has long been considered to be an important determinant of the commensal composition in mice [57].

In order to determine if the adaptive immune response is required for H2-O dependent regulation of the commensal microbiota, we are currently generating *H2-Ob*$^{-/-}$ mice on the *Rag1*$^{-/-}$ background. *Rag1*$^{-/-}$ mice lack all cells of the adaptive immune system, namely T, B, and NK T cells. Colonization of *H2-Ob*$^{+/+}$, *H2-Ob*$^{-/-}$, *Rag1*$^{-/-}$ and *H2-Ob*$^{-/-}$ *Rag1*$^{-/-}$ mice in a single experiment and subsequent analysis of the composition of bacteria in their ceca will determine whether H2-O is functioning in adaptive immune cells or perhaps is acting outside of the canonical cell type to exert its effects on the microbiota.

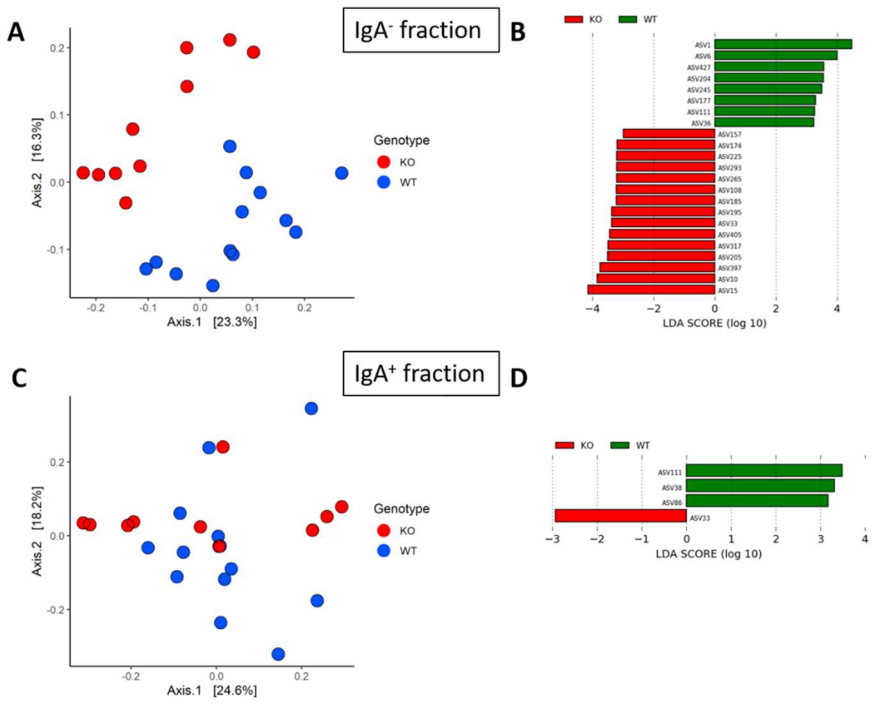

FIGURE 3.11. Analysis of IgA+ and IgA- bacterial fractions in ceca of G1 animals. The bacterial fraction of cecal contents from Fig 3.2A were sorted via MACS into IgA+ and IgA- populations. The bacterial composition of each fraction from each mouse was analyzed using 16S rRNA amplicon sequencing. The similarity of the populations to one another are visualized using principal component analysis (PCoA) built using the Bray-Curtis dissimilarity index. Differentially abundant amplicon sequence variants (ASVs) assigned by the DADA2 16s analysis pipeline were identified using the LEfSe analysis tool. ASVs denoted with green bars are significantly more abundant in *H2-Ob*$^{+/+}$ mice, and those denoted by red bars are significantly more abundant in KO mice. (A) PCoA using IgA- fraction sequences. (B) Differentially abundant ASVs in *H2-Ob*$^{+/+}$ and *H2-Ob*$^{-/-}$ mice in the IgA- fraction. (C) PCoA using IgA+ fraction sequences. (D) Differentially abundant ASVs in *H2-Ob*$^{+/+}$ and *H2-Ob*$^{-/-}$ mice in the IgA+ fraction.

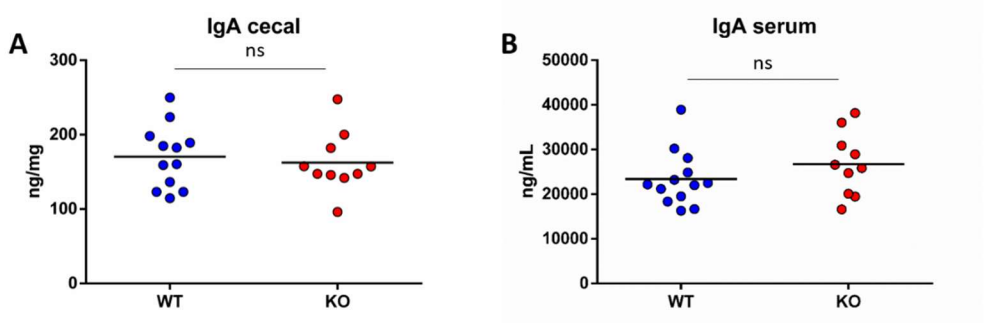

FIGURE 3.12. Intestinal and serum IgA quantification in Experiment 1 G1 colonized mice. IgA was quantified via ELISA in the cecal contents and serum of Experiment 1 G1 colonized mice.

After seeing a role for H2-O in regulating commensal bacteria, we hypothesized that other bacteria present at mucosal surfaces would also be susceptible to H2-O-dependent immune responses. To test this, we used two models of bacterial colonization: *Staphylococcus aureus* and *Citrobacter rodentium. S. aureus* is a major human pathogen responsible for over 100,000 bloodstream infections and almost 20,000 deaths in the US per year [58]. A key risk factor for systemic infection by *S. aureus* is colonization by the bacterium in the nares, the primary site of commensal *S. aureus* colonization in humans [59]. Treatment of this common infection is severely complicated by antibiotic resistance which is readily acquired by the bacterium. Attempts have been made to develop vaccines against *S. aureus,* however, none have yet been successful. In fact, immune responses mounted against the bacterium do not appear to be protective in many infected patients, as it is common for patients to become infected more than once by *S. aureus.* For these reasons, a better understanding of how the immune system interacts with commensal *S. aureus* is of great interest and importance to studies of human health. The Schneewind/Missiakas laboratory has developed a model of *S. aureus* nasopharyngeal colonization in mice [60] to accomplish this. In our studies, we adapted this model by first isolating a strain of the WU1 isolate of *S. aureus* [60] that is resistant to rifampicin, an antibiotic which inhibits the bacterial RNA polymerase. Point mutations in *rpoB,* encoding the β subunit of RNA polymerase, lead to strains of bacteria that can grow in the presence of very high concentrations of this antibiotic [61]. The purpose of this isolation was to use a strain of bacteria that could be easily differentiated from commensal bacteria by plating samples collected from mice on agar plates containing antibiotics. *H2-Ob*$^{+/+}$ and *H2-Ob*$^{-/-}$ mice were colonized intranasally with 1x10^{8} CFU rifampicin-resistant WU1 and monitored with weekly throat swabs and fecal pellet culture. We observed B6J.*Ob*$^{-/-}$ mice are more resistant to persistent WU1 colonization than *H2-Ob*$^{+/+}$ mice (**Figure 3.13**). To investigate the role of antibody responses in the clearance of WU1 from the throat and GI tract, serum Ig reactivity to a panel of 20 *Staphylococcus aureus* proteins was performed [60] (**Figure 3.14**). No particular

antigen was observed to be targeted by *H2-Ob*$^{-/-}$ antibody responses compared to *H2-Ob*$^{+/+}$ mice.

To more conclusively demonstrate a role (or lack thereof) for antibody responses in the resistance of *H2-Ob*$^{-/-}$ to persistent colonization by WU1, we generated B cell receptor monoclonal mice harboring either the wild-type or knock-out allele of *H2-Ob*. These mice were generated by crossing the MD4 transgenic mouse [62], which carries a transgene for the rearranged heavy and light chains from a BCR recognizing hen egg lysozyme, to *H2-Ob*$^{-/-}$ mice. As both the MD4 transgene and H2-Ob reside on chromosome 17, approximately 100 pups were bred to generate 4-5 recombinant pups which had both the MD4 transgene and the null allele of *H2-Ob* on the same chromosome. Next, these mice were crossed to mice lacking all endogenous B cells due to a deletion in the J_H region of the BCR, a gift from Dr. Albert Bendelac at the University of Chicago. The mice resulting from this cross lack all endogenous B cells, and have only B cells of transgene origin. The MD4 transgene was maintained at hemizygosity (i.e. only one copy) while both the J_H null and H2-Ob null alleles were maintained at homozygosity. *H2-Ob*$^{+/+}$ MD4t+ J_H $^{-/-}$ mice were bred as controls by crossing MD4 transgenic mice to Jh$^{-/-}$ to generate H2-O-sufficient but BCR monoclonal mice. H2-O-sufficient and H2-O-deficient BCR monoclonal mice were colonized with WU1 and monitored weekly for presence of bacteria (**Figure 3.17**). While we observed occasional decolonization among each group of mice, there was not a tendency for decolonization among *H2-Ob*$^{-/-}$ BCR monoclonal mice. Interestingly, these mice did have higher initial bacterial loads, which may point to a permissive microbiota in these mice. Whether the microbiota in these mice is in fact different from *H2-Ob*$^{+/+}$ BCR monoclonal mice has yet to be formally tested, however. These data suggest that BCR specificity in *H2-Ob*$^{-/-}$ mice is important for resistance to persistent *S. aureus* colonization. This could be due to either a direct effect of antibodies on the bacterium, or an indirect effect through shaping of the microbiota, and this has yet to be determined.

We also wondered if *H2-Ob*$^{-/-}$ mice would be resistant to other bacteria that replicate at mucosal surfaces, either via antibody responses or via colonization resistance imparted by the H2-O-dependent shift in the commensal microbiota. To test this, we took advantage of a well-established infection model using *Citrobacter rodentium. C. rodentium* is often used to model human infection by enteropathogenic *E. coli* (EPEC), as mice are not readily infected by EPEC. *C. rodentium* is a Gram-negative bacterium which is naturally spread via the fecal-oral route in mice. During the course of *C. rodentium* infection, mice are colonized in the distal GI tract (cecum and colon). Mice experience colitis and diarrhea which is self-limiting and resolves in approximately 3 weeks. The bacterial burden in infected mice is measured by culture of fecal pellets every 2-3 days. Typically, peak infection occurs at approximately day 10-12. Host IgG responses are critical for clearance of the bacterium, and are directed at the bacterial proteins used for attachment to host intestinal epithelium and injection of bacterial virulence factors [63]. In order to test the effect of the H2-O on infection by this bacterium, we infected *H2-Ob*$^{+/+}$ and *H2-Ob*$^{-/-}$ mice via the oral route with *C. rodentium.* Upon infection, we observed *H2-Ob*$^{-/-}$ mice were much more resistant to initial stages of bacterial replication. Furthermore, at the peak of infection, *H2-Ob*$^{-/-}$ had an overall lower bacterial burden (**Figure 3.18A**). This initial resistance against *C. rodentium* was not due to preexisting cross-reactive antibodies, as measured via ELISA using serum collected on day 01 of infection and day 28 of infection (**Figure 3.18B**). These data collectively suggest *H2-Ob*$^{-/-}$ harbor a commensal microbiota conferring resistance to bacterial replication in the early stages of infection.

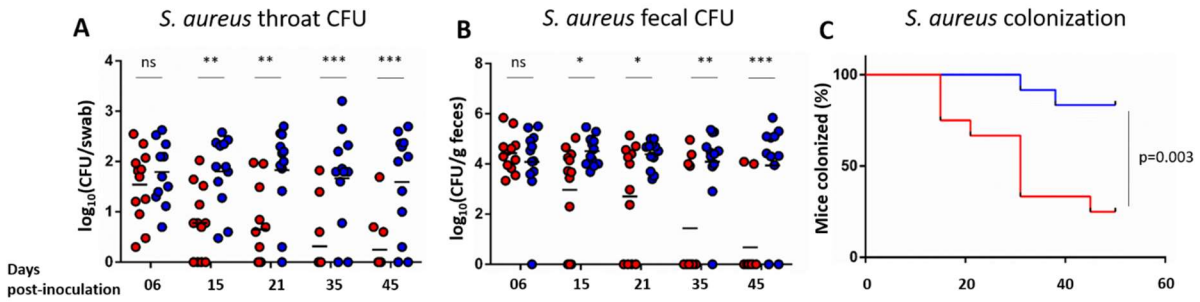

FIGURE 3.13. H2-Ob$^{-/-}$ mice are resistant to persistent colonization by S. aureus. *H2-Ob*$^{+/+}$ and *H2-Ob*$^{-/-}$ mice were colonized intranasally with 1E8 CFU and monitored weekly for bacterial load in the throat via throat swab culture and in the gut via fecal pellet culture. (A) Bacterial load in the throat over the course of 6 weeks. (B) Bacterial load in the gut over the course of 6 weeks. (C) Colonization represented as a Kaplan-Meier curve. Significance of CFU data determined using unpaired t-tests. *=p<0.05, **=p<0.01, ***=p<0.001

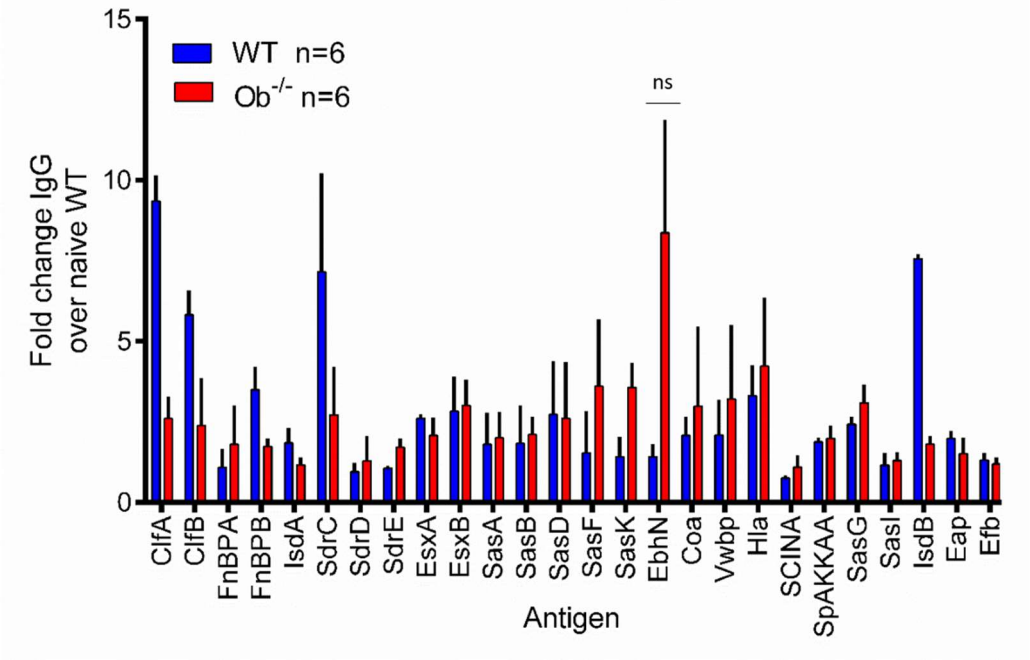

FIGURE 3.14. H2-Ob$^{-/-}$ anti-Staphylococcal antibody responses are not directed against a particular S. aureus surface protein contained in the antigen matrix panel. Serum collected from *H2-Ob*$^{+/+}$ and *H2-Ob*$^{-/-}$ mice colonized with WU1 2 weeks post-colonization was subjected to the antigen matrix panel. Significance calculated using Tukey's multiple comparisons test. ns= not significant.

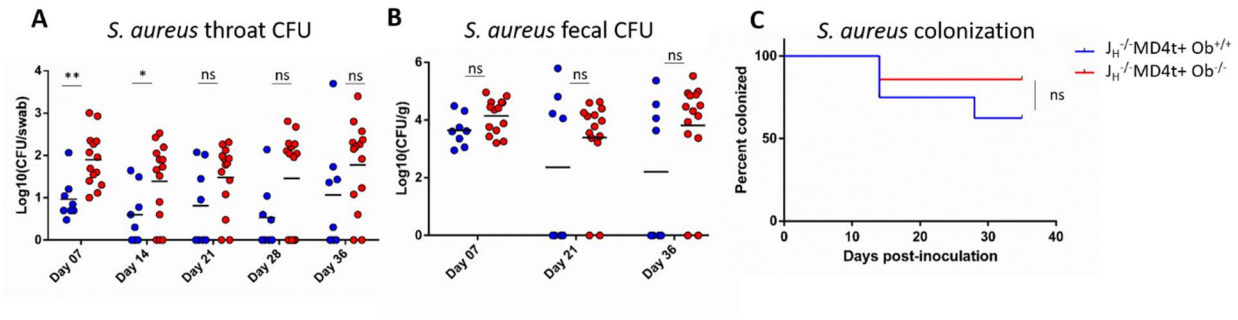

FIGURE 3.15. BCR monoclonal *H2-Ob*$^{-/-}$ mice are not resistant to persistent colonization by S. aureus.

BCR monoclonal *H2-Ob*$^{+/+}$ and *H2-Ob*$^{-/-}$ mice along with B6J wild type controls were colonized intranasally with 1E8 CFU and monitored weekly for bacterial load in the throat via throat swab culture and in the gut via fecal pellet culture. (A) Bacterial load in the throat over the course of 6 weeks. (B) Bacterial load in the gut over the course of 6 weeks. (C) Colonization represented as a Kaplan-Meier curve. Significance of CFU data determined using unpaired t-test, significance of Kaplan-Meier curve calculated using Mantel-Cox test. ns= not significant *=p<0.05, **=p<0.01.

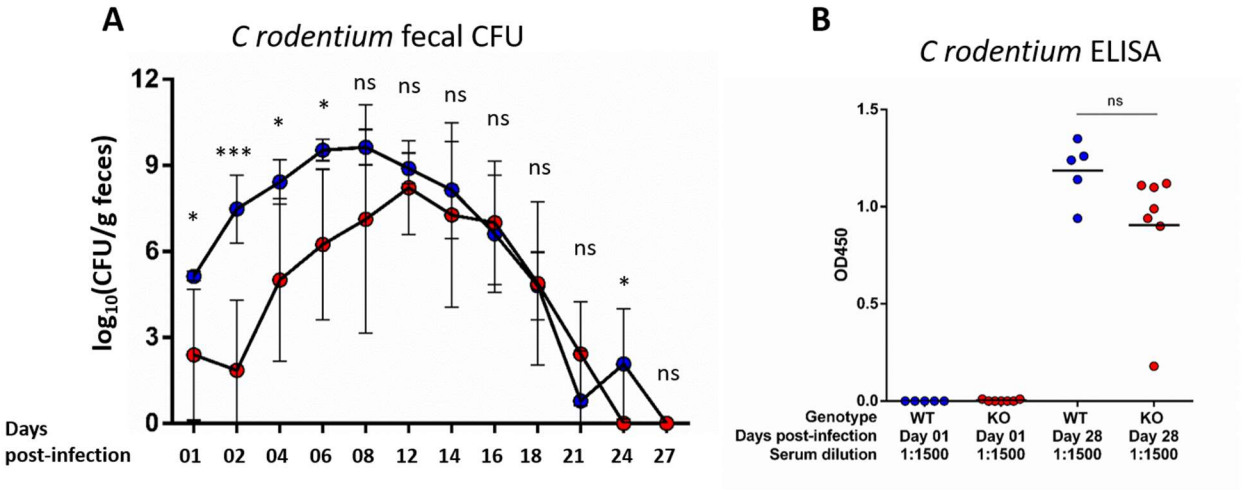

FIGURE 3.16. H2-Ob$^{-/-}$ **mice are resistant to C. rodentium infection via a mechanism independent of IgGs.** *H2-Ob*$^{+/+}$ and *H2-Ob*$^{-/-}$ were infected via oral gavage with 1E9 CFU and monitored several times per week for bacterial load in the gut via fecal pellet culture. (A) Bacterial load in the feces over the course of 4 weeks. (B) Anti-*C. rodentium* antibody titers measured via ELISA one day and 28 days post infection. Significance calculated using unpaired t-tests. ns= not significant, *=p<0.05, ***=p<0.001

Chapter 4: Investigation of the role of H2-O in predisposition to systemic and organ-specific autoimmunity

Preface

The data contained in this chapter have been recently published [64]. These studies were a collaboration between multiple graduate students. The studies concerning autoimmune phenotypes of *H2-Ob*$^{-/-}$ mice on the NOD and NZM backgrounds were performed by Jean Lee (Chervonsky Lab) with biochemical analysis of H2-M and H2-O levels done by the author. The EAE studies conducted at University of Chicago were done by the author (EAE studies conducted at Rutgers University were performed by Danielle Millick). Studies concerning infection of mice with MHV68 were performed by Kyle Stoltz. Only those figures to which I directly contributed to data generation are presented here.

Summary

It has been proposed that the function of H2-O (and HLA-DO) is to prevent autoimmunity, as it is a negative regulator of antigen presentation. However, no definitive reports of enhanced susceptibility to autoimmune disease in H2-O-deficient mice existed. Therefore, we tested the hypothesis that H2-O modulates the susceptibility of mice to autoimmune disease using three models: non-obese diabetic mice (spontaneous, organ-specific disease), B6.NZM tricongenic mice (spontaneous, systemic disease) and experimental autoimmune encephalomyelitis (EAE) in C57BL/6J mice (induced, organ-specific disease). There was no evidence of exacerbation of autoimmune disease in any model, suggesting prevention of autoimmune disease is not the role of H2-O in mice. However, the enhanced susceptibility of H2-O-deficient mice to the γherpesvirus MHV68 suggests the physiological role of this protein may be to restrict viruses that preferentially replicate in H2-O expressing cells.

H2-O helps control chronic infections rather than preempt autoimmunity

Jean Lee[1*], Emily Cullum[2*], Kyle Stoltz[3*], Niklas Bachmann[4], Zoe Strong[5], Danielle D. Millick[6] Lisa Denzin[6,7], Anthony Chang[5], Vera Tarakanova[3], Alexander Chervonsky[2,5,8§] and Tatyana Golovkina[2,4,8§]

[1]Committee on Cancer Biology, The University of Chicago, Chicago, IL, 60637

[2]Committee on Immunology, The University of Chicago, Chicago, IL, 60637

[3]Microbiology and Immunology, Medical College of Wisconsin, Milwaukee, WI 53226

[4]Department of Microbiology, The University of Chicago, Chicago, IL, 60637

[5]Department of Pathology, The University of Chicago, Chicago, IL, 60637

[6]Graduate School of Biomedical Sciences, Rutgers University, Piscataway, NJ 08854

[7]Child Health Institute of NJ, Department of Pediatrics and Pharmacology, Rutgers Robert Wood Johnson Medical School, The State University of NJ, New Brunswick, NJ, 08901

[8]Committee on Microbiology, The University of Chicago, Chicago, IL, 60637

*These authors contributed equally

[§]Address correspondence to T. Golovkina, Tel. (773) 8347988; e-mail address: tgolovki@bsd.uchicago.edu and A. Chervonsky, Tel (773)7021371: email address: achervon@bsd.uchicago.edu

Funding sources: This work was supported by PHS grant AI117535 to T. G. and L.K.D., by AI127411 to A.V.C., by P30 CA014599 to the University of Chicago, by the National Center for Advancing Translational Sciences of the National Institutes of Health through Grant Number UL1 TR000430 to the University of Chicago. Other support was provided by The Robert Wood Johnson Foundation (Grant 67038 to the Child Health Institute of New Jersey), and The Barile Children's Medical Research Trust (to L.K.D.).

Running Title: *H2-O does not preempt autoimmunity but controls γherpesvirus*

Abstract

H2-O (human HLA-DO) is a relatively conserved non-classical Major Histocompatibility Class II (MHCII)-like molecule. H2-O interaction with H2-M (human HLA-DM) edits the repertoire of peptides presented to T cell receptors by MHCII. It was long hypothesized that H2-M inhibition by H2-O provides protection from autoimmunity by preventing binding of the high affinity self-peptides to MHCII. The available evidence supporting this hypothesis, however, was inconclusive. A possibility still remained that the effect of H2-O-deficiency on autoimmunity could be better revealed by using H2-O-deficient mice that were already genetically predisposed to autoimmunity. Here, we generated and used autoimmunity-prone mouse models for systemic lupus erythematosus and organ-specific autoimmunity (Type 1 diabetes and multiple sclerosis) to definitively test whether H2-O prevents autoimmune pathology. Whereas our data failed to support any significance of H2-O in protection from autoimmunity, we found that it was critical for defense against a γherpesvirus, MHV68. Thus, we propose that H2-O editing of MHCII peptide repertoire may have evolved as a safeguard against specific highly prevalent pathogens.

Key Points

H2-O deficiency does not predispose to organ-specific or systemic autoimmunity

H2-O controls the establishment of a chronic γherpesvirus infection.

INTRODUCTION

The immune system has to maintain a delicate balance between efficient defense against pathogens and self-damaging inflammation. During an infection, pathogen-derived peptides are presented on the surface of professional antigen presenting cells (APCs) by major histocompatibility class II (MHCII) molecules to $CD4^+$T cells to initiate the adaptive immune

response. Peptide loading of MHCII molecules occurs in the endosomes and lysosomes of APCs and is catalyzed by H2-M, a non-classical MHCII-like heterodimer [65]. The final MHCII peptide array, however, is fine-tuned by another MHCII-like heterodimer, H2-O, which binds to H2-M and inhibits its function [13, 17, 18].

H2-O is an obligate αβ heterodimer, which in mice is encoded by the *H2-Oa* (*Oa*) and *H2-Ob* (*Ob*) genes [8]. Biochemical, structural, and functional analyses all supported the role of H2-O as a negative regulator of immune responses [13, 14, 17, 40, 66]. Moreover, H2-O-deficient mice and rare humans carrying loss-of-function alleles of DO generate potent neutralizing antibody responses against several viruses supporting this idea [15, 67].

Negative regulation of immunity by H2-O/DO led to prediction of its role as a guardian against autoimmunity, suggesting that autoimmune reactions should be found in H2-O/DO-deficient organisms. However, experimental evidence for autoimmunity in H2-O-deficient mice was not entirely compelling: the appearance of IgG2a anti-nuclear antibodies [18] was not confirmed by others [15, 17]; whereas a report of an enhanced development of experimental autoimmune encephalomyelitis (EAE) in B6.$Oa^{-/-}$ mice [44] had an unusually low disease score in the wild-type control mice. However, the possibility still remained that a role for H2-O in preventing autoimmunity could be more definitively shown in mice from autoimmune-prone backgrounds.

Experimental mouse models of autoimmunity have been developed for numerous human diseases, including organ-specific and systemic models. Spontaneous models of autoimmunity are of particular interest as they recapitulate many features of human diseases and are controlled by multiple (known and unknown) genes. Two broadly used models, the non-obese diabetic (NOD) mouse model of Type 1 diabetes (T1D) and the C57BL/6J.NZM (B6.NZM) model of systemic lupus erythematosus (SLE) [68], display these characteristics. Other models of autoimmunity rely on induction of disease *via* immunization, cell transfer, or other experimental manipulations. One example is an induction of experimental autoimmune

encephalomyelitis (EAE) in B6 mice immunized with MOG peptide in the presence of pertussis toxin [69].

To conclusively and definitively establish a role (or a lack thereof) for H2-O in autoimmunity, we used these three mouse models to test whether H2-O-deficiency would result in accelerated and/or exacerbated disease phenotypes. We found no significant enhancement of the disease phenotype in H2-O-deficient mice in all three models. Instead, we found that H2-O-deficient mice had an increased susceptibility to γherpesvirus MHV68. Therefore, we have to conclude that the function of H2-O is not in prevention of autoimmunity but is likely in controlling chronic viral infections.

RESULTS

H2-O does not protect against spontaneous organ-specific autoimmunity (myself and Jean Lee)

Developed in the 1970s, the NOD mouse model of T1D has been used extensively for understanding the genetic contributions to T1D [70]. T1D development in mice from this strain is dependent on multiple insulin-dependent diabetes (*Idd*) genetic loci [71]. The major contributor to T1D is *Idd1*, which contains the MHC genes on chromosome 17. The unique NOD MHC haplotype, $H2^{g7}$, is critical for development of diabetes in this strain [72]. In order to test whether H2-O deficiency would accelerate diabetes development in NOD mice, we used a CRISPR/Cas9 approach to produce H2-O-deficient NOD mice (Figure 1A). Targeting of the *Ob* gene led to the loss of Oβ protein but did not affect the levels of H2-M (Figure 1B). Diabetes development in NOD mice is a sexually dimorphic trait more penetrant in females [73, 74] and thus, diabetes incidence was tracked in female mice. Female NOD.$Ob^{+/-}$ and NOD.$Ob^{-/-}$ littermates had no difference in onset of overt diabetes or in overall disease penetrance (Figure 2A). Infiltration of the pancreatic islets by immune cells is a prerequisite to diabetes development [74]. To determine if insulitis was exacerbated in H2-O-deficient mice, H&E-stained sections from 13-week-old NOD.$Ob^{-/-}$ and NOD.$Ob^{-/+}$ mice were scored (Figures 2B and

2C). The differences in the distribution of insulitis scores observed between H2-O-deficient and H2-O-sufficient mice were not significant. If anything, NOD.*Ob*$^{-/-}$ mice had mildly reduced islet infiltration compared to NOD.*Ob*$^{+/-}$ mice. Taken together, these data demonstrate that H2-O does not influence the progression of T1D in NOD mice.

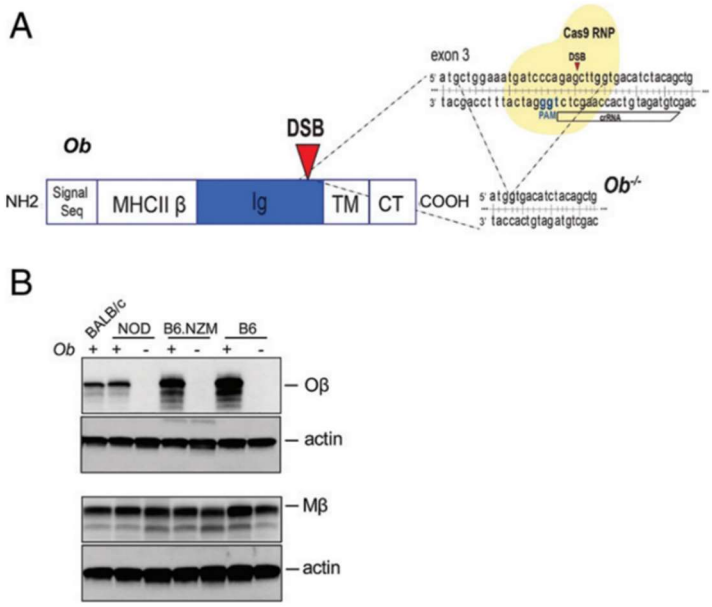

FIGURE 4.1. Generation of new H2-Oβ-negative mouse models of autoimmunity. (A) CRISPR/Cas9 targeting strategy for generation of NOD.Ob/ mice. (B) Loss of Ob in novel H2-O KO lines. Splenocyte lysates from indicated mouse strains were analyzed by Western blotting with Abs specific for the CTs of Mb and Ob proteins as well as with anti-β -actin Abs (loading control). BALB/c splenocytes served as the control for NOD splenocytes, as these strains carry an allele of Ob with the same CT sequence, which determines reactivity with anti-CT Ab. One of the two representative experiments. CT, cytoplasmic tail; DSB, double strand break; gRNA, guide RNA; MHCIIb, MHCIIb-like domain; Signal Seq, signal sequence; TM, transmembrane region.

H2-O does not protect against spontaneous systemic autoimmunity (Jean Lee, data not shown)

To address the contribution of H2-O to a systemic autoimmune disease, the New Zealand Mixed (NZM) B6J (B6.NZM) tri-congenic model was used. B6.NZM mice resulted from the transfer of three systemic lupus erythematosus (*Sle*) loci identified in New Zealand White (NZW) and New Zealand Black (NZB) onto the B6J background [75]. The hybrid NZM mouse is highly susceptible to an SLE-like disease which includes production of anti-nuclear Abs and

glomerulonephritis [68, 75]. Similar to NOD mice, SLE development in B6.NZM mice is a sexually dimorphic trait and is more penetrant in females [68]. Mice from the B6.NZM strain are overall B6J genetically with three loci, *Sle1, Sle2,* and *Sle3* present on chromosomes 1, 4, and 7, respectively, derived from NZM mice [68, 76, 77]. These mice possess the $H2^b$ haplotype of MHC like that of the conventional B6 mice [68]. To generate H2-O deficient B6.NZM mice, we crossed B6.NZM to B6.$Ob^{-/-}$ and confirmed that these mice lacked Oβ and thus H2-O, via Western blotting (Figure 1B) and had *Sle1-3* loci of the NZM background via PCR (Figure S1A). Female $Ob^{+/+}$ and $Ob^{-/-}$ B6.NZM mice were studied for three major autoimmune phenotypes at 8 months of age: 1) antinuclear antibody (ANA) titers (Figure 3A), 2) kidney glomerulonephritis (Figures 3B and S1B), and 3) kidney IgG and C3 complement deposition (Figures 3C and 3D). Measurement of these hallmarks of SLE-like autoimmune disease in multiple organ systems showed no differences between H2-O-deficient and -sufficient mice. Furthermore, no differences in splenic immune cell activation, a known and measurable precursor for SLE disease in B6.NZM mice [78-80], were observed. The frequencies of splenic T regulatory cells, T follicular helper cells and T follicular regulatory cells (Figures 3E, F and S2A) were similar between $Ob^{-/-}$ and $Ob^{+/+}$ B6.NZM mice. Furthermore, no significant differences were noted in frequencies of $CD69^+$ activated $CD4^+$ (Figure 3G) or in frequencies of activated and effector/effector memory $CD8^+$ T cells (Figures S1B and S2B). The absolute numbers of the CD4 subsets from Figure 3E-G, were also similar between the wild-type and the knock-out animals (Figure S1D). Follicular B cells and marginal zone B cells were present at similar frequencies (Figure 3H, I) and numbers (Figure S1C) in the spleens of $Ob^{-/-}$ and $Ob^{+/+}$ B6.NZM mice. Of all parameters measured, only splenic $CD4^+$ effector/effector memory T cells were slightly but significantly elevated in $Ob^{-/-}$ compared to $Ob^{+/+}$ B6.NZM mice (Figure 3J and S2E). This difference was not observed between age-matched B6.$Ob^{-/-}$ and B6.$Ob^{+/+}$ mice (Figure 3J) and, thus, was attributable to the H2-O-deficiency on the NZM background. In the absence of any evidence for augmented autoimmune pathology, however, the physiological relevance of

this elevation in $CD4^+$ activated memory T cells remains unclear. Overall, our data indicate that H2-O deficiency does not exacerbate SLE-like pathology in the B6.NZM model of autoimmunity.

H2-O does not protect against induced autoimmunity

In addition to models of spontaneous autoimmunity, we also tested whether H2-O deficiency would contribute to an acute onset of induced autoimmunity. EAE is a mouse model of multiple sclerosis (MS) and is induced by immunization of B6 mice (susceptible strain in this case) with a myelin oligodendrocyte glycoprotein (MOG) peptide emulsified in complete Freund's adjuvant (CFA) followed by the injection of pertussis toxin. MOG peptide is presented to T cells in the context of $I\text{-}A^b$ MHCII molecules, thus allowing for the use of B6.$Ob^{-/-}$ and B6.$Oa^{-/-}$ mice in testing for the role of H2-O in development of the inflammation in the CNS. Autoimmune infiltration leads to an ascending paralysis beginning in the tail approximately 9 days post-immunization that progresses to the hind limb and, in some cases, forelimb paralysis several days after symptom onset. To test whether H2-O-deficient mice were differentially susceptible to EAE compared to H2-O-sufficient mice, EAE was induced by immunization in B6.$Oa^{-/-}$, B6.$Ob^{-/-}$ and control B6J mice. Immunized mice were monitored for the next 28 days for the symptoms of neuroinflammation. No statistically significant differences in disease development in H2-O-deficient (B6.$Ob^{-/-}$ mice) compared to H2-O-sufficient mice were observed when all mice experimental mice from The University of Chicago and Rutgers University (males and females) were combined (Figure 4A, B) or only when female mice were compared (Figure 4C, D). Similarly, B6.$Oa^{-/-}$ mice did not develop EAE disease with kinetics or severity that was different from their controls (Figure 4E, F). A recent study [44] found that B6.$Oa^{-/-}$ mice were more susceptible to EAE than control B6J animals. However, that conclusion was based on a single experiment, in which control B6J mice developed very mild EAE disease (with average score 1; only 2 of 8 B6J mice had a disease score $\geq$ 2 and 4 of 8 did not develop any disease) which is far lower than the penetrance and disease scores published by other groups [81-83] and

observed in our study. Thus, in this inducible model of autoimmunity H2-O deficiency does not contribute to either disease development and severity.

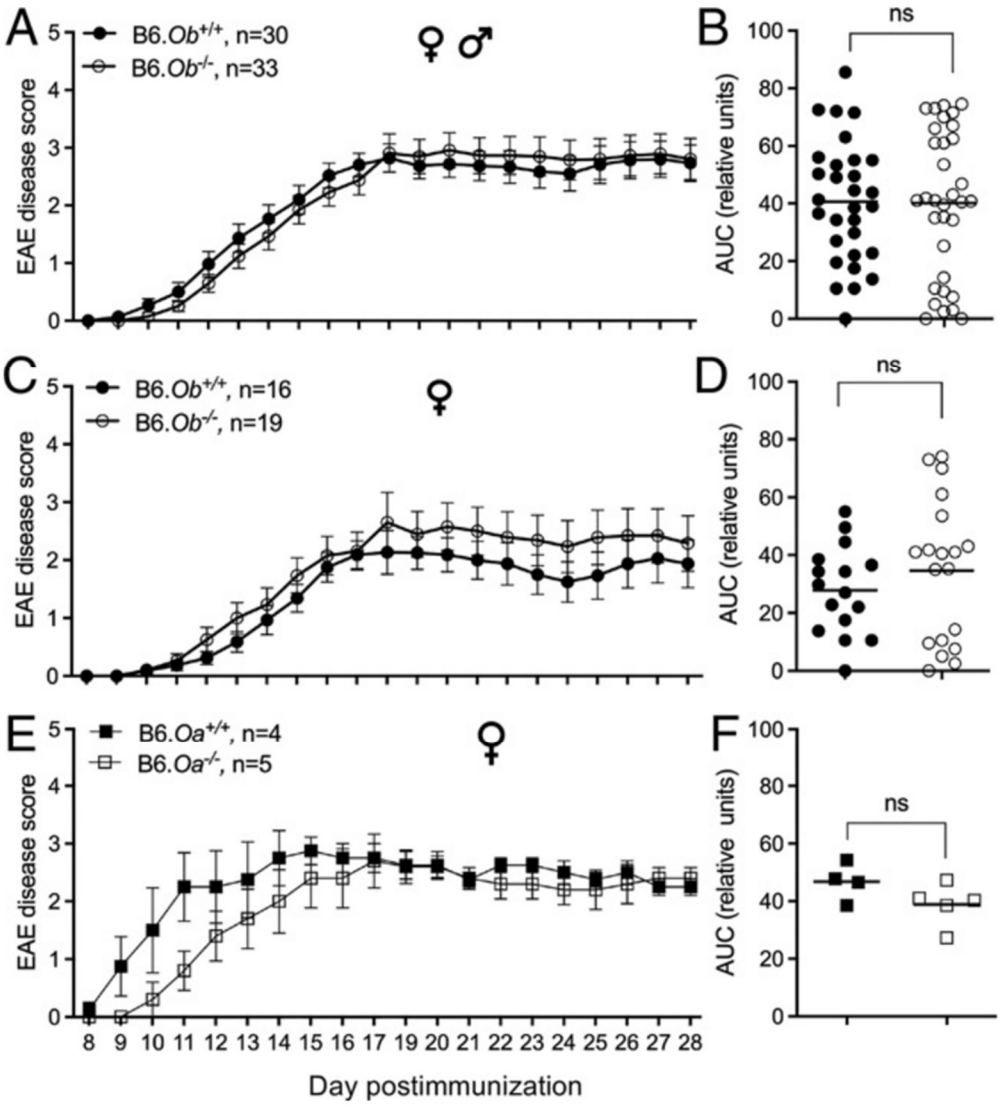

FIGURE 4.2. EAE development in B6 and B6.Ob$^{-/-}$ mice. Disease scores (A) and area under the curve (AUC) analysis (B) for male and female B6.Ob$^{+/+}$ and B6.Ob$^{-/-}$ mice. Data combined from three independent experiments performed at two institutions. (C) and (D) show females only. (E and F) is a similar analysis of B6.Oa$^{+/+}$ and B6.Oa$^{-/-}$ mice. Mice were immunized with MOG35-55 in CFA alongside pertussis toxin administration. Daily disease scoring started 8 d after immunization. Score 0/5 no paralysis, 1/5 limp tail, 2/5 partial hind limb paralysis, 3/5 total hind limb paralysis, 4/5 partial forelimb and total hind limb paralysis, and 5/5 death. Significance was calculated using an unpaired t test. Error bars indicate SEM.

H2-O contributes to control of a chronic γherpesvirus infection (Kyle Stoltz, data not shown)

Thus far we have not found a support for any substantial involvement of H2-O in prevention of autoimmunity. Moreover, our own findings in mice [15] and relevant human data [67] suggested that the loss of H2-O/HLA-DO function could be beneficial for promotion of strong neutralizing antiviral antibody responses. However, since H2-O is highly conserved throughout mammalian evolution [6, 84], its function must be important. To search for such a function, we broadened the scope of testing an importance of H2-O in viral infections.

For that, we turned to the mouse βherpesvirus 68 (MHV68, also known as murid herpesvirus 4), a natural rodent pathogen which shares high levels of genetic conservation with Epstein-Barr virus (EBV) and Kaposi Sarcoma-associated herpesvirus (KSHV) [85-87] infecting humans. Like EBV, MHV68 initially infects naïve B cells and drives both infected and bystander B cells to become germinal center (GC) B cells [88-90]. Virally-induced GC B cells require T follicular helper (Tfh) cells [91, 92] and harbor both virus-specific and virus non-specific B cells. [91, 93, 94]. These GC B cells transition to memory B cells that support life-long latent infection, or to plasma cells, where the viral 'latent to lytic' switch occurs [95, 96]. After a brief acute lytic replication in a naive host, MHV68 establishes latency in several organs, including the spleen [97, 98]. Viral latency in the spleen peaks at 14 to 18 days post-infection, with most of the latent virus being present in the germinal center B cells [99, 100].

To determine if H2-O has a role in controlling γherpesvirus infection, B6.$Ob^{-/-}$ and B6.$Ob^{+/+}$ mice were infected with MHV68, and parameters of viral latency and reactivation were determined at 16 days post-infection. To compare the frequencies of latently infected splenic cells in B6.$Ob^{-/-}$ and B6.$Ob^{+/+}$ mice, we performed a limiting dilution PCR assay amplifying the MHV68 genome from pooled cells in multiple replicates. The frequency of latently infected cells in a given sample was determined by a number of cells added per well needed to achieve 62.5% MHV68 positivity of all replicates. Splenocytes from infected B6.$Ob^{-/-}$ mice contained about 6 times more latently infected cells as B6.$Ob^{+/+}$ splenocytes (Figure 5A). Similarly, for the *ex vivo* reactivation assay, splenocytes were added to microplate wells containing mouse embryonic fibroblasts (MEFs),

and the cytopathic effect of the virus (loss of viable MEFs) was scored after three weeks of co-culture. The frequency of infected cells was determined similarly to the PCR assay. The viral reactivation was 5 times higher in B6.*Ob*$^{-/-}$ mice than in B6.*Ob*$^{+/+}$ mice (Figure 5B). Furthermore, flow cytometry analyses of individual spleens demonstrated that compared to B6.*Ob*$^{+/+}$ mice, B6.*Ob*$^{-/-}$ mice had significantly increased frequencies of GC B cells, Tfh cells, and class-switched plasma cells (Figures 5C-E, gating strategy is shown in Figure S3), reflecting the γherpesvirus-driven B cell differentiation. Thus, functional H2-O attenuates the establishment of chronic MHV68 infection.

DISCUSSION

By interacting with H2-M/HLA-DM, H2-O/HLA-DO edits the repertoire of peptides presented by MHCII to T cells. Indeed, small but significant differences were found in MHCII peptidomes between H2-O/DO-deficient and DO-sufficient cells with the latter containing many peptides that were absent from or present at much lower frequency in the H2-O/DO-deficient cells [23, 44]. The data suggested a potential predisposition to autoimmunity in the absence of H2-O/DO due to an aberrant presentation of some high affinity self-peptides by MHCII or due to the loss of some low affinity tolerogenic peptides. Some findings of autoimmune phenotype [18] were not confirmed by others [15, 17], whereas other findings were obtained using control mice developing very mild disease [44]. Since we were not convinced that prevention of autoimmunity is the major function of H2-O/DO, we aimed at testing this hypothesis in three distinct disease models, in which H2-O deficiency was introduced in animals already prone to autoimmunity. That should have increased the chances to detect higher susceptibility of H2-O-deficient to autoimmunity. These models included spontaneous autoimmunity (T1D in NOD mice and SLE in B6.NZM mice), as well as induced autoimmunity (EAE in B6, B6.*Oa*$^{-/-}$ and B6.*Ob*$^{-/-}$ mice). In sum, except for a small increase in CD4^{+} T cells with memory phenotype in B6.NZM.*Ob*$^{-/-}$ mice compared to B6.NZM mice (model of SLE), which had no visible effect on any other parameters

of pathology reflecting disease severity, we found no evidence in favor of H2-O being a negative regulator of autoimmunity. This small increase might be a result of interaction between *Ob* and an unknown gene mapped in one of the three SLE loci, which may be interesting to dissect in the future.

Interestingly, overexpression of human DO in NOD mouse dendritic cells led to the amelioration of T1D disease development [34]. These studies showed that protection was mediated by the increased propensity of human DO to suppress mouse H2-M function and, hence, presentation of diabetogenic peptides. Apparently, endogenous mouse H2-O that co-evolved with H2-M was not capable of reaching such level of suppression of H2-M function.(the point of this sentence is unclear to me) Thus, at the steady state, even if the loss of H2-O-mediated MHCII peptidome editing abrogates the removal of self-peptides that can drive autoimmune disease, other major mechanisms of self-tolerance (negative selection, lack of co-stimulatory signals, Tregs etc.) must be sufficient to prevent activation of autoreactive T and B cells.

Since our data do not support a role for H2-O as a protector from autoimmune disease development, we posit that the key to understanding the functions of H2-O/HLA-DO should be found by studying the involvement of these molecules in resistance to pathogens. However, this idea seemingly does not seat well with our own previous findings that H2-O-deficient mice produced potent neutralizing antibody responses against MMTV, a mouse retrovirus and some rare individuals with loss of function DOA and DOB alleles clear HCV and HBV [15, 67]. Moreover, the presence of some gain of function alleles of DOA and DOB in humans correlated with persistence of HCV and HBV [15, 67]. Therefore, the presence of functional H2-O/DO genes appears to benefit some pathogens and yet, these genes are highly conserved among all mammals [6]. One reasonable explanation for H2-O/DO conservation throughout mammalian evolution could be in its possible role in protection from some highly prevalent pathogens. Such pathogens are likely to be intracellular, targeting MHCII-positive cells that can present an array of pathogen-derived peptides. Indeed, it has been found that mice of I/St strain carrying a

defective *Ob* allele were uniquely sensitive to mycobacteria tuberculosis (MTB) compared to B6 and A/Sn mice carrying functional alleles of *Ob* [101, 102]. Although MTB can cause an antibody response [103], this response cannot provide pathogen clearance and could even become detrimental by enhancing pathogen uptake through Fc receptor-mediated phagocytosis [104]. In the current study, we have identified one such microorganism – γherpesvirus MHV68, a prototype of cancer-associated human γherpesviruses such as EBV and Kaposi's Sarcoma-associated herpesvirus (KSHV) [105] which is controlled by H2-O.

γherpesviruses are highly prevalent in multiple mammalian species. These viruses infect B cells and rely on robust B cell differentiation reaction to establish a life-long infection of memory B cells [106]. Although B cells are usurped by the virus as hosts of latent infection and viral reactivation, they are required as APCs [107] for inducing virus-specific $CD8^+$ and $CD4^+$ T cell responses [108-110]. $CD4^+$ T cells have a dual role during γherpesvirus infection. Whereas $CD4^+$ T cells are proviral during establishment of latency (as they are required for GC reactions induced by the virus ([92])), they are (together with $CD8^+$ T cells) anti-viral during the control of reactivation of the virus from latency ([111]). We found that MHV68-mediated GC B cell and Tfh cell expansion was significantly increased in H2-O-deficient mice compared to H2-O-sufficient mice (Figures 5C-5E) coinciding with a rise in the number of latently infected cells (Figure 5A). These results indicate that proper expression of H2-O puts the pressure on the virus during the establishment of latency restricting the overall pathogen burden.

Most of adults worldwide are chronically infected with EBV and KSHV reaches 50% seroprevalence in Sub-Saharan Africa and approximately 10% in central Europe or Northern America [105]. These viruses can cause severe illnesses in immunocompromised patients, however, they are well controlled by the immune system in most immunocompetent hosts. Our data suggest that the control of γherpesviruses is dependent on the presence and proper functioning of the HLA-DO. The precise mechanism by which H2-O/DO controls the establishment of viral latency is yet to be determined, but one can speculate that it is based on

reduction of DM-dependent presentation of high affinity peptides leading to negative regulation of GC reactions triggered by the $CD4^+$ T cells.

Chapter 5: Investigation of the role of H2-O in antibody responses against retroviruses in neonatal mice infected via the natural oral route.

Preface

The data in this chapter have been recently published [46]. Many of the data in this paper were generated by other authors, and are outside the scope of this thesis. Those data which were generated by the author, with help from Tatyana Golovkina, are presented here as they relate to the influence of *H2-Ob* on antibody responses against retrovirus acquired via the natural oral route by neonates.

Summary

Previous work in the laboratory [112] has shown that C57BL/6J mice that are infected with MMTV via viremic foster mothers are unresponsive to MMTV antigens upon immunization as adults. This tolerance to viral antigens allows the virus to persist indefinitely in these mice. We wanted to understand to what extent this tolerance depends on H2-O. We used *H2-Ob*$^{-/-}$ and wild-type controls fostered on viremic mothers and immunized with MMTV and observed that *H2-Ob*$^{-/-}$ mice are incompletely tolerant of viral antigens. We also show that *H2-Ob*$^{-/-}$ mice appear to be completely tolerant to other dietary antigens, such as ovalbumin and soy protein, suggesting this incomplete tolerance is virus-specific and viral tolerance may be induced by the virus via a mechanism dependent on H2-O or H2-Oβ. In order to better understand how this state of tolerance is maintained by the immune system, we took a splenocyte transfer approach. We transferred wild-type or *H2-Ob*$^{-/-}$ splenocytes into neonatally infected (i.e. tolerant) adult mice to ask if transferred splenocytes would produce antibodies in the tolerant environment of the recipient. We observed that the *H2-Ob*$^{-/-}$ transferred splenocytes did produce antibodies in the tolerant host, suggesting H2-O-dependent tolerance may be maintained in via a cell-intrinsic mechanism.

Results

In the vast majority of experiments conducted in the lab, infection of mice with retroviruses is done via intraperitoneal injection of purified viral particles. The natural route of infection for both MMTV and MuLV is via breastmilk, although mice can become infected with MuLV via biting, scratching, or fighting which results in exposure of blood to infectious bodily fluids.

Previous work in the lab established that neonates infected with MMTV are tolerant to antigens as adults [112], meaning no virus-specific antibody response is mounted even after immunization of purified virus in the presence of CFA. We were specifically interested in understanding the role of H2-O in this neonatal form of tolerance, as clearly loss of H2-O is sufficient to prevent this tolerance from forming in adult mice.

These results were recently published [46], but will be summarized in below.

To test the contribution of H2-O to the establishment of tolerance to viral antigens in neonates, we produced uninfected *H2-Ob*$^{+/+}$ and *H2-Ob*$^{-/-}$ pups and placed them with a viremic foster mother. Both H2-O-sufficient and H2-O-deficient mice failed to produce antibodies upon infection alone in the absence of immunization, indicating H2-O deficiency alone is not sufficient to prevent formation of tolerance to viral antigens in the neonate (this finding is also explored in detail in [46], but those experiments outside the scope of this chapter were performed by other co-authors) (**Figure 5.1**).

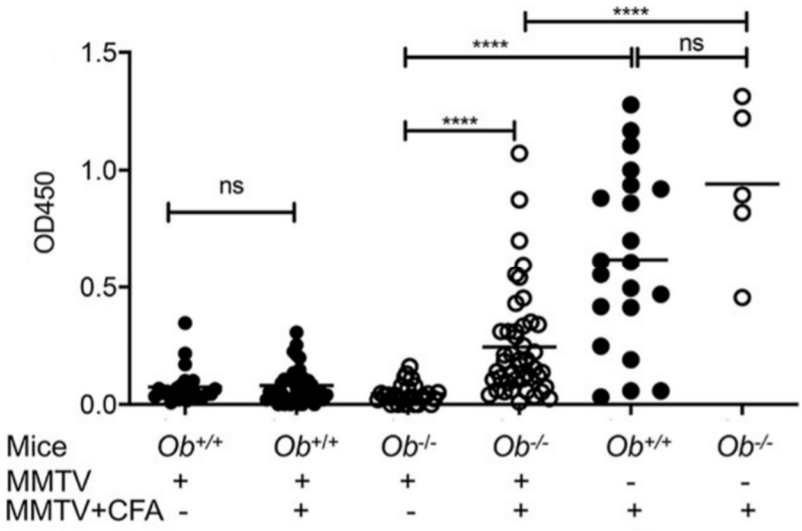

FIGURE 5.1. Neonatally infected Ob$^{-/-}$ mice fail to respond to infection, but are not fully tolerant to viral antigens later in life. B6 mice of indicated genotypes infected by fostering on MMTV(LA)-infected females were immunized with Triton X-100-treated MMTV(LA) virions in complete Freund's adjuvant (CFA) at 8 weeks of age and bled at the age of 3 months along with unimmunized mice. Production of specific Abs to viral antigens was tested by ELISA. Uninfected mice were immunized with MMTV(LA) proteins in CFA as controls. P values were calculated using the Mann-Whitney test. ns, not significant; ****, $p < 0.0001$.

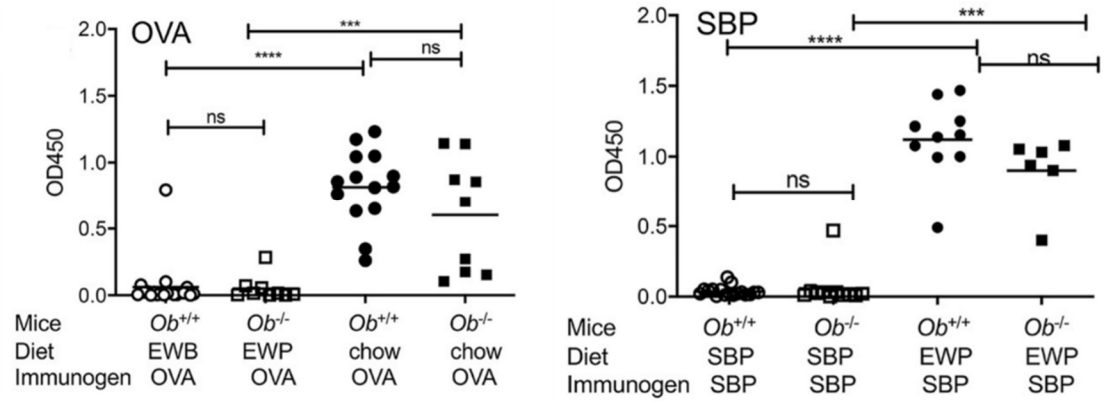

FIGURE 5.2. *H2-Ob*$^{-/-}$ mice are tolerant to non-viral antigens acquired via the oral route. Pregnant B6.*Ob*$^{-/-}$ and B6.*Ob*$^{+/+}$ females were fed either an egg white protein diet (EWP, in which the major protein is OVA) (top graph) or soybean protein diet (SBP) (bottom graph), so the pups were exposed to the specific Ag-containing food since birth. At 8 weeks of age, mice were immunized with OVA or SBP in CFA, respectively. Antibody responses to OVA and SBP were measured via ELISA. As normal mouse chow contains SBP, control uninfected mice were fed an EWP diet (bottom graph). p values were calculated using the Mann-Whitney test. ns, not significant; ***, $p < 0.001$; ****, $p < 0.0001$.

Interestingly, H2-Ob-deficient mice do exhibit some loss of this tolerance, evidenced by their elevated antibody response to immunization compared to *H2-Ob*$^{+/+}$ mice. However, this break of tolerance is not complete, as uninfected *H2-Ob*$^{+/+}$ and *H2-Ob*$^{-/-}$ mice mount more robust antibody responses to immunization. Importantly, these groups of uninfected mice do not differ from one another, indicating no intrinsic difference in response to immunization in general.
To determine if H2-O-deficient mice were more susceptible to loss of tolerance to antigens acquired via the oral route, we placed *H2-Ob*$^{+/+}$ and *H2-Ob*$^{-/-}$ pregnant mothers on diets containing either ovalbumin (OVA) or soy as the protein source and weaned the subsequent litters onto these diets. H2-O-deficient mice did not mount a response to either dietary antigen, indicating loss of tolerance is specific to MMTV antigens (**Figure 5.2**).

Lastly, we were interested in understanding on what cellular level this tolerance is maintained. We hypothesized that tolerance would either be maintained by T cells preventing virus specific antibodies from being produced or by B cells intrinsically preventing secretion of antiviral antibodies. To test this, we took a splenocyte transfer approach. We generated CD45.1+ IgG2a+ B6 mice which were neonatally infected via foster mothers and administered a sublethal dose of irradiation. After irradiation, CD3-depleted splenocytes from CD45.2+ IgG2c+ *H2-Ob*$^{+/+}$ or *H2-Ob*$^{-/-}$ mice were transferred, creating chimeric animals containing lymphocytes from both recipient and donor animals. Recipient cells are CD45.1+ and secrete IgG2a antibodies while donor cells are CD45.2+ and secrete IgG2c antibodies. Mice were confirmed to be chimeric, and although CD3-depletion of donor splenocytes was performed, residual CD3+ cells proliferated in recipient animals to result in chimeric T cell and B cell compartments (**Figure 5.3**). MMTV-specific IgG2c antibody titers were higher in mice receiving *H2-Ob*$^{-/-}$ splenocytes than in mice receiving *H2-Ob*$^{+/+}$ splenocytes, indicating that tolerance to viral antigens may B cell intrinsic, as recipient-derived tolerant lymphocytes were not capable of blocking antibody production (**Figure 5.4**).

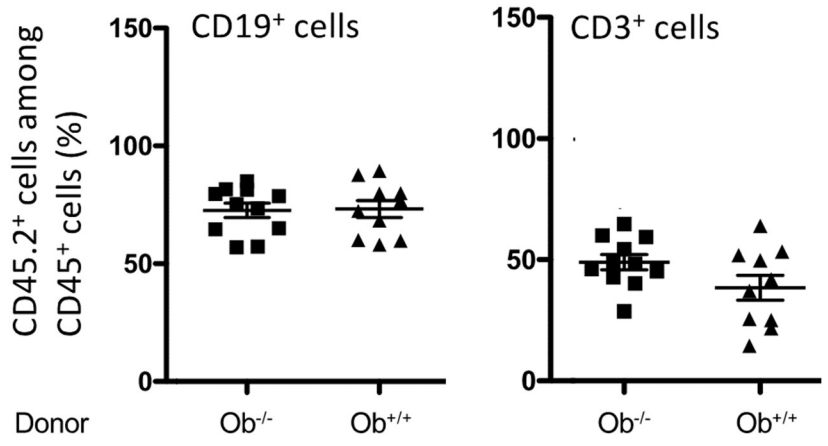

FIGURE 5.3. Recipient mice are chimeric in both B cell and T cell compartments. Peripheral white blood cells were stained with antibodies recognizing CD45.1 (recipient CD45 allele), CD45.2 (donor CD45 allele), CD3 (T cells), and CD19 (B cells). Data are expressed as percent of total CD45+ cells that are CD45.2+ (i.e. of donor origin) among CD19+ cells (left) or CD3+ cells (right). Data indicate that both the B cell and T cell compartments in recipient animals are chimeric.

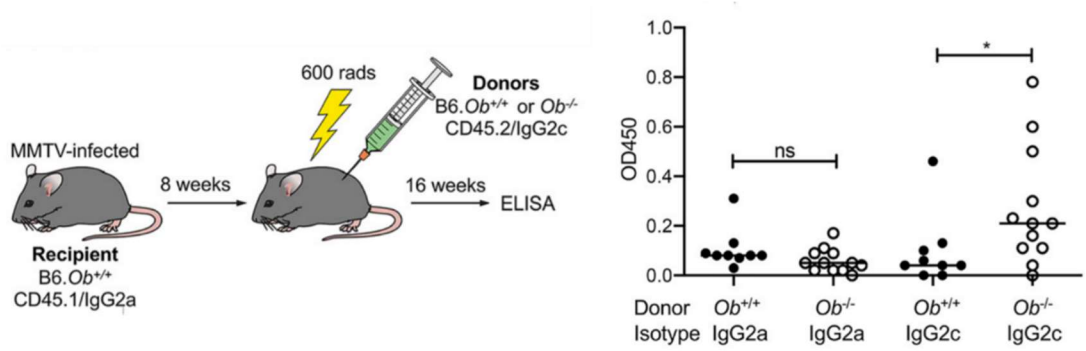

FIGURE 5.4. Experimental approach to test whether Ob-deficient cells from adult mice were responsive to the virus when placed into virus-tolerant mice. Chimeras contained 50 to 85% of B cells of the donor origin (data not shown). (D) Chimeric mice were bled 16 weeks post-transfer, and their sera were tested for antivirus Abs by ELISA. Either IgG2c (donor-related)- or IgG2a (recipient-related)-specific secondary Abs were used to develop ELISA. Results are expressed as the mean OD. p values were calculated using the Mann-Whitney test. ns, not significant; *, $p < 0.05$

MATERIALS AND METHODS

Mice

B6.SJL-Ptprca Pepcb/BoyJ (B6.CD45.1^{+}) and B6.Cg-Gpi1a Thy1a Igha/J (IgG2a^{+}), purchased from The Jackson Laboratory (JAX), were crossed and CD45.1-, IgG2a-positive mice were further intercrossed to produce B6.CD45.1 IgG2a mice. I/LnJ, C57BL/6J (B6) and BALB/cJ (BALB) (JAX) were bred and maintained at The University of Chicago. C3H/HeN (C3H) MMTV-free mice were originally purchased from the National Cancer Institute Frederick Cancer Research Facility, Frederick, MD, and maintained in colony at The University of Chicago. C3H^{vic1RR}, BALB^{vic1RR} and C3H^{vic1RR} congenic lines carrying the non-recombinant *vic1* locus from I/LnJ mice, and B6.*Ob*$^{-/-}$ mice were described in [15].

I/LnJ, C57BL/6J (B6J), C57BL/6NJ (B6N), and CAST/Ei were purchased from The Jackson Laboratory (TJL) and bred at The University of Chicago. B6J.*H2*-*Ob*$^{-/-}$ mice (line 134) and B6$^{vic1I/LnJ}$ congenic mice carrying the non-recombinant virus infectivity controller 1 (*vic1*) locus from I/LnJ mice were generated by us and have been described previously [15]. C3H/HeN MMTV-free mice were originally purchased from the National Cancer Institute Frederick Cancer Research Facility, Frederick, MD, and maintained at The University of Chicago. In addition, colonies of B6J, B6J.*H2*-*Oa*$^{-/-}$ [17], B6J.*H2*-*Ob*$^{-/-}$ [15], B6J.*H2*-*Ma*$^{-/-}$ [113] were maintained at the animal facility of Rutgers University. For bone marrow chimera (BMC) experiments, B6N, B6J and B6.129S2-Ighm^{tm1Cgn}/J (B6J.μMT) were purchased from TJL and maintained in the Rutgers University Animal Facility.

NOD/ShiLtJ (NOD), C57BL/6J (B6), B6;NZM-*Sle1*$^{NZM2410/Aeg}$ *Sle2*$^{NZM2410/Aeg}$ *Sle3*$^{NZM2410/Aeg}$/LmoJ (B6.NZM) mice were purchased from The Jackson Laboratory (TJL). B6.*Ob*$^{-/-}$ produced by us [15] were maintained at The University of Chicago, at Rutgers University and at Medical College of Wisconsin (MCW). *B6.Oa*$^{-/-}$ mice [17] were maintained at Rutgers University. NOD.*Ob*$^{-/-}$ mice were produced at Transgenic Facility of The University of Chicago using CRISPR/Cas9

technology. The 5'CTGTAGATGTCACCAAGCTC3' guide targeting exon 3 was used to produce NOD.*Ob*$^{-/-}$ mice. Mice from one line (#19), which have a 22bp deletion in the exon 3, were used in the studies. Founder of the line mouse #19 was crossed to NOD mice to ensure the germ-line transmission of the KO allele. Heterozygous female mice were crossed to homozygous males to generate homozygous and heterozygous mice inheriting the same microbiota from their mothers.

B6.NZM mice were crossed to B6.*Ob*$^{-/-}$ and resulting B6.NZM.*Ob*$^{-/+}$ mice were intercrossed to obtain B6.NZM.*Ob*$^{-/-}$ and B6.NZM.*Ob*$^{+/+}$ mice. PCRs specific for the NZM *Sle1/2/3* loci mapped to chromosomes 1, 4, and 7 were done with primers at proximal, intermediate and distal locations of each of the loci using the following primers. Proximal *Sle1* forward: GTGTCTGCCTTTGCACCTTT; proximal *Sle1* reverse: 5'CTGCTGTCTTTCCATCCACA3'. Intermediate *Sle1* forward: 5'TCCACAGAACTGTCCCTCAA3'; intermediate *Sle1* reverse: 5'ATACACTCACACCACCCCGT3'; distal *Sle1* forward: 5'CTGACCTCCACACGACCC3'; distal *Sle1* reverse: 5'GCTTGGGAAACTGGATGAAA3'. Proximal *Sle2* forward: 5'TGGCCAACCTCTGTGCTTCC3'; proximal *Sle2* reverse: 5'ACAGTTGTCCTCTGACATCC3'. Intermediate *Sle2* forward: 5'GGCTTTGCAATGCTATGCAT3'; intermediate *Sle2* reverse: 5'TGGCAGGAGGTATGACAGAA3'. Distal *Sle2* forward: 5'GCTTGCTTTAGGAGTGTGCC3'; distal *Sle2* reverse: 5'TATTTGCTCTCCATTTCCCC3'. Proximal *Sle3* forward: 5'CCAGACCATCTGATCCAGATC3'; proximal *Sle3* reverse: 5'GGAGGTTGCAGTGAATTCAAG3'. Intermediate *Sle3* forward: 5'CCCACCAGAGATCACCAAGT3'; intermediate Sle3 reverse: 5'CACAATGAAGGCTGAAAGCA3'. Distal *Sle3* forward: 5'CACTTGGGGAACGTCAAGAC3'; distal *Sle3* reverse: 5'TGTAGACCATAGCCCATAAGCC3'. Only PCRs with distal and proximal primers are shown in Figure S1C. C.B10-H2b/LilMcdJ (BALB/c mice carrying the H2b locus derived from C57BL/10 mice, i.e. BALB.B mice) (stock #001952) were purchased from Jackson Laboratories (Bar Harbor, ME).

Production of B6 Ob knock-in mice

B6J mice with single and combination amino acid substitutions found in I/LnJ Ob were generated using a CRISPR/Cas9 approach. Two single guide RNAs (CTGTAGATGTCACCAAGCTC and sgRNA: CACTTGACACTTATGTCCCC) were used to target the Ig domain to replace S, V, and L with
N, I, and H amino acids, and two single guide RNAs (AGAATGAGACTCTCTCTTG and GATCTTACTAGGGTTGAGAA) were used to target the cytoplasmic domain to replace ES with KL. Guide sites were identified using Integrated DNA Technologies' selection tool (https://www.idtdna.com/site/order/designtool/index/CRISPR_CUSTOM). Individual guide sites were selected based on their on-target scores and off-target scores. The 500-bp ssDNA oligos containing sequences corresponding to the knock-in (KI) amino acids were coinjected with the RNA guides, and Cas9 was injected into fertilized B6J embryos at Transgenic/Embryonic Stem Cell Technology Mouse Core Facility at The University of Chicago and at TJL. The founder mice were identified by PCR. The carriers of the KI Ob alleles were bred to B6Jmice for two generations and heterozygous mice from each line were intercrossed to produce Ob KI homozygous mice. Genomic DNA and splenic cDNA produced from the Ob KI alleles were sequenced to confirm mutations. Wild-type (*H2-Ob*$^{+/+}$) (*H2-Ob*$^{+/+}$ / *H2-Ob*$^{+/+}$ and *H2-Ob*$^{+/+}$ /KI) control B6J mice were generated from either breeding the colony of B6J mice or from breeding Ob.KI/+ × Ob.KI/+ mice.

Generation of BMPR2 knock out and knock in mice

B6J.Bmpr2KI mice were produced at the Transgenic and Embryonic Stem Cell Core of the University of Chicago using CRISPR/Cas9 technology. The 5'-CACACAGAATTACCACGAGGAGG-3' guide (final concentration 100ng/uL in injection mixture,

purchased from Integrated DNA Technologies) targeting exon 7 was coinjected into embryos along with the homology directed repair template oligonucleotide

5'-

AATGTTTGATATCTTTTTTCCTTTATACAGGGATCTCTGTGCAAATATCTGAGTCTCCACACA AGTGATTGGGTAAGCTCTTGCCGTCTGGCTCATTCTGTGACTAGAGGACTGGCTTATCTTC ACACAGAATTACCACGAGGAGGTAAGATGAATGAAATTTTAATCATATTTTAGAAGAAAAAT AATAATTTATACTG-3' (final concentration 120ng/uL in injection mixture, purchased from Integrated DNA Technologies). Genotyping was performed with PCR primers flanking the HDR template (Forward: TGCCTTTTCTTGTTGAAGCA, Reverse: GTTTCTTCATGCTGGATCTTTCA) to identify insertions and deletions and Sml1 digestion (New England Biolabs, cat# R0597S) to identify the presence of the KI allele.

FACS analysis

To measure viral infection, mononuclear PBLs were stained with FITC-coupled mAbs against the $V\beta6^+$ TCR chain (BD Biosciences). Anti-CD4 Abs coupled to PE (BD Biosciences) were used in the second dimension. Leukocytes were recovered from heparinized blood samples by centrifugation through a Ficoll-Hypaque cushion. PBLs were analyzed using a Fortessa (BD Biosciences) flow cytometer and the FlowJo software (BD).

To measure MHCII-CLIP, H2-M, and H2-O levels, the following monoclonal Abs for FACs analysis were purchased from eBiosciences or BD Biosciences: CD19-PE (clone 1D3), CD11c-PE-Cy7 (clone HL3), MHCII-biotin (clone M5/114) and CD3-PerCP-Cy5.5 (clone 145-2C11). Strepavidin-Alexa 647 was purchased from Molecular Probes. The α-Oβ cytoplasmic tail specific mAb Mags.Ob3 [114], the α-H2-M specific mAb 2C3A [114] and the $I\text{-}A^b$-CLIP-specific monoclonal Ab 15G4 [17] (provided by A. Rudensky, Memorial Sloan Kettering Cancer Center)

were purified from bioreactor supernatants using standard Protein G chromatography and then conjugated with Alexa 647, Alexa 488, or biotin, respectively (ThermoFisher Scientific). Single cell suspensions of splenic cells were blocked with mouse Fc Block (BD Biosciences) plus normal mouse sera and incubated at 4ºC with Abs specific for surface proteins for 30 min followed by washing. After washing, cells were incubated with streptavidin-Alexa 647 for 20 min at room temperature, washed and analyzed by flow cytometry. For intracellular measurement of H2-M and H2-O, cells were surface stained and fixed and permeabilized (BD Cytofix/Cytoperm™ Fixation/Permeabilization Kit) prior to the addition of Abs, washing, and analysis. For FACS analysis where both splenic B cells and dendritic cells were analyzed, spleens were digested in 400 U/ml collagenase D and 100 mg/ml DNase I for 30 min at 37ºC prior to blocking and staining. Data was acquired using a BD LSRII cytometer and analyzed using FlowJo software (BD Biosciences). Dead cells (DAPI or Zombie dye; BioLegend) and doublets were excluded from analyses. For experiments analyzing only splenic B cells, B cells were identified as $CD19^+$. For experiments analyzing both B cells and DCs, B cells were identified as $CD3^-$ $CD11c^-$ and $CD19^+$ and DCs identified as $CD3^-$ $CD19^-$ and $CD11c^+$. Staining to measure MHCII and MHCII-CLIP ($I\text{-}A^b$-CLIP) were always performed as two separate stains since the individual Abs to each of these species interfered when stained simultaneously. To correct for small differences in total MHCII levels among different samples, the ratio of MHCII-CLIP:(total) MHCII was calculated by dividing the gMFI obtained for MHCII-CLIP by that obtained for MHCII for each independent sample. In order to compare multiple independent experiments, the MHCII-CLIP:MHCII ratio for control mice was set to 100%, and the MHCII-CLIP:MHCII ratios for all other samples were normalized to this control. Three-five control mice were included in each independent experiment.

To measure T cell activation, red blood cells-depleted splenocytes were stained with: anti-CD4-FITC (eBioscience), anti-CD8a-PacBlue (Invitrogen), anti-CD62L-PECy7 (BioLegend), anti-

CD44-APCCy7 (BioLegend), anti-CD69-PE (Invitrogen) Abs in the presence of Fc-Block (BD Biosciences). To compare B cells subpopulations, the same samples were stained with: anti-B220-APCCy7 (BioLegend), anti-CD93-APC (BioLegend), anti-CD23-PECy7 (BioLegend), anti-IgM-eF450 (Invitrogen), anti-CD21/35-FITC (BioLegend) and anti-CD1d-PE (Invitrogen) Abs in the presence of Fc-Block. To compare Tfh, Tfr and Treg cell populations, the samples were stained with: anti-CD4-PacBlue (BioLegend), anti-CXCR5-APC (BioLegend), anti-PD-1-FITC (Invitrogen), anti-Foxp3-PECy7 (Invitrogen) and anti-Bcl6-PE (Invitrogen). For MHV68 studies, the following antibodies were purchased from Biolegend (San Diego, CA): CD3 (17A2), CD4 (RM4-5), CD95 (Jo2), PD-1 (29f.1A12), B220 (RA3-6B2), GL7 (GL-7). CXCR5 (2G8) was purchased from BD Pharmingen (San Jose, CA). All stainings mentioned above were preceded by incubating cells with Fc-Block (BD Biosciences). For intracellular staining, cells were permeabilized using Foxp3/Transcription factor staining buffer (Invitrogen). Dead cells were gated out by staining with Propidium Iodide (Sigma-Aldrich) or Zombie Aqua (BioLegend). Data were acquired using Fortessa flow cytometers (Becton, Dickinson & Company). Data analysis was performed using *FlowJo*™ software (Becton, Dickinson & Company).

Virus neutralization

Sera from MMTV-infected *vic1*^{RR}, *vic1,2*^{RR} and control mice were tested for their ability to neutralize virus. Each serum diluted at $1x10^{-1}$ with PBS was incubated with purified MMTV(LA) for 2 h at room temperature and injected into 2 footpads of BALB/cJ mice. Four days after injection, cells isolated from the draining popliteal lymph node were analyzed by FACS for the percentage of $CD4^+/V\beta6^+$ T cells among $CD4^+$ T cells. MMTV-encoded SAg stimulates cognate T cells to proliferate during initial stages of infection [115] and thus, the proliferation of SAg cognate T cells was used as indicator of virus infectivity [116]. The amount of virus prep used in the experiments was first titrated to give an increase from 10% to 25% of SAg-reactive T cells four days after virus injection. Neutralization (%) was calculated as follows: (a-c)-(b-c):(a-c)X100

where a= mean of $CD4^+/V\beta6^+$ (%) in mice injected with virus plus sera from uninfected mice, b= mean of $CD4^+/V\beta6^+$ (%) in experimental mice and c=mean of $CD4^+/V\beta6^+$(%) in uninfected mice.

EAE induction

The MOG_{35-55}/CFA Emulsion PTX kit for EAE induction was purchased from Hooke Laboratories and was used according to the manufacturer protocol. Male and female mice between the ages of 9 and 12 weeks were used in these studies. Mice were monitored for 28 days after EAE induction using the company's scoring guide. In experiments performed at Rutgers University, litters of B6.*Oa*$^{-/-}$ and wildtype B6J pups or B6.*Ob*$^{-/-}$ and wildtype B6J pups were mixed and cross-fostered in two groups on B6 dams to normalize the microbiota, For experiments at U of C either *Ob*$^{+/+}$ littermates of *Ob*$^{-/-}$ mice (sharing the microbiota source) or B6J mice purchased from TJL were used as control.

Cryosectioning and Immunohistochemistry

Kidney samples embedded in O.C.T. (Sakura Tissue Tek®) were cut with cryostat into 8µm-thick sections, which were transferred to microscope slides. Slides were fixed in -20°C acetone, dried and stained with TRITC-coupled anti-mouse IgG (Jackson ImmunoResearch) or anti-mouse FITC-labeled C3a antibody (MP Biomedicals, LLC) in FACS buffer (1%FBS, 0.02% NaN_3, 1XPBS). After washes in FACS buffer (1xPBS/1%FBS/0.1% sodium azide), slides were wetted with 50% glycerol and covered with coverglass (IMEB Inc). The slides were stored at 4°C until imaging using DMLB microscope (Leica Microsystems IR GmbH) equipped with SPOT camera (Diagnostic Instruments, Inc.)

Anti-nuclear antibody (ANA) staining

HEp-2 slides (Bio-Rad) were incubated with serum samples diluted at 1:100 in FACS buffer and counterstained with TRITC-labeled donkey anti-mouse IgG (Jackson ImmunoResearch) diluted

at 1:100 in FACS buffer. After washes in FACS buffer, slides were wetted with 50% glycerol and covered with coverglass (IMEB Inc). The imaging and scoring were performed on the Leica DMLB fluorescent microscope.

Viral strains and infection

MMTV(LA), a naturally occurring exogenous virus [117], was propagated in C3H/HeN mice. Virus was isolated from the skim milk of lactating females via a series of centrifugation including a 30% sucrose cushion centrifugation. Virions were resuspended in PBS and injected intraperitoneally (i. p.). Each mouse received an equivalent of 20 ul of milk. MMTV(LA) consists of three different exogenous MMTVs, BALB2, BALBLA, and BALB14, with Vβ2-, Vβ6-, and Vβ14-specific superantigens (SAgs), respectively [117, 118]. The Vβ6-specific SAg encoded by BALBLA can be presented by both the I-E and I-A molecules of MHC-II and thus, is capable of efficiently infecting I-E-negative mice, like B6 mice [119]. All MMTV-infected mice demonstrate deletion of SAg-cognate T cells after 8 weeks post infection [15, 120] and thus, deletion of $CD4^{+}V\beta6^{+}$ SAg-cognate T cells was used to confirm MMTV infection. Fluorescence-activated cell sorter (FACS) analysis of peripheral blood lymphocytes was used to measure T cell deletion rates. MMTV(LA)-injected mice were considered to be infected if the percentages of their $CD4^{+}V\beta6^{+}$ T cells among peripheral $CD4^{+}$ T cells were decreased by more than 50% compared to the percentages in uninfected mice. Rauscher-like Murine Leukemia Virus (RL-MuLV) which consists of N, B tropic ecotropic and mink cell focus forming (MCF) virus [121] was isolated from tissue culture supernatant of infected SC-1 cells (described elsewhere in this section).

Immunization with MMTV and Ab detection

Preimmune and immune sera were collected from MMTV(LA)-infected or uninfected mice before and after immunization with 1% Triton X-100-treated MMTV(LA) virions purified from milk

in complete Freund's adjuvant (CFA [Thermo Fisher]). Mice immunized with MMTV plus CFA were boosted with the same dose of MMTV in incomplete Freund's adjuvant (IFA [Thermo Fisher]) 14 days after initial immunization. Serum samples collected for ELISA were obtained 10 days postboost. Ab responses to MMTV(LA) virion proteins were compared by ELISA. Donkey anti-mouse IgGs plus anti-IgG2c Abs (Jackson ImmunoResearch, West Grove, PA) coupled to horseradish peroxidase (HRP) were used at the second step. All tests were done in triplicate. Readings obtained with the preimmune samples were subtracted. Mice were immunized at 8 weeks of age.

Immunization with ovalbumin and soy

Pregnant B6.*Ob*-/- and B6.*Ob*-/- females were put on either an egg white protein or soybean protein diet (Harland-Envigo), so the pups were exposed to the specific-Ag-containing food since birth. Mice were immunized with respective Ag in CFA at 8 weeks of age, boosted at 14 days (Ag plus IFA), and bled 10 days postboost. The immunization doses of ovalbumin (OVA [Sigma]) and soy protein (Thermo Fisher) were 100 and 200 µg per mouse, respectively. Mice fed on regular chow were used as controls for OVA diet-fed mice, while mice fed on OVA-containing diet were used as controls for the soy diet-fed mice.

ELISA

To detect MMTV- or MuLV-specific Abs in mouse sera, an enzyme-linked immunosorbent assay (ELISA) was performed. Purified virus (see virus purification from milk) was bound to wells in borate buffered saline at empiricially dermined dilutions (usually 1:100-1:400) overnight at 4C. Wells were blocked with 10% fecal calf serum in 1x PBS (MMTV) or 2% ovalbumin in 1xPBS + 0.05% Tween-20 at 37C for one hour. Sera were diluted in PBS/tween and used at a $1x10^{-2}$ dilution (splenocyte transfer

experiment), $5x10^{-3}$ (MMTV immunization experiments, infection experiments), or $2.5x10^{-3}$ (MuLV immunization experiments). Anti-mouse total IgG- plus anti-IgG2c or IgG2a- or IgG2c-specific secondary antibodies coupled to horseradish peroxidase (HRP [Jackson ImmunoResearch]) were used to detect antivirus antibodies. Backgrounds obtained from incubation with secondary antibodies alone were subtracted from the values obtained from sera of infected mice. In addition, for the corresponding ELISAs the following procedure was used. To detect OVA- and soy protein-specific Abs, the Ags (OVA, fraction VI [Sigma] and soy protein [Thermo Fisher]) were bound to plastic at final concentrations of 2 and 5 ug/ml, respectively, in borate-buffered saline (BBS). Plates were then blocked with 10% fetal bovine serum (FBS) in 1x phosphate-buffered saline (PBS). Mouse sera were used at a $5x10^{-3}$ dilution. Anti-mouse total IgG plus anti-IgG2c or IgG2a- or IgG2c-specific secondary antibodies coupled to HRP were used to detect antivirus antibodies.

Splenocyte transfer

Eight-week-old B6.*Ob*-/- and *Ob*-/- mice were used as donor animals for splenocyte transfer. Red blood cell lysed splenocytes were first incubated with anti-CD3-biotin antibodies (Invitrogen) following by incubation with streptavidin-labeled magnetic beads (Miltenyi). Washed cells were flowed over a magnetic column (Miltenyi), and the CD3-depleted fraction was collected. The CD3-depleted fraction contained ~80% of CD19+ cells as determined by FACS. To produce chimeric mice, $20x10^6$ CD3-depleted splenocytes were intravenously injected into 8-week-old sublethally irradiated (600 rads) recipient MMTV(LA)-infected B6.*Ob*-/- mice. Even though CD3+ cells were depleted from the donor cell pool, a residual population of these cells proliferated in a lymphopenic environment, contributing to ~50% of T cells in the chimeras. Mice were bled 16 weeks after injection, and the sera were assayed by ELISA for anti-MMTV Abs.

Mouse genomic DNA extraction, genotyping, and sequencing

Mouse genomic DNA was extracted from toe or ear samples using 150uL tail digestion buffer (1x STE/0.05% lauryl sarcosine/0.2mg/mL proteinase K) with 4-16 hour incubation at 55C followed by heat inactivation at 85C for 45 mins. One uL of the resulting digestion was used for genotyping PCR. The PCR products were separated on 5% acrylamide gel (Bio-Rad Laboratories) or 2% agarose gels. For genomic analysis of the NOD.Ob KO allele and Bmpr2 KI allele, PCR reactions were treated with ExoSAP-IT (Thermo Fisher Scientific) before submission for sequencing.

Diabetes tracking

Diabetes development was monitored by weekly testing of urine glucose with Diastix Reagent Strips (Bayer, Elkhart, IN).

Histology

Insulitis was scored on ~100 islets per pancreas using 5-mm, H&E-stained sections with 40-mm intervals and scored as follows: 0, no visible infiltration; 1, peri-insulitis; 2, insulitis with <50% islet infiltration; and 3, insulitis with >50% islet infiltration. Kidney pathology was scored using 5-mm, PAS-stained sections with 40-mm intervals and scored as follows by a renal pathologist: 0, no visible change; 1, focal mesangial proliferative changes; 2, diffuse mesangial proliferative disease; 3, diffuse proliferative glomerulonephritis (GN) with focal crescents; and 4, diffuse GN with crescents in >50% of glomeruli.

Purification of B cells

B cells were purified from the spleens of the indicated strains of mice using biotin-conjugated Ab specific for CD19 (eBioscience) followed by MACS (Miltenyi Biotec) using streptavidin-conjugated or a-biotin microbeads, according to the manufacturer's protocol. Purified B cells were >95% pure as determined by FACS analysis.

BM chimeras

Lineage-negative BM cells from 8-12week old B6J, B6N, or B6J.uMT mice were purified using a Lineage Cell Depletion Kit (Miltenyi Biotec). The resulting B6J, B6N, or a 50:50 mix of B6N plus B6J.uMT lineagenegative cells were transplanted by i.v. injection (4-7 $x10^5$ cells per recipient) into lethally irradiated B6J- or B6N-recipient mice as indicated. Each mouse received 1200 rads administered as a split dose of 600 rads, each with 4 h between doses. Posttransplant, BMC recipient mice were maintained on antibiotic-supplemented water for the first two weeks. MHCII-CLIP and MHCII levels were measured on the surface of splenic or peripheral blood B cells from the BMC mice 9-12 wk posttransplant.

Biochemical analyses

H2-M and H2-O coimmunoprecipitation

Purified B cells ($5x10^6$) from the indicated strains of mice were lysed in 20 mM Tris-HCl, 130 mM NaCl pH 7.4 containing 1.2% CHAPS (ThermoFisher Scientific) and protease inhibitors (Roche Life Science) for 30 min on ice. Following the removal of nuclei and cellular debris by centrifugation, the lysates were transferred to new, pre-chilled tubes and precleared for 30-60 min at 4ºC by incubation with 5µg rat or hamster IgG (α-H2-M or α -H2-O immunoprecipitations, respectively) and 25µl of Protein G-Sepharose (GE Healthcare Life Sciences). After centrifugation, 5µg of mAbs specific for the H2-M heterodimer [mAb 2C3A; [114]] or the Oβ cytoplasmic tail [Mags.Ob1; [114]] and 25µl of Protein G Sepharose were added to the precleared lysates. The immunoprecipitations were rotated for 2 hours 4ºC and washed three times with 20 mM Tris-HCl, 130 mM NaCl pH 7.4 containing 0.6% CHAPS. The resulting Protein G pellets were stored at -20ºC until analysis. Immunoprecipitations from B cells purified from *Ma*- and *Ob*-deficient mice were used as negative controls for the H2-O and H2-M immunoprecipitation.

The precipitated H2-O and H2-M was released from the immunoprecipitation pellets by the addition of Laemmli sample buffer and incubated at 95ºC for 5 min prior to separation by 10%–20% gradient SDS-PAGE gels (Criterion, Bio-Rad) and transferred to polyvinylidene fluoride membrane (Millipore). Aliquots of the B cell lysates generated for the immunoprecipitations were also blotted as lysate blotting controls. The lysates were mixed with Laemmli sample buffer containing 20 mM DTT and incubated at 95°C for 5 min prior to analysis by SDS-PAGE. Membranes were blocked with 1% BSA or 5% skim milk powder and incubated with a rabbit serum to the cytoplasmic tails of Mβ (R.Mb/c; see below) or Oβ [R.Ob/c [114]], the luminal domain of Oβ [R.Obeta1; [15]], a mAb specific for Mβ [YoDMA.1; (Fallas et al., 2004)], or β-actin (clone AC-74; Sigma). The blots were washed and bound Abs were detected by incubation with HRP-conjugated goat α-rabbit, -mouse, or -hamster Abs (Jackson ImmunoResearch). After extensive washing blots were developed with SuperSignal West Pico chemiluminescent peroxidase substrate (Pierce Biotechnology) and exposure to film.

To determine the relative levels of Oβ, Mα and Mβ in B cells from the different strains of mice, films were scanned and bands were quantitated using ImageJ (NIH) or Image Studio Lite (LI-COR) software. For the lysate blots, the band density was normalized to that obtained for β-actin to control for differences in loading. To allow data to be combined across multiple independent experiments, the resulting β-actin corrected values were subsequently normalized to the values obtained for H2-O and H2-M from B cells from mice of the indicated control strains. To determine the relative ratio of H2-M and H2-O after immunoprecipitation of H2-O or H2-M, the band density for H2-M was divided by that obtained for H2-O which was then normalized to the value obtained for B cells from mice of the indicated control groups to allow data from independent experiments to be combined.

Polyclonal Abs to the Mβ cytoplasmic tail, were produced in rabbits after multiple immunizations with the Mβ cytoplasmic tail (Mβ/c)-specific peptide (YTPLSGSTYPEGRH) conjugated to

keyhole limpet hemocyanin. Mβ/c-specific Abs were purified from the serum by affinity chromatography using Mβ/c peptide-agarose beads.

H2-M and H2-O Western Blotting

Pellets of $1x10^7$ red blood cell-depleted splenocytes were lysed in 20 mM Tris-HCl, 130 mM NaCl pH 7.4 containing 1% Triton X-100 and protease inhibitor cocktail (Roche Life Sciences) for 30 minutes on ice. Following centrifugation to eliminate nuclei and cellular debris, lysates were incubated at 98^0C for 10 min in Laemmli buffer and resolved on a 15% SDS-PAGE gel (BioRad). After electrotransfer, PVDF membranes were blocked in 5% non-fat dry milk and incubated with a rabbit serum to the cytoplasmic tails of Mβ (R.Mb/c; see below) or Oβ [R.Ob/c [114]], or β-actin (clone AC-74; Sigma). The membranes were washed and probed with HRP-conjugated anti-rabbit Ig secondary Abs (Jackson ImmunoResearch). After extensive washing blots were developed with chemiluminescent peroxidase substrate and visualized by Image LAS 3000 (FujiFilms).

Polyclonal Abs to the Mβ cytoplasmic tail (R.Mb/c) were produced in rabbits after multiple immunizations with a peptide encoding the Mβ cytoplasmic tail (M□/c; YTPLSGSTYPEGRH) conjugated to keyhole limpet hemocyanin. Mβ/c-specific Abs were purified from the sera by affinity chromatography with an Mβ/c peptide column.

BMPR2 Western Blotting

Frozen pellets of purified B cells or bulk bone marrow cells ($5 x10^6$) from the indicated strains of mice were lysed in 400uL SDS lysis buffer (1% SDS/50mM Tris-HCl/5mM DTT) by boiling in a boiling water bath for 10 mins. Supernatants were collected following centrifugation at 15,000rpm x 10 mins. The lysates were mixed with Laemmli sample buffer containing 20 mM DTT and incubated at 95C for 5 min prior to analysis by SDS-PAGE. Membranes were blocked with 5% skim milk powder and incubated with monoclonal antibodies against BMPR2 (Invitrogen

cat#MA5-15827) The blots were washed, and bound Abs were detected by incubation with HRP-conjugated anti-mouse (Jackson ImmunoResearch). After extensive washing, blots were developed with chemiluminescent substrate prior to imaging.

Quantification and statistical analysis

Significance was determined by performing Student unpaired t tests using GraphPad Prism software.

***Staphylococcus aureus* colonization and monitoring**

To grow bacteria for inoculation, a frozen stocks were streaked onto trypic soy agar (TSA) plates containing 100ug/mL rifampicin (stock 100mg/mL rifampicin in DMSO) and incubated overnight at 37C. A single colony was isolated to grow in trypic soy broth (TSB) overnight at 37C with shaking. The following day, 1mL of overnight culture was diluted with 99mL fresh TSB and grown to OD600=1.0 (approximately 3 hours) at 37C with shaking. Cultures were then spun down (8000g x 10 min at 4C) and resuspended in an equal volume of 1x PBS and spun down again. The resulting pellet was resuspended in 1mL 1x PBS and the final volume adjusted such that a 1:100 dilution gave OD600=0.40 (approximately 1E8 CFU/mL in cuvette, or 1E10 CFU/mL in culture). A 1:1 dilution of this stock culture (~5E7 CFU/mL) was made with 1x PBS and 10uL used for intranasal colonization of mice.

Mice were monitored by weekly throat swab and fecal pellet culture on TSA containing 100ug/mL rifampicin. Throat swabs were performed with CONSTIX swabs (pointed 0.08x0.30 in, cat# SC-4). Throats of mice were swabbed to a depth of approximately 17mm, and streaked across 2 agar plates each (approximately 100 streaking motions per plate). Fecal pellets were collected into sterile pre-weighed tubes and homogenized in 500uL 1x PBS and 10uL was plated in duplicate and 100uL was also plated in the case 0 CFU were found on 10uL plates to

confirm loss of colonization. Plates with samples from mice were incubated overnight at 37C before counting. Data are expressed as log10(CFU/throat swab +1) and log10(CFU/gram feces +1).

Generation of rifampicin-resistant *Staphylococcus aureus*

To generate a strain of rifampicin resistant *S. aureus* WU1, a single colony of wild type WU1 was grown overnight in 100mL Mueller Hinton broth (MHB) at 37C with shaking. The following day, the 100mL culture was spun down (600g x 15 mins) and resuspended in 10mL MHB. 100uL of concentrated bacteria were plated on MHA plates containing various amounts of rifampicin (0.008ug/mL to 8ug/mL) to isolate a single spontaneous mutant resistant to the antibiotic. A single colony isolated was tested for resistance to higher concentrations of antibiotic by streaking on MHA plates containing rifampicin concentrations up to 100ug/mL. As 100ug/mL effectively restricted growth of all other microorganisms found in fecal samples from mice in the colony and also allowed for rapid growth of the resistant mutant, this concentration was used for future experiments. Frozen stocks of bacteria were made by resuspending overnight cultures of bacteria grown in trypic soy broth (TSB) in cryopreservation medium (5% monosodium glutamate/5% bovine serum albumin) at -80C.

DNA extraction, 16S rRNA amplicon sequencing and analysis

Cecal contents and IgA-coated and non-coated bacterial fractions were collected and snap frozen at -80C. DNA was extracted from the samples using the DNeasy PowerSoil HTP 96 Kit (QIAGEN, Germantown, MD) according to the manufacturer's instructions. The V4 region of the 16S rRNA-encoding gene (515F-806R) was PCR amplified to survey the total bacterial community in the extracted samples using the Illumina MiSeq platform as described (Walters et al., 2015; Caporaso et al., 2012). PCR reactions were carried out in triplicate for each sample using sterile, DNase-free 96 well plates with appropriate (DNA template-free) negative controls

using the 5 PRIME HotMasterMix kit (Quantabio, Beverly, MA). PCR reactions were conducted using an initial denaturation step of 95C for 3 min, followed by 35 cycles at 95C for 30 s, 55C for 45 s, then 72C for 1.5 min. A single extension step at 72C for 10 min was used at the end. Triplicate PCR reactions were then pooled together, primer dimers were removed from the pooled products using the UltraClean 96 PCR Cleanup Kit (QIAGEN, Germantown, MD) and total DNA was quantified using the PicoGreen dsDNA Assay (Invitrogen/Thermo Fisher Scientific, Carlsbad, CA) and resuspended at 2 ng/ml. Amplicons were sequenced on an Illumina MiSeq using 151x151 base pair paired-end sequencing at the Environmental Sample Preparation and Sequencing Facility at Argonne National Laboratory. 16S rRNA amplicon sequences were analyzed using the DADA2 pipeline (version 1.16) [53] in R Studio. Briefly, reads were verified to be high quality and the leftmost 14 bases trimmed. Amplicon sequence variants (ASVs) were identified and taxonomy was assigned using the Silva NR99 database (release 138.1). PCoA plots were generated using the Bray-Curtis dissimilarity distance in the Phyloseq package in R Studio [122].

IgA-sequencing

To sort IgA+ and IgA- bacteria from frozen cecal contents, approximately 30-35mg frozen cecal contents were resuspendended in 350uL 1X PBS containing protease inhibitor (Roche, cat# 11 836 153 001). Cecal contents were homogenized by vortexing for 5 mins at high speed and bacteria isolated from debris by centrifugation at 400g for 5 mins. The supernatant was filtered through nylon mesh and bacteria were pelleted at 8000g for 5 mins. Bacteria were blocked using 0.25% BSA/10% normal goat serum (Jackson ImmunoResearch cat# 005-000-121) on ice for 20 mins. Bacteria were diluted 1:2 in blocking buffer and stained with anti-IgA-biotin (1:400, Southern biotech, cat# 1040-08) in a total volume of 500uL on ice for 20 mins. Bacteria were washed with 0.25% BSA in PBS and subsequently incubated with streptavidin-APC at 1:800 on ice for 20 mins. Bacteria were washed again and incubated with 10uL anti-APC magnetic beads

(Miltenyi cat# 130-090-855) in a total volume of 500uL. Bacteria were washed and resesupended in 1mL 0.25% BSA in PBS and sorted using an autoMACS (posselds program first, and positive fraction re-sorted using posseld2 program). Double-sorted positive fraction and negative fraction from first sort were pelleted and stored at -80C before processing for sequencing.

Citrobacter rodentium infection, monitoring, and ELISA

C. rodentium strain DBS120 was streaked from a frozen stock onto LB agar plates containing 50ug/mL kanamycin (stock 50mg/mL in water) and incubated overnight at 37C. A single colony was used to start an overnight culture in LB broth incubated at 37C with shaking. The following day, the overnight culture was diluted 1:50 into fresh LB broth for a final volume of 100mL. Cultures were grown to OD600=1.2, washed with an equal volume of PBS, and resuspended in a final volume of 5mL 1x PBS. The final volume was adjusted so a 1:100 dilution of the culture OD600=0.20 (approximately 1E10 CFU/mL). 200uL of this culture was delivered into mice via oral gavage without prior sodium bicarbonate treatment, antibiotic treatment, or fasting.

After infection, mice were monitored every other day starting the day following infection (day 01) by collecting fecal pellets into preweighed sterile tubes and homogenizing fecal pellets in 500uL 1x PBS. Serial dilutions of homogenate were plated in triplicate on LBA containing 50ug/mL kanamycin. Data were expressed as log10(CFU/gram feces +1).

To generate the *C. rodentium* preparation for binding to the ELISA plate, a single colony is first grown at 37C in DMEM overnight without shaking in 5% CO2 conditions in a 100mL volume. The culture is then washed with PBS 1X and adjusted to OD600 = 1 (~1x109 CFU/ml). The culture was then heat killed by incubation at 80C for 45 mins. Heat killed preparations were diluted 1:10 in 1x carbonate buffer (15mM carbonate/35mM bicarbonate, pH 9.6) and incubated in wells overnight at 4C. Wells were blocked with 10% FBS for 1 hour at 37C. Sera were used at a dilution of $6.67x10^{-4}$. Anti-mouse total IgG- plus anti-IgG2c secondary antibodies coupled to

horseradish peroxidase (HRP [Jackson ImmunoResearch]) were used to detect antibacterial antibodies. Backgrounds obtained from incubation with secondary antibodies alone were subtracted from the values obtained from sera of infected mice.

Genome-wide scan of N2 mice and analysis of genome-wide scan data

Tail DNA samples collected from N2 mice phenotyped for MHCII-CLIP levels were selected for genome-wide SNP analysis. Genome-wide SNP analysis was carried out via the Mini Mouse Universal Genotyping Array (miniMUGA) platform offered by Transnetyx [49]. In addition to the SNPs included in the miniMUGA panel, additional SNP assays were designed Genotypes of selected mice were either homozygous for the B6N allele or heterozygous for the B6N and B6J alleles. Percent heterozygosity at each SNP within each phenotype group (i.e. high CLIP or low CLIP) was calculated to identify regions of >60% heterozygosity in high CLIP animals and <40% heterozygosity in low CLIP animals. Plots and data analysis were done in R Studio.

RNA isolation

RNA isolation for the purposes of qPCR analysis was performed from whole spleen with the PureLink RNA Mini Kit (Invitrogen, cat# 12183025) according to the manufacturer's instructions with on column DNAse treatment to remove contaminating genomic DNA. Purified RNA was stored as a precipitate in ethanol at -20C. RNA quality was determined using gel electrophoresis (samples showing degradation were discarded).

RNA isolation for the purpose of RNA-seq was peformed via a cesium chloride gradient. First, B cells were purified from whole spleen via MACS on CD19 (see B cell isolation). Approximately 40 million B cells were resuspended in 3mL guanidine thiocyanate lysis buffer (60% guanidine thiocyanate/0.5% sodium lauryl sarcosine/0.5% beta-EtSH/50mM sodium citrate pH 7.0) and layered over 2mL of CsCl buffer (5.7M CsCl/50mM EDTA). Samples were spun for 16 hours at 36,000 rpm at 25C on an SW 55.1 ultracentrifuge rotor. The resulting pellet was resuspended in

water, 200-proof ethanol precipitated, 160-proof ethanol washed, and resuspended in water. Quality of RNA samples were verified via gel electrophoresis.

cDNA generation

cDNA was produced from 5ug of purified RNA by first incubating RNA with 0.75 mM dNTPs and 4.6uM random primer mix (New England Biolabs, cat# S1330S) at 65C for 5 mins in a final volume of 13uL. After reaction had cooled the following were added and incubated at 55C for 10 mins and then 80C for 10 mins: 400U of SuperScript IV reverse transcriptase (Invitrogen, cat#18090050), RNAseOUT recombinant ribonuclease inhibitor (Invitrogen, cat# 10777019) to a final concentration of 5mM, DTT to a final concentration of 5mM and 5x SuperScript IV buffer to a final concetration of 1x in a final volume of 20uL. PCR with primers specific for the *Actb* gene (Forward: GTATCCTGACCCTGAAGTACC Reverse: TGAAGGTCTCAAACATGATCTG) was carried out to ensure high quality cDNA.

qPCR reactions and data analysis

qPCR reactions were performed in duplicate 20uL reactions containing 1uL cDNA (generated as described in these methods), 2x Gene Expression Master Mix (ThermoFisher, cat#4369016), and 20x TaqMan primer/probe assays (ThermoFisher) for *Obsl1* (Mm00619110_m1), *Bmpr2* (Mm00432134_m1), *Wdfy1* (Mm00840455_m1), or *Pydc3* (Mm04206759_mH). Control reactions with the housekeeping gene *Actb* were performed similarly (probe cat# 4352341E). Amplification was carried out on an AppliedBiosystems QuantStudio3 instrument with the following cycling conditions: 50C for 2 mins, 95C for 10 mins followed by 40 cycles of 95C for 15 sec and 60C for 1 min.

XC plaque assay

Quantification of MuLV infectious virus was performed using the XC plaque assay. First, SC-1 cells (ATCC, cat# CRL-1404) are plated in 6cm tissue culture treated dishes at a density of 2E5 cells/dish in Click's medium (Irvine Scientific, cat# 9195) (day 01) such that they are 30-60% confluent the next day. The following day (day 02), splenocytes (including red blood cells) are isolated from mice and are gamma-irradiated (2000 rad dose) to stop cell proliferation and 1E4 and 1E5 cells are added to the adhered SC-1 cells per dish. Splenocytes are incubated overnight with SC-1 cells in Click's medium containing 10ug/mL polybrene. The medium on the cells is changed the following day (day 03), and once again three days later (day 06). On day 07, cells are exposed to 30 seconds of high-intensity UV light to kill SC1 cells and are immediately overlayed with 1E6 XC cells (ATCC, cat # CCL-165) grown in minimal essential medium (Gibco, cat# 11095-080). On day 09, the medium is changed (MEM) and on day 11 medium is removed and plates are stained with ~4 mL XC plaque stain (0.5% methylene blue/0.17% carbol fuschin in methanol) for 10 mins. After 10 mins, plates are rinsed with distilled water and plaques counted after plates have fully dried.

RNA-seq

RNASeq libraries were prepared using Illumina TotalRNA TruSEQ kits (RiboZero depletion) and sequenced using an Illumina NovaSeq6000 (paired-end 50bp). RNA-seq reads were aligned to the Mus musculus reference C57BL/6J transcriptome with Ensembl gene annotation (GRCm38) by Kallisto (v0.46.1; default settings) [123] in order to generate mRNA expression quantifications. Differential expression analysis downstream of Kallisto processing was performed with the R package DESeq2 (3.14) [124]. Transcripts were considered to be differentially regulated if they had at least a 1.5-fold change compared to B6J and a multiple testing adjusted p-value of <0.05.

Isolation of virus from milk

Virus (MMTV or MuLV) isolation from the milk of viremic females was performed first by collection of milk-filled stomachs from pups fostered on viremic mothers, which were stored at -80C until sufficient quantities of stomachs were collected for isolation. Isolation was performed with approximately 75 stomachs per batch. Stomachs were first homogenized in 1x PBS using a tissue homogenizer (Polytron PT 10-35 GT) in tubes containing 2-15 stomachs each with 2mL PBS. Homogenate was pooled and spun down (3000g x 15 mins at 4C) to separate tissue debris from milk and milkfat. The milk layer was collected. 3mL of milk was carefully layered on top of 2mL endotoxin-free 30% sucrose (Sigma, cat# 84097-1KG) in 1xPBS and spun at 31,000 rpm for 1 hour at 4C using a SW55.1 ultracentrifuge rotor. Pellets were collected and resuspended in 1xPBS and kept on ice overnight to solubilize. The following day, virus was vortexed for 10 mins at high speed and debris was further removed from the virus preparation by centrifugation at 2,350g for 5 mins. Supernatant was collected and 1/10 volume of 10% triton-X100 was added to kill the virus. Virus was then aliquotted and stored at -80C until use.

Germ free mice and sterility monitoring

Germ free (sterile) mice were maintained in the University of Chicago Gnotobiotic Facility in sterile isolators and maintained on sterile food and water. Sterility of mice in the germ free isolators was monitored weekly via PCR screening of the 16S rRNA gene in DNA extracted from fecal samples from individual cages. DNA was extracted by bead beating fecal samples in extraction buffer (500uL 200mM NaCl/200mM Tris-HCl/20mM EDTA + 210 uL 20% SDS +500uL phenol:chloroform 24:24) and further purifying the resulting aqueous fraction by another round of phenol:chloroform extraction. The DNA from this resulting aqueous fraction was precipitated (1/10 volume 3M sodium acetate pH 7.0, 2.5 volumes 200-proof EtOH), washed, and resuspended in sterile water for use in PCR. PCR was performed using universal 16S primers [125] (Forward: 5'-AGAGTTTGATCCTGGCTCAG-3' Reverse: 5'-GACGGGCGGTGWGTRCA-3') using the following cycling conditions: 95C for 2 mins, followed

by 27 cycles of 94C for 40 sec, 56C for 1 min, and 72C for 1 min 20 sec, and a final extension at 72C for 10 mins.

Additionally, microbiological cultures were set up with GF fecal pellets, positive (SPF mouse fecal pellets), sham (sterile saline), and negative (sterile culture medium) controls for each sample batch. Samples were inoculated into BHI, Nutrient, and Sabaroud Broth tubes. Every sample in each of the respective culture media was incubated at 37C and 42C in both aerobic and anaerobic environments. Cultures were monitored daily for evidence of growth and were followed for 5 days until cultures were declared negative.

Gnotobiotic colonization

Ex-germ free mice colonized with cecal contents or defined bacterial consortia were maintained in specific gnotobiotic isolators for the entire course of the experiment. Specific pathogen free cecal contents used for colonization were obtained from C57BL/6NTac mice purchased from Taconic Farms. Cecal contents for Altered Shaedler's Flora colonization was obtained from ASF-colonized mice mainlined by Dr. Eugene Chang at the University of Chicago. Bacterial stock for 22-mix colonization was obtained from Dr. Federico Rey at the University of Wisconsin-Madison. Colonization was performed in 8 week old mice via oral gavage of either frozen bulk cecal contents (for C57BL/6.Tac and Altered Schedler's Flora) or frozen bacterial stock (for 22-mix) homogenized in sterile 1x PBS immediately prior to gavage.

MuLV isolation from tissue culture for ELISA

SC-1 cells infected with MuLV were continuously passaged while collecting tissue culture medium. Approximately 1.5 L pooled medium was used for each isolation. Isolation was performed by mixing 1 part 3x polyethylene glycol (24% PEG 6,000, Sigma cat# 81260-5KG) with 2 parts medium and stirred overnight at 4C. The following day, the mixture was centrifuged at 10,000 rpm for 40 min at 4C and the precipitate resuspended in 30mL 1x PBS. 3mL of virus

was carefully layered on top of 2mL endotoxin-free 30% sucrose (Sigma, cat# 84097-1KG) in 1xPBS and spun at 31,000 rpm for 1 hour at 4C using a SW55.1 ultracentrifuge rotor. Pellets were collected and resuspended in 1xPBS aliquotted and stored at -80C until use. Each virus preparation was tested back to back with the previous preparation to determine the best dilution for use in ELISA.

MuLV isolation for infection

MuLV for infection was isolated from the spleens of infected preleukemic BALB/cJ mice. Virus isolation was performed first by collection of spleens from preleukemic mice which were stored at -80C until isolation. Isolation was performed with approximately 3-4 spleens with a combined approximate weight of 1.0 grams. Spleens were first homogenized in 1x PBS using a tissue homogenizer (Polytron PT 10-35 GT). Homogenate was spun down (3000g x 15 mins at 4C) to separate tissue debris from virus and the virus fraction was collected. 3mL of virus fraction was carefully layered on top of 2mL endotoxin-free 30% sucrose (Sigma, cat# 84097-1KG) in 1xPBS and spun at 31,000 rpm for 1 hour at 4C using a SW55.1 ultracentrifuge rotor. Pellets were collected and resuspended in 1xPBS aliquotted and stored at -80C until use. An aliquot of virus was then used for titration to quantify virus in the preparation.

MuLV infection

Eight week old mice were infected via intraperitoneal injection of 1000 PFU of MuLV diluted in 1x PBS in a 200uL final volume. Mice were bled and sacrificed 3 months post-infection and spleens weighed and used for virus quantification via the XC plaque assay.

References

1. Akira, S., S. Uematsu, and O. Takeuchi, *Pathogen Recognition and Innate Immunity.* Cell, 2006. **124**(4): p. 783-801.
2. Roh, J.S. and D.H. Sohn, *Damage-Associated Molecular Patterns in Inflammatory Diseases.* Immune network, 2018. **18**(4): p. e27-e27.
3. Iwasaki, A. and R. Medzhitov, *Control of adaptive immunity by the innate immune system.* Nature Immunology, 2015. **16**(4): p. 343-353.
4. Chaplin, D.D., *Overview of the immune response.* The Journal of allergy and clinical immunology, 2010. **125**(2 Suppl 2): p. S3-S23.
5. Netea, M.G., et al., *Innate and Adaptive Immune Memory: an Evolutionary Continuum in the Host's Response to Pathogens.* Cell Host & Microbe, 2019. **25**(1): p. 13-26.
6. Flajnik, M.F., *A cold-blooded view of adaptive immunity.* Nat Rev Immunol, 2018. **18**(7): p. 438-453.
7. Karlsson, L., et al., *A novel class II MHC molecule with unusual tissue distribution.* Nature, 1991. **351**(6326): p. 485-8.
8. Liljedahl, M., et al., *HLA-DO is a lysosomal resident which requires association with HLA-DM for efficient intracellular transport.* EMBO J, 1996. **15**(18): p. 4817-24.
9. Sanderson, F., et al., *Accumulation of HLA-DM, a Regulator of Antigen Presentation, in MHC Class II Compartments.* Science, 1994. **266**(5190): p. 1566-1569.
10. Fung-Leung, W.P., et al., *Antigen presentation and T cell development in H2-M-deficient mice.* Science, 1996. **271**(5253): p. 1278-81.
11. Denzin, L.K. and P. Cresswell, *HLA-DM induces CLIP dissociation from MHC class II alpha beta dimers and facilitates peptide loading.* Cell, 1995. **82**(1): p. 155-65.
12. Sloan, V.S., et al., *Mediation by HLA-DM of dissociation of peptides from HLA-DR.* Nature, 1995. **375**(6534): p. 802-6.
13. Denzin, L.K., et al., *Negative regulation by HLA-DO of MHC class II-restricted antigen processing.* Science, 1997. **278**(5335): p. 106-9.
14. van Ham, S.M., et al., *HLA-DO is a negative modulator of HLA-DM-mediated MHC class II peptide loading.* Curr Biol, 1997. **7**(12): p. 950-7.
15. Denzin, L.K., et al., *Neutralizing Antibody Responses to Viral Infections Are Linked to the Non-classical MHC Class II Gene H2-Ob.* Immunity, 2017. **47**(2): p. 310-322.e7.
16. Denzin, L.K., *Inhibition of HLA-DM Mediated MHC Class II Peptide Loading by HLA-DO Promotes Self Tolerance.* Front Immunol, 2013. **4**: p. 465.
17. Liljedahl, M., et al., *Altered antigen presentation in mice lacking H2-O.* Immunity, 1998. **8**(2): p. 233-43.
18. Gu, Y., P.E. Jensen, and X. Chen, *Immunodeficiency and autoimmunity in H2-O-deficient mice.* J Immunol, 2013. **190**(1): p. 126-37.
19. Welsh, R.A., et al., *Lack of the MHC class II chaperone H2-O causes susceptibility to autoimmune diseases.* PLOS Biology, 2020. **18**(2): p. e3000590.
20. Gu, Y., P.E. Jensen, and X. Chen, *Immunodeficiency and Autoimmunity in H2-O–Deficient Mice.* The Journal of Immunology, 2013. **190**(1): p. 126-137.
21. Poluektov, Y.O., et al., *HLA-DO as the Optimizer of Epitope Selection for MHC Class II Antigen Presentation.* PLOS ONE, 2013. **8**(8): p. e71228.
22. Perraudeau, M., et al., *Altered major histocompatibility complex class II peptide loading in H2-O-deficient mice.* Eur J Immunol, 2000. **30**(10): p. 2871-80.
23. Nanaware, P.P., et al., *HLA-DO Modulates the Diversity of the MHC-II Self-peptidome.* Mol Cell Proteomics, 2019. **18**(3): p. 490-503.
24. Guce, A.I., et al., *HLA-DO acts as a substrate mimic to inhibit HLA-DM by a competitive mechanism.* Nature structural & molecular biology, 2013. **20**(1): p. 90-98.

25. Golovkina, T.V., *A novel mechanism of resistance to mouse mammary tumor virus infection.* J Virol, 2000. **74**(6): p. 2752-9.
26. Andervont, H.B., *FATE OF THE C3H MAMMARY TUMOR AGENT IN MICE OF STRAINS C57BL, 1, AND BALB/C.* J Natl Cancer Inst, 1964. **32**: p. 1189-98.
27. Dudley, J.P., T.V. Golovkina, and S.R. Ross, *Lessons Learned from Mouse Mammary Tumor Virus in Animal Models.* ILAR Journal, 2016. **57**(1): p. 12-23.
28. Ross, S.R., et al., *Mouse transferrin receptor 1 is the cell entry receptor for mouse mammary tumor virus.* Proceedings of the National Academy of Sciences, 2002. **99**(19): p. 12386.
29. Held, W., et al., *Superantigen-reactive CD4+ T cells are required to stimulate B cells after infection with mouse mammary tumor virus.* J Exp Med, 1993. **177**(2): p. 359-66.
30. Beutner, U., et al., *B cells are essential for murine mammary tumor virus transmission, but not for presentation of endogenous superantigens.* J Exp Med, 1994. **179**(5): p. 1457-66.
31. Golovkina, T.V., J.P. Dudley, and S.R. Ross, *B and T cells are required for mouse mammary tumor virus spread within the mammary gland.* J Immunol, 1998. **161**(5): p. 2375-82.
32. Case, L.K., et al., *Replication of beta- and gammaretroviruses is restricted in I/LnJ mice via the same genetic mechanism.* J Virol, 2008. **82**(3): p. 1438-47.
33. Purdy, A., et al., *Unique resistance of I/LnJ mice to a retrovirus is due to sustained interferon gamma-dependent production of virus-neutralizing antibodies.* J Exp Med, 2003. **197**(2): p. 233-43.
34. Yi, W., et al., *Targeted regulation of self-peptide presentation prevents type I diabetes in mice without disrupting general immunocompetence.* J Clin Invest, 2010. **120**(4): p. 1324-36.
35. Belov, K., M.K.-P. Lam, and D.J. Colgan, *Marsupial MHC Class II β Genes Are Not Orthologous to the Eutherian β Gene Families.* Journal of Heredity, 2004. **95**(4): p. 338-345.
36. Cullum, E., et al., *MHC Class II Presentation Is Affected by Polymorphism in the H2-Ob Gene and Additional Loci.* The Journal of Immunology, 2021. **207**(1): p. 5.
37. Kane, M., L.K. Case, and T.V. Golovkina, *Vital role for CD8+ cells in controlling retroviral infections.* J Virol, 2011. **85**(7): p. 3415-23.
38. Case, L.K., A. Purdy, and T.V. Golovkina, *Molecular and cellular basis of the retrovirus resistance in I/LnJ mice.* J Immunol, 2005. **175**(11): p. 7543-9.
39. Mellins, E.D. and L.J. Stern, *HLA-DM and HLA-DO, key regulators of MHC-II processing and presentation.* Curr Opin Immunol, 2014. **26**: p. 115-22.
40. Guce, A.I., et al., *HLA-DO acts as a substrate mimic to inhibit HLA-DM by a competitive mechanism.* Nat Struct Mol Biol, 2013. **20**(1): p. 90-8.
41. Kropshofer, H., et al., *A role for HLA-DO as a co-chaperone of HLA-DM in peptide loading of MHC class II molecules.* EMBO J, 1998. **17**(11): p. 2971-81.
42. Yoon, T., et al., *Mapping the HLA-DO/HLA-DM complex by FRET and mutagenesis.* Proc Natl Acad Sci U S A, 2012. **109**(28): p. 11276-81.
43. Kremer, A.N., et al., *Endogenous HLA class II epitopes that are immunogenic in vivo show distinct behavior toward HLA-DM and its natural inhibitor HLA-DO.* Blood, 2012. **120**(16): p. 3246-55.
44. Welsh, R.A., et al., *Lack of the MHC class II chaperone H2-O causes susceptibility to autoimmune diseases.* PLoS Biol, 2020. **18**(2): p. e3000590.
45. Graves, A.M., et al., *Human Hepatitis B Viral Infection Outcomes Are Linked to Naturally Occurring Variants of HLA-DOA That Have Altered Function.* J Immunol, 2020.

46. Cullum, E., et al., *Genetic Control of Neonatal Immune Tolerance to an Exogenous Retrovirus.* J Virol, 2020. **94**(24).
47. Keane, T.M., et al., *Mouse genomic variation and its effect on phenotypes and gene regulation.* Nature, 2011. **477**(7364): p. 289-94.
48. Simon, M.M., et al., *A comparative phenotypic and genomic analysis of C57BL/6J and C57BL/6N mouse strains.* Genome Biol, 2013. **14**(7): p. R82.
49. Sigmon, J.S., et al., *Content and Performance of the MiniMUGA Genotyping Array: A New Tool To Improve Rigor and Reproducibility in Mouse Research.* Genetics, 2020. **216**(4): p. 905-930.
50. Beppu, H., et al., *BMP type II receptor is required for gastrulation and early development of mouse embryos.* Dev Biol, 2000. **221**(1): p. 249-58.
51. Agnew, C., et al., *Structural basis for ALK2/BMPR2 receptor complex signaling through kinase domain oligomerization.* Nature Communications, 2021. **12**(1): p. 4950.
52. Britt, W.J. and B. Chesebro, *H-2D control of recovery from Friend virus leukemia: H-2D region influences the kinetics of the T lymphocyte response to Friend virus.* J Exp Med, 1983. **157**(6): p. 1736-45.
53. Callahan, B.J., et al., *DADA2: High-resolution sample inference from Illumina amplicon data.* Nature Methods, 2016. **13**(7): p. 581-583.
54. Segata, N., et al., *Metagenomic biomarker discovery and explanation.* Genome Biol, 2011. **12**(6): p. R60.
55. Khan, A.A., et al., *Polymorphic Immune Mechanisms Regulate Commensal Repertoire.* Cell Reports, 2019. **29**(3): p. 541-550.e4.
56. Wymore Brand, M., et al., *The Altered Schaedler Flora: Continued Applications of a Defined Murine Microbial Community.* ILAR journal, 2015. **56**(2): p. 169-178.
57. Donaldson, G.P., et al., *Gut microbiota utilize immunoglobulin A for mucosal colonization.* Science (New York, N.Y.), 2018. **360**(6390): p. 795-800.
58. Kourtis AP, H.K., Baggs J, et al., *Vital Signs: Epidemiology and Recent Trends in Methicillin-Resistant and in Methicillin-Susceptible Staphylococcus aureus Bloodstream Infections — United States.* MMWR Morb Mortal Wkly Rep, 2019. **68**: p. 214-219.
59. Tacconelli, E., et al., *Antibiotic usage and risk of colonization and infection with antibiotic-resistant bacteria: a hospital population-based study.* Antimicrob Agents Chemother, 2009. **53**(10): p. 4264-9.
60. Sun, Y., et al., *Staphylococcal Protein A Contributes to Persistent Colonization of Mice with Staphylococcus aureus.* Journal of Bacteriology, 2018. **200**(9): p. e00735-17.
61. Aubry-Damon, H., C.J. Soussy, and P. Courvalin, *Characterization of mutations in the rpoB gene that confer rifampin resistance in Staphylococcus aureus.* Antimicrob Agents Chemother, 1998. **42**(10): p. 2590-4.
62. Goodnow, C.C., et al., *Altered immunoglobulin expression and functional silencing of self-reactive B lymphocytes in transgenic mice.* Nature, 1988. **334**(6184): p. 676-82.
63. Kamada, N., et al., *Humoral Immunity in the Gut Selectively Targets Phenotypically Virulent Attaching-and-Effacing Bacteria for Intraluminal Elimination.* Cell host & microbe, 2015. **17**(5): p. 617-627.
64. Lee, J., et al., *Mouse Homologue of Human HLA-DO Does Not Preempt Autoimmunity but Controls Murine Gammaherpesvirus MHV68.* The Journal of Immunology, 2021: p. ji2100650.
65. Blum, J.S., P.A. Wearsch, and P. Cresswell, *Pathways of antigen processing.* Annu Rev Immunol, 2013. **31**: p. 443-73.
66. Chen, X., et al., *Regulated expression of human histocompatibility leukocyte antigen (HLA)-DO during antigen-dependent and antigen-independent phases of B cell development.* J Exp Med, 2002. **195**(8): p. 1053-62.

67. Graves, A.M., et al., *Human Hepatitis B Viral Infection Outcomes Are Linked to Naturally Occurring Variants of HLA-DOA That Have Altered Function.* J Immunol, 2020. **205**(4): p. 923-935.
68. Morel, L., et al., *Genetic reconstitution of systemic lupus erythematosus immunopathology with polycongenic murine strains.* Proceedings of the National Academy of Sciences, 2000. **97**(12): p. 6670-6675.
69. Lyons, J.A., et al., *B cells are critical to induction of experimental allergic encephalomyelitis by protein but not by a short encephalitogenic peptide.* European Journal of Immunology, 1999. **29**(11): p. 3432-3439.
70. Leiter, E. and M. Atkinson, *Nod Mice and Related Strains: Research Applications in Diabetes, AIDS, Cancer, And Other Diseases* 1998: R.G. Landes Company.
71. Driver, J.P., D.V. Serreze, and Y.-G. Chen, *Mouse models for the study of autoimmune type 1 diabetes: a NOD to similarities and differences to human disease.* Seminars in Immunopathology, 2011. **33**(1): p. 67-87.
72. Miyazaki, T., et al., *Direct evidence for the contribution of the unique I-ANOD to the development of insulitis in non-obese diabetic mice.* Nature, 1990. **345**(6277): p. 722-4.
73. Yurkovetskiy, L., et al., *Gender bias in autoimmunity is influenced by microbiota.* Immunity, 2013. **39**(2): p. 400-12.
74. Makino, S., et al., *Breeding of a Non-Obese, Diabetic Strain of Mice.* Experimental Animals, 1980. **29**(1): p. 1-13.
75. Rudofsky, U.H., et al., *Differences in expression of lupus nephritis in New Zealand mixed H-2z homozygous inbred strains of mice derived from New Zealand black and New Zealand white mice. Origins and initial characterization.* Lab Invest, 1993. **68**(4): p. 419-26.
76. Morel, L., et al., *Functional dissection of systemic lupus erythematosus using congenic mouse strains.* J Immunol, 1997. **158**(12): p. 6019-28.
77. Morel, L., et al., *Production of congenic mouse strains carrying genomic intervals containing SLE-susceptibility genes derived from the SLE-prone NZM2410 strain.* Mamm Genome, 1996. **7**(5): p. 335-9.
78. Mohan, C., et al., *Genetic dissection of SLE pathogenesis. Sle1 on murine chromosome 1 leads to a selective loss of tolerance to H2A/H2B/DNA subnucleosomes.* J Clin Invest, 1998. **101**(6): p. 1362-72.
79. Mohan, C., et al., *Genetic dissection of systemic lupus erythematosus pathogenesis: Sle2 on murine chromosome 4 leads to B cell hyperactivity.* J Immunol, 1997. **159**(1): p. 454-65.
80. Mohan, C., et al., *Genetic Dissection of Sle Pathogenesis: Sle3 on Murine Chromosome 7 Impacts T Cell Activation, Differentiation, and Cell Death.* The Journal of Immunology, 1999. **162**(11): p. 6492-6502.
81. Terry, R.L., I. Ifergan, and S.D. Miller, *Experimental Autoimmune Encephalomyelitis in Mice.* Methods Mol Biol, 2016. **1304**: p. 145-60.
82. Marusic, S., et al., *Cytosolic phospholipase A2 alpha-deficient mice are resistant to experimental autoimmune encephalomyelitis.* J Exp Med, 2005. **202**(6): p. 841-51.
83. Mendel, I., N. Kerlero de Rosbo, and A. Ben-Nun, *A myelin oligodendrocyte glycoprotein peptide induces typical chronic experimental autoimmune encephalomyelitis in H-2b mice: fine specificity and T cell receptor V beta expression of encephalitogenic T cells.* Eur J Immunol, 1995. **25**(7): p. 1951-9.
84. Kumanovics, A., T. Takada, and K.F. Lindahl, *Genomic organization of the mammalian MHC.* Annu Rev Immunol, 2003. **21**: p. 629-57.
85. Efstathiou, S., Y.M. Ho, and A.C. Minson, *Cloning and molecular characterization of the murine herpesvirus 68 genome.* J. Gen. Virol, 1990. **71**: p. 1355-1364.

86. Efstathiou, S., et al., *Murine herpesvirus 68 is genetically related to the gammaherpesviruses Epstein-Barr virus and herpesvirus saimiri.* J. Gen. Virol, 1990. **71**: p. 1365-1372.
87. Virgin, H.W., et al., *Complete sequence and genomic analysis of murine gammaherpesvirus 68.* J. Virol, 1997. **71**(8): p. 5894-5904.
88. Coleman, C.B., M.S. Nealy, and S.A. Tibbetts, *Immature and transitional B cells are latency reservoirs for a gammaherpesvirus.* J Virol, 2010. **84**(24): p. 13045-52.
89. Flano, E., et al., *Latent murine gamma-herpesvirus infection is established in activated B cells, dendritic cells, and macrophages.* J Immunol, 2000. **165**(2): p. 1074-81.
90. Thorley-Lawson, D.A., *Epstein-Barr virus: exploiting the immune system.* Nat Rev Immunol, 2001. **1**(1): p. 75-82.
91. Gauld, S.B., et al., *Modulation of B-cell tolerance by murine gammaherpesvirus 68 infection: requirement for Orf73 viral gene expression and follicular helper T cells.* Immunology, 2013. **139**(2): p. 197-204.
92. Collins, C.M. and S.H. Speck, *Expansion of murine gammaherpesvirus latently infected B cells requires T follicular help.* PLoS Pathog, 2014. **10**(5): p. e1004106.
93. Sangster, M.Y., et al., *Analysis of the virus-specific and nonspecific B cell response to a persistent B-lymphotropic gammaherpesvirus.* J Immunol, 2000. **164**(4): p. 1820-8.
94. Darrah, E.J., et al., *Conserved Gammaherpesvirus Protein Kinase Selectively Promotes Irrelevant B Cell Responses.* J Virol, 2019. **93**(8).
95. Flano, E., et al., *Gamma-herpesvirus latency is preferentially maintained in splenic germinal center and memory B cells.* J Exp Med, 2002. **196**(10): p. 1363-72.
96. Matar, C.G., et al., *Murine gammaherpesvirus 68 reactivation from B cells requires IRF4 but not XBP-1.* J Virol, 2014. **88**(19): p. 11600-10.
97. Weck, K.E., et al., *Mature B cells are required for acute splenic infection, but not for establishment of latency, by murine gammaherpesvirus 68.* J Virol, 1996. **70**(10): p. 6775-80.
98. Weck, K.E., et al., *Macrophages are the major reservoir of latent murine gammaherpesvirus 68 in peritoneal cells.* J Virol, 1999. **73**(4): p. 3273-83.
99. Willer, D.O. and S.H. Speck, *Long-term latent murine Gammaherpesvirus 68 infection is preferentially found within the surface immunoglobulin D-negative subset of splenic B cells in vivo.* J Virol, 2003. **77**(15): p. 8310-21.
100. Collins, C.M. and S.H. Speck, *Tracking murine gammaherpesvirus 68 infection of germinal center B cells in vivo.* PLoS One, 2012. **7**(3): p. e33230.
101. Nikonenko, B.V., et al., *Comparative analysis of mycobacterial infections in susceptible I/St and resistant A/Sn inbred mice.* Tuber Lung Dis, 2000. **80**(1): p. 15-25.
102. Korotetskaia, M.V., et al., *[A locus involved in tuberculosis infection control in mice locates in the proximal part of the H2 complex].* Mol Biol (Mosk), 2011. **45**(1): p. 68-76.
103. Radaeva, T.V., et al., *Direct comparison of low-dose and Cornell-like models of chronic and reactivation tuberculosis in genetically susceptible I/St and resistant B6 mice.* Tuberculosis (Edinb), 2005. **85**(1-2): p. 65-72.
104. Ernst, J.D., *Macrophage receptors for Mycobacterium tuberculosis.* Infect Immun, 1998. **66**(4): p. 1277-81.
105. Cesarman, E., *Gammaherpesviruses and lymphoproliferative disorders.* Annu. Rev. Pathol, 2014. **9**: p. 349-372.
106. Johnson, K.E. and V.L. Tarakanova, *Gammaherpesviruses and B Cells: A Relationship That Lasts a Lifetime.* Viral Immunol, 2020. **33**(4): p. 316-326.
107. McClellan, K.B., et al., *Antibody-independent control of gamma-herpesvirus latency via B cell induction of anti-viral T cell responses.* PLoS Pathog, 2006. **2**(6): p. e58.
108. Hu, Z., et al., *Functional heterogeneity in the CD4+ T cell response to murine gamma-herpesvirus 68.* J Immunol, 2015. **194**(6): p. 2746-56.

109. Sparks-Thissen, R.L., et al., *CD4 T cell control of acute and latent murine gammaherpesvirus infection requires IFNgamma.* Virology, 2005. **338**(2): p. 201-8.
110. Tibbetts, S.A., et al., *Immune control of the number and reactivation phenotype of cells latently infected with a gammaherpesvirus.* J Virol, 2002. **76**(14): p. 7125-32.
111. Cardin, R.D., et al., *Progressive loss of CD8+ T cell-mediated control of a gamma-herpesvirus in the absence of CD4+ T cells.* J Exp Med, 1996. **184**(3): p. 863-71.
112. Kane, M., et al., *Successful transmission of a retrovirus depends on the commensal microbiota.* Science (New York, N.Y.), 2011. **334**(6053): p. 245-249.
113. Miyazaki, T., et al., *Mice lacking H2-M complexes, enigmatic elements of the MHC class II peptide-loading pathway.* Cell, 1996. **84**(4): p. 531-41.
114. Fallas, J.L., et al., *Expression patterns of H2-O in mouse B cells and dendritic cells correlate with cell function.* J Immunol, 2007. **178**(3): p. 1488-97.
115. Acha-Orbea, H. and H.R. MacDonald, *Superantigens of mouse mammary tumor virus.* Annu Rev Immunol, 1995. **13**: p. 459-86.
116. Finke, D., S.A. Luther, and H. Acha-Orbea, *The role of neutralizing antibodies for mouse mammary tumor virus transmission and mammary cancer development.* Proc Natl Acad Sci U S A, 2003. **100**(1): p. 199-204.
117. Piazzon, I., et al., *Transmission of an Mls-1a-like superantigen to BALB/c mice by foster-nursing on F1 Mls-1bxa mothers. Sex-influenced onset of clonal deletion.* J. Immunol., 1994. **153**(4): p. 1553-1562.
118. Golovkina, T.V., et al., *Generation of a tumorigenic milk-borne mouse mammary tumor virus by recombination between endogenous and exogenous viruses.* J. Virol., 1997. **71**(5): p. 3895-3903.
119. Buggiano, V., et al., *Characterization of two infectious mouse mammary tumour viruses: superantigenicity and tumorigenicity.* Scand. J. Immunol., 1999. **49**(3): p. 269-277.
120. Marrack, P., E. Kushnir, and J. Kappler, *A maternally inherited superantigen encoded by mammary tumor virus.* Nature, 1991. **349**: p. 524-526.
121. Hook Lauren, M., et al., *Characterization of a Novel Murine Retrovirus Mixture That Facilitates Hematopoiesis.* Journal of Virology, 2002. **76**(23): p. 12112-12122.
122. McMurdie, P.J. and S. Holmes, *phyloseq: An R Package for Reproducible Interactive Analysis and Graphics of Microbiome Census Data.* PLOS ONE, 2013. **8**(4): p. e61217.
123. Bray, N.L., et al., *Near-optimal probabilistic RNA-seq quantification.* Nature Biotechnology, 2016. **34**(5): p. 525-527.
124. Love, M.I., W. Huber, and S. Anders, *Moderated estimation of fold change and dispersion for RNA-seq data with DESeq2.* Genome Biology, 2014. **15**(12): p. 550.
125. Turner, S., et al., *Investigating Deep Phylogenetic Relationships among Cyanobacteria and Plastids by Small Subunit rRNA Sequence Analysis1.* Journal of Eukaryotic Microbiology, 1999. **46**(4): p. 327-338.

Supplemental Materials available online

TABLE S1: Complete RNAseq results table (available online)

TABLE S2: Differentially expressed transcripts in B6J and B6N B cells (available online)

TABLE S3: 16S rRNA sequencing ASV results table, bulk cecal contents (available online)

TABLE S4: 16S rRNA sequencing ASV results table, IgA-seq (available online)